MIXED LUBRICATED LINE CONTACTS

Irinel Cosmin Faraon

De promotiecommissie is als volgt samengesteld:
Prof. dr. ir. M.F.A.M. Maarseveen, Universiteit Twente, Voorzitter en secretaris
Prof. dr. ir. D.J. Schipper, Universiteit Twente, Promotor
Prof. dr. ir. J. Huetink, Universiteit Twente
Prof. ir. H.M.J.R. Soemers, Universiteit Twente
Prof. dr. M.C. Elwenspoek, Universiteit Twente
Prof. dr. ing. S. Cretu, Universiteit Gh. Asachi, Roemenië
Prof. dr. ir. P. De Baets, Universiteit Gent, België

Faraon, Irinel Cosmin
MIXED LUBRICATED LINE CONTACTS
Ph.D. Thesis, University of Twente, Enschede, The Netherlands
November 2005

ISBN 90-365-2280-3

Key words: Stribeck curve; mixed lubrication, boundary lubrication; film thickness; starved lubrication; shear thinning; statistic contact model; deterministic contact model

MIXED LUBRICATED LINE CONTACTS

PROEFSCHRIFT

ter verkrijging van
de graad van doctor aan de Universiteit Twente,
op gezag van de rector magnificus,
prof.dr. W.H.M. Zijm,
volgens besluit van het College voor Promoties,
in het openbaar te verdedigen
op donderdag 24 november 2005 om 15.00 uur

door

Irinel Cosmin Faraon
geboren op 28 april 1977
te Onesti, Roemenië

Dit proefschrift is goedgekeurd door:

de promotor, prof.dr.ir. D.J. Schipper

to Irina and Ştefan
my family in Romania
in memory of my son, Teodor

Summary

The present work deals with friction in mixed lubricated line contacts. Components in systems are becoming smaller and due to, for instance power transmitted, partial contact may occur. In industrial applications, friction between the moving contacting surfaces cannot be avoided, therefore it is essential that an engineer is able to predict friction. A very important parameter in lubricated tribo-system is the roughness of the surfaces i.e. the micro geometrical irregularities of the surfaces. The roughness may influence the transition between the friction situation when the surfaces carry all the load by having direct contact (so called Boundary Lubrication regime) and the friction situation when the surfaces are separated by the lubricant, so called (Elasto) Hydrodynamic Lubrication (E)HL regime. The transition between these two aforementioned lubrication regimes is called Mixed Lubrication (ML), and the three lubrication regimes BL, ML and (E)HL can be distinguished in a friction curve named after Stribeck (1902).
Many tribo-systems (machine components, production processes, etc.) operate in the ML or even in the BL regime and therefore it is very important to know prior to the design in which lubrication regime a tribo-system operates. In this thesis the influence of parameters such as velocity, load etc. on the coefficient of friction are studied and a mixed lubrication model, able to predict Stribeck curves, is developed by taking into account those different parameters.

An overview is presented on the three lubrication regimes, i.e. (Elasto) Hydrodynamic Lubrication, Mixed Lubrication and Boundary Lubrication with the emphasis on the formation mechanisms of boundary layers and the factors which influence the friction in the Boundary Lubrication regime.

Statistical Stribeck curve models for two rough surfaces in contact, shear thinning of lubricants and starved lubrication are developed. By using the statistic Stribeck curve model for two rough surfaces, the separation between the contacting surfaces is smaller than for a single rough surface Stribeck contact model and as a consequence the Stribeck curve changes.
When shear thinning of the lubricant occurs, the viscosity of that lubricant decreases and as a consequence the film thickness decreases which has an influence on the Stribeck curve by shifting the mixed lubrication regime to the high velocity region. The results of calculations show that the shift of the mixed lubrication regime depends on the properties of the lubricant.
The results of calculations for starved lubricated contacts show that for values of oil layer thickness applied to the contact over roughness ratio (h_{oil}/σ_s) larger than

approximately 6, the Stribeck curve does not change. If oil layer thickness over roughness ratio is in the range of 6 to 0.7, the friction starts to increase and when oil layer thickness over roughness ratio is less than approximately 0.7, the Stribeck curve tends to transform into a straight line (constant friction level).

When the distribution of the asperity is not Gaussain, then a deterministic contact model for rough surfaces is desirable. A deterministic contact model has been developed in order to be able to calculate the Stribeck curve for a real distribution of the asperities. It is shown based on comparisons between measurements and calculations that the deterministic Stribeck curve model is in good agreement with the experiments, and the calculations given by the statistical Stribeck curve model are in agreement with the experiments when the height distribution of the asperities of a surface is close to the Gaussian distribution.

Samenvatting

Dit werk behandelt de wrijving in gemengd gesmeerde contacten. Componenten in systemen worden steeds kleiner en als gevolg van bijvoorbeeld vermogensoverdracht kan gedeeltelijk contact optreden. In industriële toepassingen kan wrijving tussen de bewegende contactoppervlakken niet worden voorkomen, daarom is het essentieel dat een ingenieur in staat is om de wrijving te voorspellen. Een zeer belangrijke parameter in een gesmeerd tribo-systeem is de ruwheid van de oppervlakken, dat wil zeggen de micro geometrische onregelmatigheden van de oppervlakken. De ruwheid kan de transitie tussen de verschillende wrijvingssituaties beïnvloeden; als de oppervlakken de gehele belasting dragen door direct contact, het zogenaamde grenssmeringsgebied BL en de wrijvingssituatie als de oppervlakken worden gescheiden door het smeermiddel, het zogenaamde (elasto)hydrodynamische smeringsgebied (E)HL. De transitie tussen de twee bovengenoemde smeringsgebieden wordt gemengde smering genoemd ML. De drie smeringsgebieden BL, ML en (E)HL kunnen worden onderscheiden in een wrijvingsgrafiek de zogenoemde Stribeckcurve genoemd naar Stribeck (1902).
Veel tribo-systemen (machine componenten, productieprocessen, enz.) opereren in het ML of zelfs in het BL gebied en daarom is het zeer belangrijk om van tevoren te weten van het ontwerp in welk smeringsgebied het tribo-systeem opereert. In dit proefschrift is de invloed van de parameters zoals snelheid, belasting enz. op de wrijvingscoëfficiënt bestudeerd en een gemengde smeringsmodel, in staat om de Stribeckcurves te voorspellen, is ontwikkeld rekening houdend met deze verschillende parameters.

Een overzicht is gepresenteerd van de drie smeringsgebieden, d.w.z. (elasto) hydrodynamische smering, gemengde smering en grenssmering met de nadruk op het effect van de grenslagen en de invloedsfactoren op de wrijving in het grenssmeringsgebied.

Er zijn statistische Stribeckcurve modellen ontwikkeld voor 1) twee ruwe oppervlakken in contact, 2) viscositeits vermindering door afschuiving van smeermiddelen en 3) marginale smering (“starved lubrication”). Bij toepassing van het statistisch Stribeckcurve model voor twee ruwe oppervlakken wordt een kleinere scheiding tussen de contactoppervlakken voorspeld dan voor een enkel ruw oppervlak Stribeck contactmodel en als gevolg daarvan verandert de Stribeckcurve.

Als “shear thinning” van het smeermiddel plaatsvindt, neemt als gevolg daarvan de filmdikte af hetgeen een invloed heeft op de Stribeckcurve. Het gemengde smeringsgebied verschuift naar het hoge snelheidsgebied. De resultaten van de berekeningen laten zien dat de verschuiving van het gemengde smeringsgebied afhangt van de eigenschappen van het smeermiddel.
De resultaten van berekeningen voor marginaal gesmeerde contacten laten zien dat de waardes voor de ratio olielaagdikte toegevoerd naar het contact over de ruwheid (h_{iol}/σ_s) groter dan ongeveer 6 de Stribeckcurve niet verandert. Als de toegevoerde olielaagdikte over ruwheids ratio is in de range van 0.7 tot 6 begint de wrijving toe te nemen en wanneer de olielaagdikte over ruwheids ratio is kleiner dan ongeveer 0.7 de Stribeckcurve neigt te transformeren in een rechte lijn (constant wrijvingsniveau).

Als de verdeling van de ruwheidhoogten niet Gaussisch is, dan is een deterministisch contactmodel voor ruwe oppervlakken wenselijk. Er is een deterministisch contactmodel ontwikkeld teneinde in staat te zijn om een Stribeckcurve te berekenen voor een werkelijke hoogteverdeling van ruwheidstoppen. Er wordt aangetoond op basis van vergelijking tussen metingen en berekeningen dat a) de deterministische Stribeckcurve model in goede overeenstemming is met de experimenten en b) de berekeningen behorend bij het statistisch Stribeckcurve model in overeenkomst zijn met de experimenten wanneer de hoogteverdeling van de ruwheidstoppen de Gaussische verdeling benadert.

Acknowledgement

Many people have contributed to this thesis by their physical or intellectual support.

First I would like to thank to my supervisor and promoter Prof. Schipper for his support and ideas in writing this thesis. He guided me very well during my studies and preparation of this thesis.

I would also like to thank the other committee members: Prof. dr. ir. M.F.A.M. Maarseveen, Prof. dr. ir. J. Huetink, Prof. ir. H.M.J.R. Soemers, Prof. dr. M.C. Elwenspoek, Prof. dr. ing. S. Cretu, Prof. dr. ir. P. De Baets.

I am grateful to ir. Arjen Brandsma and ir. Mark van Drogen for their support, collaboration and discussion in our meetings.

Special thanks to Erik de Vries and Willie Kerver for their help with design and Walter Lette for his solution to the problems related to computers. Many thanks to Belinda Bruinink for her support in the bureaucratic difficulties I faced.

During the past four years I have enjoyed the pleasant working environment in the Tribology group and I want to thank the (ex-) staff members: Wijtze ten Napel, Dik Schipper, Kees Venner, Matthijn de Rooij, Erik de Vries, Walter Lette, Belinda Bruinink, Willie Kerver and the (former) PhD students: Ako, Bert, Bernd, Caner, Ellen, George, Gerrit, Isaias, Jamari, Jan Willem, Loredana, Mark, Marc, Rihard and Quiang.

I want to thank George, Izabela, Loredana, Szabolcs, Liviu, Oxana, Gratiela, Bogdan, Octav, Rita, Emad and Kitam for their friendship and support during my stay in the Netherlands.

Finally I express my deep gratitude and love to my wife Irina for her care and her never-ending support in my work. I express my love to my son Stefan who brings happiness and harmony in my life. I want to thank to my beloved family in Romania for their love and support.

Contents

Nomenclature

a	Hertzian contact radius	[m]
a_i	fit parameter (i=1, 2, 3, 4)	[-]
A_C	real area of asperity contact	[m^2]
A_{iep}	local elastic-plastic contact area	[m^2]
A_i	local contact area	[m^2]
A_{ip}	local plastic contact area	[m^2]
A_{ie}	local elastic contact area	[m^2]
A_H	total area of the hydrodynamic component in contact	[m^2]
A_{nom}	nominal or apparent contact area	[m^2]
A_r	real contact area	[m^2]
$\overline{A}$	dimensionless real contact area	[-]
b	half Hertzian width	[m]
b^*	half width of deformed line contact	[m]
$\overline{b}^*$	normalized half width of deformed line contact	[-]
B	length of the cylinder	[m]
d_d	distance between mean plane of the heights of summits and mean plane of the surface heights	[m]
D_d	dimensionless distance between mean plane of the heights of the summits and mean plane of the surface heights	[-]
E'	combined elasticity modulus	[Pa]
E_i	elasticity modulus of contacting surface i (i=1, 2)	[Pa]
f	coefficient of friction	[-]
f_i	microscopic coefficient of friction	[-]
f_{BL}	coefficient of friction of boundary layer	[-]
f_F	coefficient of friction for fully flooded conditions	[-]
f_s	coefficient of friction for starved conditions	[-]
$f(s)$	Gaussian height distribution	[1/m]
F_{iep}	local elastic-plastic asperity normal load	[N]
F_i	local asperity normal load	[N]
F_{ip}	local plastic asperity normal load	[N]
F_{ie}	local elastic asperity normal load	[N]
F_f	friction force	[N]
F_j	integral identity (with j a number)	[-]
f_c	coefficient of friction in the BL regime	[-]
F_N	normal force	[N]
F_C	load carried by the asperities	[N]
F_H	load carried by the hydrodynamic component	[N]
G	lubricant number	[-]

h	film thickness, separation	[N]
h_c	critical value of the film thickness	[m]
h_{oil}	lubricant layer thickness supplied to the contact	[m]
$\overline{h}$	dimensionless film thickness	[-]
h^*	starved film thickness	[m]
h_∞^*	film thickness for fully flooded conditions	[m]
h_{00}	integration constant	[m]
h_{cen}	central film thickness	[m]
H	dimensionless separation	[-]
H_∞	integration constant	[-]
H_C	dimensionless central separation	[-]
H_{cen}	dimensionless central film thickness	[-]
H_h	dimensionless separation	[-]
H_{HS}	dimensionless separation for shear thinning lubricants	[-]
H_{EI}	elastic / isoviscous asymptote	[-]
H_{EP}	elastic / piezoviscous asymptote	[-]
H_{RI}	rigid / isoviscous asymptote	[-]
H_{RP}	rigid / piezoviscous asymptote	[-]
L	lubrication number (Schipper parameter)	[-]
M	load number	[-]
N	number of asperities in contact	[-]
$\overline{N}$	normalized number of asperities in contact	[-]
n	density of asperities	[$1/m^2$]
n_i	density of asperities of the contacting surfaces (i=1, 2)	[$1/m^2$]
$\overline{n}$	density of asperities number	[-]
p	pressure	[Pa]
$\overline{p}$	dimensionless contact pressure	[-]
p_{av}	average contact pressure	[Pa]
p_h	maximum Hertzian pressure	[Pa]
p_c	central pressure	[Pa]
p_C	asperity pressure	[Pa]
p_H	hydrodynamic pressure	[Pa]
p_{iep}	local elastic-plastic average pressure	[Pa]
p_r	constant ($p_r = 196.2 \cdot 10^6$)	[Pa]
p_T	total pressure	[Pa]
P	dimensionless nominal contact pressure	[-]
P_c	dimensionless central contact pressure	[-]
q	reduced pressure	[-]
q_{HS}	reduced pressure for shear thinning lubricants	[-]
R	reduced radius of cylinder	[m]
R_a	CLA surface roughness	[m]
s	argument of the height distribution $\phi(s)$	[m]

t	time	[s]
T_t	transition temperature	[ºC]
T_m	melting temperature	[ºC]
U_Σ	velocity number	[-]
v_i	surface velocity (i=1, 2)	[m/s]
v	velocity	[m/s]
v^+	sum velocity	[m/s]
$\overline{U}$	average velocity	[m/s]
v^{dif}	sliding velocity	[m/s]
W	load number	[-]
w	deformation	[m]
w_e	local elastic deformation	[m]
w_i	local deformation	[m]
w_p	local plastic deformation	[m]
x	spatial coordinate	[m]
x_i	lubricant inlet length	[m]
x_i'	lubricant inlet length for surface tension case	[m]
X	dimensionless spatial coordinate	[-]
y	spatial coordinate	[m]
z	viscosity-pressure index (Roelands)	[-]
z_i	asperity height (i=1, 2..n)	[m]

Greek symbols

α	viscosity-pressure coefficient (Barus)	[1/Pa]
β	radius of asperity	[m]
β_{ei}	local effective asperity radius	[m]
β_i	local asperity radius (i=1, 2..n)	[m]
β^*	influence of starvation upon h^* $[=h^*/h^*_\infty]$	[-]
γ_1	adaptation parameter for hydrodynamic component in ML	[-]
γ_2	adaptation parameter for asperity contact component in ML	[-]
$\dot{\gamma}$	shear rate	[s^{-1}]
$\dot{\gamma}_c$	critical shear rate	[s^{-1}]
η	viscosity	[Pa·s]
η_0	viscosity at ambient pressure	[Pa·s]
η_∞	constant ($\eta_\infty = 6.315 \cdot 10^{-5}$)	[Pa·s]
φ	anisotropy surface coefficient	[-]
ν	Poison's ratio	[-]
ρ	density	[kg/m^3]
ρ_0	density at ambient pressure	[kg/m^3]

σ_s	standard deviation of the asperity height distribution	[m]
σ	standard deviation of the surface height distribution	[m]
$\overline{\sigma}_s$	dimensionless roughness	[-]
τ	shear stress	[Pa]
τ_C	shear stress of asperity contact	[Pa]
τ_H	shear stress of the hydrodynamic component	[Pa]
τ_l	lubricant limiting shear stress	[Pa]
τ_0	Eyring shear stress	[Pa]
ϕ	non-dimensional co-ordinate	[-]
$\phi(s)$	distribution of the asperities	[-]

Dimensionless numbers

$$\overline{A} = \frac{A_r}{bB}$$

$$\overline{b}^* = \frac{b^*}{b}$$

$$D_d = \frac{\pi}{8}\frac{d_d BE'}{F_N}$$

$$G = \alpha E'$$

$$\overline{h} = \frac{h}{R}$$

$$H = \frac{h}{R}\sqrt{\frac{E'R}{\eta_0 v^+}}$$

$$H_h = \frac{\pi}{8}\frac{hBE'}{F_N}$$

$$L = \frac{\eta_0 v^+}{p_{av} R_a}$$

$$L = \alpha E'\left(\frac{\eta_0 v^+}{E'R}\right)^{1/4}$$

$$M = \frac{F_N}{BE'R}\sqrt{\frac{E'R}{\eta_0 v^+}}$$

$$\overline{N} = \frac{N}{Bbn}$$

$$\overline{n} = \frac{32}{\pi}\frac{nF_N}{E'B}\sqrt{\beta \cdot R}$$

$$\overline{p} = \frac{p}{p_h}$$

$$U_\Sigma = \frac{\eta_0 v^+}{E'R}$$

$$W = \frac{F_N}{BE'R}$$

$$X = \frac{x}{b}$$

$$\beta^* = \frac{h^*}{h^*_\infty}$$

$$\overline{\sigma}_s = \frac{\pi}{8}\frac{\sigma_s BE'}{F_N}$$

Abbreviations

BL	Boundary Lubrication
(E)HL	(Elasto) Hydrodynamic Lubrication
G & W	Greenwood and Williamson
ML	Mixed Lubrication
EP	Extrem pressure lubricant
SFA	Surface Force Apparatus
AFM	Atomic Force Microscop

Chapter 1

Introduction

1.1 Tribology and friction

Friction is essential in our daily life. Friction makes it possible to walk, cycle, skate etc. On one hand, there are cases where a high friction is demanded, as for instance in brakes, traction drives and clutches. But on the other hand, in many industrial applications low friction between the contacting surfaces is required, such as gears, bearings and cam & tappet system.

One of the developments in design is to reduce the size of the components in constructions while transmitting the same or even higher loads resulting in severe operational contact conditions. Therefore, a higher quality of the materials is required and the need of tribological knowledge increases as well. Furthermore the tribo-systems are optimized with respect to low friction and wear. This is often realised by lubrication. When the lubricant is able to separate the surfaces, then friction is considerably less, compared to the situation when the surfaces are in direct contact. If the surfaces are separated by a fluid film due to motion, the lubrication mechanism is called hydrodynamic lubrication (HL) and when the contacting bodies deform elastically due to the contact pressure the lubrication mechanism refers to as elasto-hydrodynamic lubrication (EHL).

A very important aspect in the tribo-system is the roughness of the surfaces i.e. the micro geometrical irregularities of the surfaces. The roughness may influence the transition between the friction situation when the surfaces have direct contact (so called Boundary Lubrication regime) and the friction situation when the surfaces are separated by the lubricant ((E)HL). The transition between the two aforementioned lubrication regimes is called Mixed Lubrication (ML), and the three lubrication regimes (BL, ML and (E)HL) can be distinguished in the curve named after Stribeck who published a series of papers in 1902 on the influence of the velocity of the contacting surfaces and the load on the coefficient of friction for plain

journal bearings as well as for roller bearings. In the next section the so called generalized Stribeck curve will be described.

1.2 Stribeck curve

The contact between surfaces in the three lubrication regimes are schematically presented in Fig.1.1.

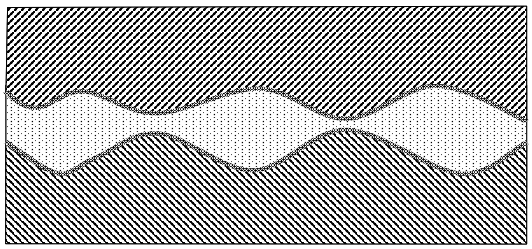

(a) (E)HL

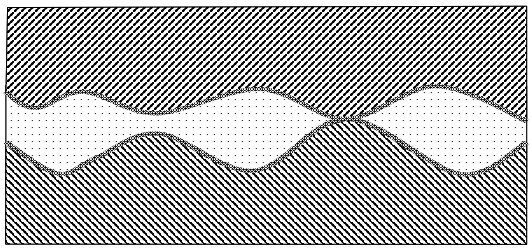

(b) ML

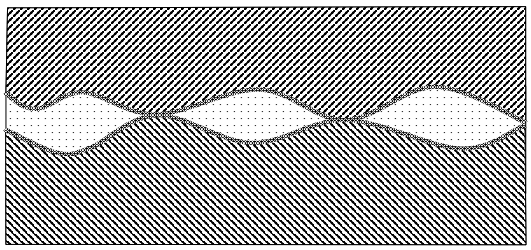

(c) BL

Fig.1.1: The three lubrication regimes: a) elasto-hydrodynamic lubrication regime ((E)HL), b) mixed lubrication regime (ML) and c) boundary lubrication regime (BL).

When the sliding velocity is high, due to hydrodynamic effects, the two surfaces are fully separated by the lubricant (see Fig.1.1[a]). In this situation the pressure of the fluid in the contact is high enough to separate the surfaces, the (Elasto-) Hydrodynamic Lubrication regime. In this situation the velocity difference between the surfaces is accommodated by the lubricant. The coefficient of friction in this case is governed by the lubricant properties and is typically of the order 0.01. When the velocity decreases the pressure of the fluid in the contact decreases (less hydrodynamic action) and as a consequence the asperities of the surfaces start to touch each other and a part of the load is carried by the asperities which leads to an increase in friction. In this situation the friction is given by shear between the interacting asperities as well as by the shear of the lubricant. This is a transition regime and is called Mixed Lubrication (ML), see Fig.1.1[b]. By decreasing the velocity further, the pressure of the lubricant in the contact becomes equal to the ambient pressure and as a result more asperities are in contact and the total normal load is carried by interacting asperities. This regime is called Boundary Lubrication (BL), see Fig.1.1[c]. In the BL regime the friction is controlled by the shear stress of the boundary layers built on the surfaces of the solid bodies. The value of the coefficient of friction in this regime is of the order 0.1.

The boundary layers on the solid bodies are usually formed by the additives in the lubricant or by the lubricant itself. The boundary layer protects the surface from wear and the shear stress of these layers is in most of the cases constant with pressure and velocity but there are also layers where the shear stress varies with these parameters (pressure and velocity). When the boundary layer cannot be formed on the surfaces, the coefficient of friction in the “BL regime” approaches the “dry” value (e.g. 0.4 - 1) while for boundary layered surfaces it is in the order of 0.1-0.15. This thesis deals with lubricated contacts which have protective boundary layers on the surfaces.
In Fig.1.2 the generalized Stribeck curve is depicted. The coefficient of friction (i.e. the ratio between the friction force and the normal force) between the two moving surfaces is plotted against velocity or lubrication number. The horizontal axis in Fig.2.1 has a logarithmic scale. For details about the lubrication number the reader is referred to Schipper (1988).

The increase in the technical demands (small sized components in combination with high loads) leads to a decrease in the film formation and as a consequence the contacts do not operate in the (E)HL but in the ML regime. There are also tribological applications where a higher coefficient of friction is desired and as a result the contacts should operate in the BL and ML regime. Therefore, prior to the design of machine components, it is very important to know their operational position in one of the three lubrication regimes as a function of the velocity or lubrication number for the tribo-system which has to be designed. There are many

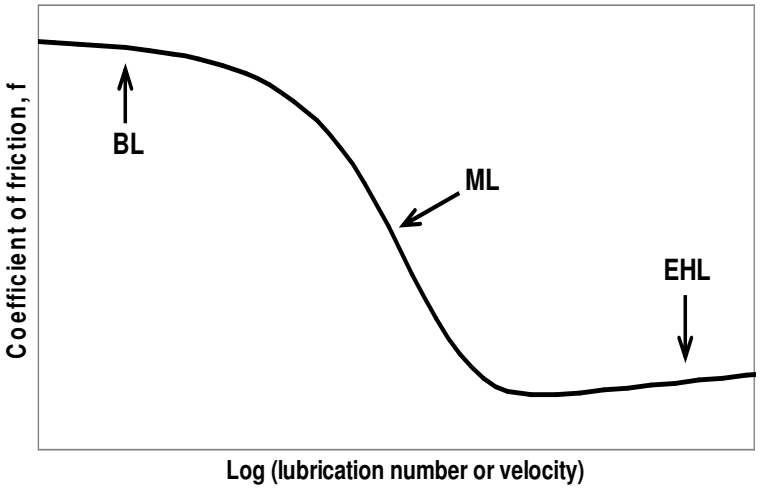

Fig.1.2: The generalized Stribeck curve.

factors which influence the friction curve such as surface roughness, type of boundary layer, amount of oil which is supplied to the contact etc. Therefore, the prediction of the ML regime becomes complicated and all the influencing parameters have to be considered.

1.3 Objective of this thesis

As presented in the previous section, many tribo-systems (machine components, production processes) operate in the ML or even in the BL regime and therefore it is very important to know prior to the design in which lubrication regime a tribo-system operates. In this thesis the influence of parameters such as velocity, pressure, load etc. on the coefficient of friction are studied and a mixed lubrication model, able to predict Stribeck curves, is developed by taking into account those different parameters. The experimentally validated model is restricted to the isothermal line contact situation. The influence of the pressure on the coefficient of friction in the boundary lubrication regime is also an issue of this thesis.

1.4 Outline

The objective of this thesis has been presented previously.
Chapter 2 presents a literature overview on the three lubrication regimes, i.e. (elasto) hydro-dynamic lubrication, mixed lubrication and boundary lubrication.
In Chapter 3 mixed lubrication models for statistical rough surfaces will be presented. In this chapter the influence of shear thinning lubricants, two rough surfaces and the starved lubrication situation is studied.
In Chapter 4 a mixed lubrication model for deterministic rough surfaces is developed and the influence of pressure on the coefficient of friction in the boundary lubrication regime is investigated.
In Chapter 5 the pin-on-disc machine is presented for validation of the mixed lubrication model as well as the Surface Force Apparatus for measuring the shear stress-pressure behaviour of boundary layers.
In Chapter 6 results of the shear stress-pressure measurements are presented and comparisons between measured and calculated Stribeck curves are made. Finally in Chapter 7 conclusions are pointed out and recommendations are given.

References

Gelinck, E.R.M. (1999), “Mixed lubrication of line contacts”, PhD thesis, University of Twente Enschede, The Netherlands.

Schipper, D.J. (1988), “Transitions in the lubrication of concentrated contacts”, PhD thesis, University of Twente Enschede, The Netherlands.

Stribeck, R. (1902), “Die wesentlichen Eigenschaften der Gleit- und Rollenlager”, VDI-Zeitschrift, Vol. 46, 1341-1348, 1432-1438 and 1463-1470.

Chapter 2

Literature

As it was presented in the previous chapter the Stribeck curve comprises three lubrication regimes. The Mixed Lubrication (ML) regime is the transition between the Boundary Lubrication (BL) regime and the Elasto-Hydrodynamic Lubrication (EHL) regime and therefore the lubrication mechanism is a combination of these two lubrication regimes. This chapter presents a literature review on the elasto-hydrodynamic lubrication, boundary lubrication and mixed lubrication regime. In the following sections the frictional behaviour of lubricated contacts operating in these regimes is also described.

2.1 Elasto-Hydrodynamic Lubrication theory

Hydrodynamic lubrication is the best described regime in literature and is based on the so called Reynolds equation (1886). For detailed information regarding hydrodynamic lubrication the reader is referred to Moes (1997). This equation describes the relation between the pressure and film shape as a function of the viscosity and the velocity. The Reynolds equation can be written as:

$$\frac{\partial}{\partial x}\left(\frac{\rho h^3}{\eta}\frac{\partial p}{\partial x}\right)+\frac{\partial}{\partial y}\left(\frac{\rho h^3}{\eta}\frac{\partial p}{\partial y}\right)=\overbrace{6v^+\frac{\partial(\rho h)}{\partial x}}^{\text{wedge}}+\underbrace{6\rho h\frac{\partial(v^+)}{\partial x}}_{\text{stretch}}+\overbrace{12\frac{\partial(\rho h)}{\partial t}}^{\text{squeeze}}, \quad (2.1)$$

with:

v^+	: the sum velocity of the moving surfaces ($v^+ = v_1 + v_2$)
x, y	: spatial Cartezian coordinates
t	: time
p	: pressure
h	: film thickness
ρ	: density

η : viscosity

The right-hand-side of Eq. 2.1 denotes three possible effects that generate pressure in the gap between the opposing moving surfaces. The first term is referred to as the wedge term, the second as the stretch term and the last as the squeeze term. The stretch term is omitted in this thesis, i.e. the sum velocity is constant in the direction of motion. The chosen moving direction is the x-direction. This thesis deals with line-contacts, the pressure is constant along the y-direction and therefore the second term in the left-hand side of Eq. 2.1 can be omitted. In this thesis the steady-flow case is considered. The squeeze term in the Reynolds equation can thus be left out as well. The remaining Reynolds equation reads:

$$\frac{\partial}{\partial x}\left(\frac{\rho h^3}{\eta}\frac{\partial p}{\partial x}\right) = 6(v^+)\frac{\partial(\rho h)}{\partial x} \tag{2.2}$$

In order to solve the Reynolds equation boundary conditions are needed. The pressure is defined as zero at the edges of the gap, thus:

$$p(x_a) = p(x_b) = 0 \text{ and } \frac{\partial p(x_a)}{\partial x} = \frac{\partial p(x_b)}{\partial x} = 0 \tag{2.3}$$

By solving the Reynolds equation, pressure distribution is obtained.
The integral over pressure distribution in the gap results into the load applied to the contact:

$$F_N = B\int_{-\infty}^{\infty} p(x)dx \tag{2.4}$$

with B the length of the cylinder.

Reynolds' equation includes parameters like the geometry or shape of the surfaces (i.e. the film thickness), the viscosity η and the density ρ. These three parameters are pressure dependent. The next three sections present a literature review on the relationships between these three parameters and pressure.

2.1.1 Density-pressure relation

When the generated pressure in the contact is much larger than the ambient pressure, the compressibility of the lubricant must be taken into account. In this thesis the well-known relation proposed by Dowson and Higginson (1966) is used. This reads:

$$\rho(p) = \rho_0 \frac{0.59\text{GPa} + 1.34p}{0.59\text{GPa} + p} \tag{2.5}$$

with: ρ_0 the density at ambient pressure and p is the pressure in GPa. According to Hamrock (1994) the density-pressure relation of Dowson and Higginson must be restricted to pressures up to 1 GPa.

2.1.2 Viscosity-pressure index

Two relationships are frequently used in literature defininig the viscosity-pressure dependency; i.e. the Barus equation (1893) and the Roelands relation (1966). The equation of Barus reads:

$$\eta(p) = \eta_0 e^{\alpha p} \tag{2.6}$$

with:

η_0 : viscosity at ambient pressure
α : viscosity-pressure coefficient

This analytical relation is simple and easily applied in analytical equations but is only accurate for rather low pressure (up to 0.1 GPa).

Another widely used viscosity-pressure relation which accounts for higher pressures is the Roelands equation. This equation is accurate for pressures up to 1 GPa. Roelands' equation reads as:

$$\eta(p) = \eta_0 \exp[\{(1 + \frac{p}{p_r})^z - 1\} \cdot \ln(\frac{\eta_0}{\eta_\infty})] \tag{2.7}$$

with:

η_∞ : constant ($\eta_\infty = 6.315 \cdot 10^{-5}\,\text{Pa} \cdot \text{s}$)
η_0 : viscosity at ambient pressure

p_r : constant (p_r =196.2 MPa)
p : pressure
z : viscosity-pressure index

For most mineral oils $0.6 \le z \le 1$. The calculations in this thesis are performed by using the relation of Roelands.

2.1.3 Film shape

Due to the pressure generated in the contact the surface may deform. If this is the case elasto-hydrodynamic lubrication takes place. The distribution of the pressure in the gap is solved by using the Reynolds equation when the geometry or shape of the surface is known. The equation which describes the film shape between two deformed cylinders can be written by using a parabolic approximation:

$$h(x) = h_\infty + \frac{x^2}{2R} + w(x) \tag{2.8}$$

with:

h_∞ : constant
R : reduced radius of the undeformed cylinders
w : deformation.

The reduced radius is defined by:

$$\frac{1}{R} = \frac{1}{R_1} + \frac{1}{R_2} \tag{2.9}$$

with R_1 and R_2 the radii of cylinder 1 and 2 respectively.
The deformation of a cylinder by a pressure distribution is calculated according to Timosenko and Goodier (1982) as:

$$w(x) = -\frac{4}{\pi E'} \int_{-\infty}^{\infty} p(s) \ln|x - s| ds \tag{2.10}$$

where E' is reduced elasticity modulus.
The reduced elastic modulus is given by:

$$\frac{2}{E'} = \frac{1-\nu_1^2}{E_1} + \frac{1-\nu_2^2}{E_2} \tag{2.11}$$

with E_1 and E_2 the elasticity modulus and ν_1 and ν_2 the Poisson ratios of surfaces 1 and 2 respectively.

2.1.4 Result of EHL calculations

In order to simplify the elasto-hydrodynamic lubrication problem dimensionless numbers are introduced, Dowson and Higgison (1996) and Moes (1992).
Two sets of dimensionless numbers has been introduced, Dowson and Higginson derived the first set of four numbers:

$$\bar{h} = \frac{h}{R},\ U_{\Sigma} = \frac{\eta_0 v^+}{E'R},\ W = \frac{F_N}{BE'R} \text{ and } G = \alpha E' \tag{2.12}$$

with:

$\bar{h}$	:	dimensionless film thickness
W	:	dimensionless load number
U_{Σ}	:	dimensionless speed number
G	:	dimensionless lubricant number

And h is the film thickness, R the reduced radius, η_0 the inlet viscosity, v^+ the sum velocity, E' the reduced elasticity modulus, F_N the normal load, B the contact length and α the viscosity-pressure coefficient of Barus.
A second set has been derived by Moes (1992) from the first one and contains three dimensionless numbers:

$$H = \bar{h}U_{\Sigma}^{-\frac{1}{2}},\ M = WU_{\Sigma}^{-\frac{1}{2}} \text{ and } L = GU_{\Sigma}^{\frac{1}{4}} \tag{2.13}$$

with:

H	:	dimensionless film thickness
M	:	dimensionless load number
L	:	dimensionless lubricant number

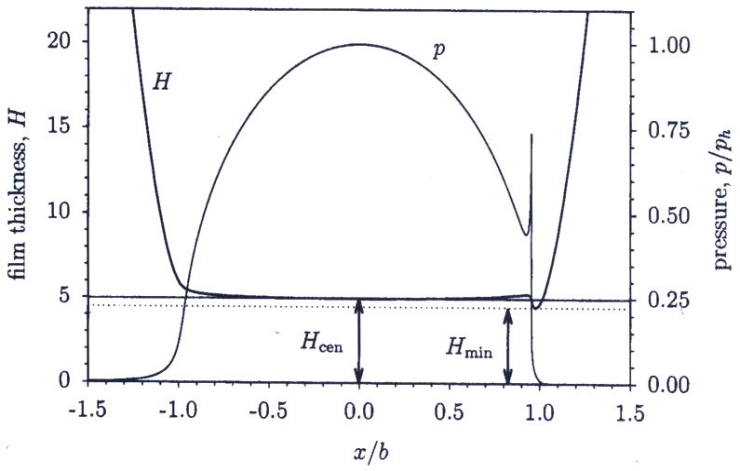

Fig.2.1: Film thickness and pressure distribution (Gelinck (1999)), for M=50 and L=15.

Having these dimensionless numbers the film thickness and pressure distribution can be calculated. In Fig.2.1 an example of such a calculation is presented (M = 50, L = 15). As it can be seen in this figure for high loads the central film thickness is a good parameter to indicate the separation between the opposing surfaces, therefore in this thesis the central film thickness is used. A function fit for the central film thickness in line contacts has been derived by Moes (1997) using his dimensionless parameters. The expression reads:

$$H_C = \left[\left(H_{RI}^{\frac{7}{3}} + H_{EI}^{\frac{7}{3}} \right)^{\frac{3}{7}s} + \left(H_{RP}^{-\frac{7}{2}} + H_{EP}^{-\frac{7}{2}} \right)^{-\frac{2}{7}s} \right]^{s^{-1}} \tag{2.14}$$

with s as auxiliary variable defined as:

$$s = \frac{1}{5}\left(7 + 8e^{-2\frac{H_{EI}}{H_{RI}}} \right) \tag{2.15}$$

In Eq. 2.14 H_{RI}, H_{EI}, H_{RI} and H_{RP}, are the film thicknesses for the Rigid-Isoviscous (RI), Rigid-Piezoviscous (RP), Elasto-Isoviscous (EI) and Elasto-Piezoviscous (EP) regime. These parameters read:

$$H_{RI} = 3M^{-1} \qquad \text{RI-asymptote} \qquad (2.16)$$

$$H_{RP} = 1.287L^{\frac{2}{3}} \qquad \text{RP-asymptote} \qquad (2.17)$$

$$H_{EI} = 2.621M^{-\frac{1}{5}} \qquad \text{EI-asymptote} \qquad (2.18)$$

$$H_{EP} = 1.311M^{-\frac{1}{8}}L^{\frac{3}{4}} \qquad \text{EP-asymptote} \qquad (2.19)$$

Eq. 2.14 can be plotted in a diagram as shown in Fig.2.2 in which the four asymptotes have been indicated as well. Heavy loaded line contacts operate in the Elasto-Piezoviscous regime. In 1962 Koets settled the condition for the Elasto-Piezoviscous regime as:

$$L\sqrt{M} > 13.3 \text{ and } M > 0.1L^{\frac{2}{3}} \qquad (2.20)$$

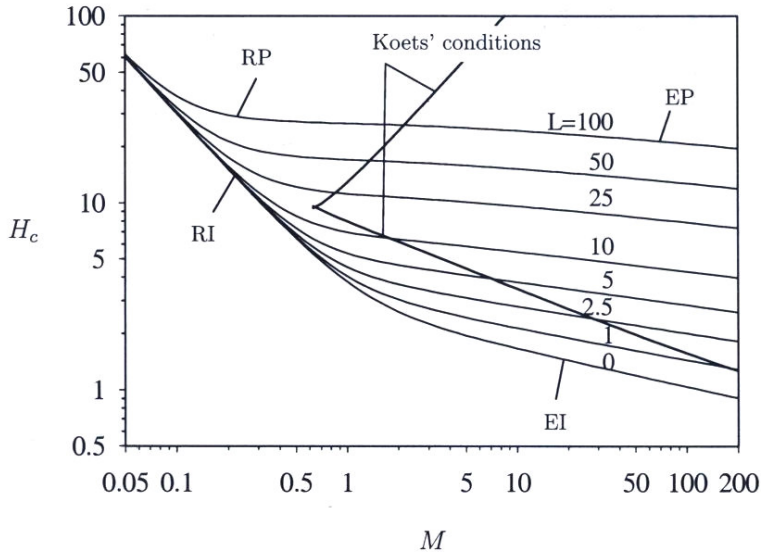

Fig.2.2: The film thickness for EHL line contacts (Moes (1997)).

2.1.5 Friction in EHL regime

Friction in the EHL regime, for highly loaded contacts, is mainly due to sliding. In sliding contacts friction is caused by shearing the lubricant in the contact zone. Generally the shear stress in the lubricant can be written as a function of the shear rate $\dot{\gamma}$:

$$\tau_H = f(\dot{\gamma}) \tag{2.21}$$

The sliding friction can be written as:

$$F_f = \iint_{A_H} \tau_H(\dot{\gamma}) dA_H \tag{2.22}$$

in which A_H is the hydrodynamic contact area.
The shear stress of the lubricant depends on the rheological behaviour of the lubricant. In Fig.2.3 (Evans (1983)) four typical friction curves and three distinct regions ($\tau < \tau_0$, $\tau_0 < \tau < \tau_l$ and $D > 1$) are presented. When the shear stress of the lubricant varies linearly with the shear rate, the lubricant behaves like a Newtonian fluid represented in Fig.2.3 with curve I, ($\tau < \tau_0$). In the second region the shear stress does not behave linearly at higher shear rates; the shear stress increases slowly until a maximum is reached. The curves in this region describe the non-Newtonian behaviour of the fluid ($\tau_0 < \tau < \tau_l$).

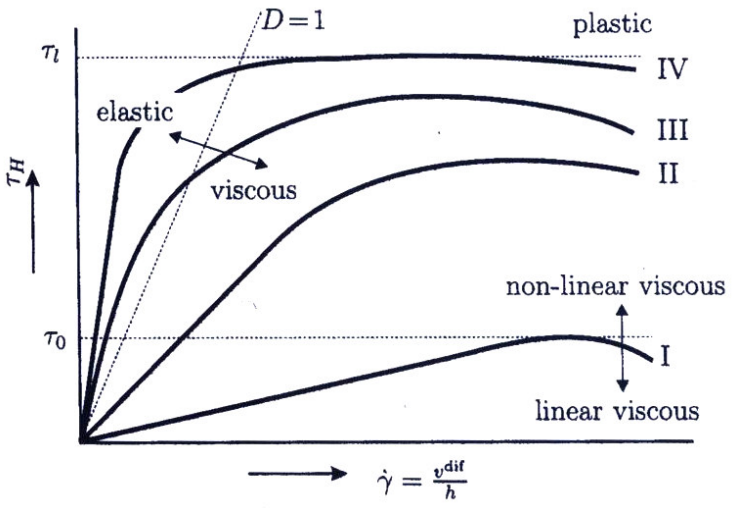

Fig.2.3: Types of friction curves (Evans (1983)). Shear stress, τ_H, as a function of the shear rate $\dot{\gamma}$. τ_0 is the Eyring shear stress, τ_l the lubricant limiting shear stress and D the Deborah number.

Curve II in Fig.2.3 represents the non-linear viscous behaviour of the lubricant. According to Bell, Kannel and Allen (1964) the fluid model of Eyring is applicable in this region:

$$\dot{\gamma} = \frac{\tau_0}{\eta} \sinh\left(\frac{\tau_H}{\tau_0}\right) \tag{2.23}$$

where τ_0 is the Eyring shear stress.
For the friction model developed in this thesis, the Eyring model is applied.
With curve III the elastic and non-linear viscous behaviour of the lubricant is represented and is described by a relation proposed by Johnson and Tevaarwerk (1977):

$$\dot{\gamma} = \dot{\gamma}_e + \dot{\gamma}_v = \frac{\dot{\tau}_H}{G} + \frac{\tau_0}{\eta} \sinh\left(\frac{\tau_H}{\tau_0}\right) \tag{2.24}$$

with $\dot{\gamma}_e$ and $\dot{\gamma}_v$ the elastic and viscous component of the shear rate respectively and G is the shear modulus of the lubricant.
Curve IV (Fig.2.3) represents the elastic/plastic shear stress behaviour of a lubricant which reaches its limiting shear stress value (τ_l). In the model of Johnson and Tevaarwerk the shear stress can increase without limitation. However in reality at a certain shear rate, the shear stress remains constant. Bair and Winer (1979) have introduced a shear stress shear rate model based on the limiting shear stress value:

$$\dot{\gamma} = \frac{\tau_l}{\eta} \arctan h\left(\frac{\tau}{\tau_l}\right) \tag{2.25}$$

with τ_l the limiting shear stress.
The transition from viscous to elastic behaviour is determined by the Deborah number D which is the ratio of the relaxation time of the lubricant ($\eta / \overline{G}$) and the time for the lubricant to pass the contact. The Deborah number is defined as:

$$D = \frac{\eta v_{av}}{2Gb} \tag{2.26}$$

with v_{av} the average velocity, b the half Hertzian contact width and G the shear modulus of the lubricant. If the Deborah number is much larger than the unit, elastic behaviour is dominant, and when Deborah number is smaller than the unit, the lubricant behaves like a viscous fluid.

2.2 Boundary Lubrication

Boundary lubrication is perhaps the most complex aspect of the subject of friction and wear prevention. The complexity arises from the large number of variables. Larsen and Perry (1950) listed 29 variables, and this list is probably not complete.
In the first part of this section a review of the literature on boundary lubrication is presented. What the boundary layer is and what its mechanisms of formation are, is explained in subsection 2.2.1. Next, subsection 2.2.2 deals with the factors which influence boundary lubrication and focuses on friction and durability of the boundary layer.
The second part of this section attempts to give a background on the analysis of the pressure influence on the shear stress of a boundary layer which is one of the topics of this thesis. The mechanism of the τ-p diagram and the behaviour of different boundary layers with pressure are presented.

2.2.1 Boundary lubrication and boundary layer mechanism

Lubricants are used for reducing friction and wear. In some applications, the solid surfaces are so close together that some asperities come into contact and others are separated by a layer Fig.2.4. The physical and chemical interaction of the lubricant with the solid body control friction and wear. Even a single layer of adsorbed molecules may provide some protection against wear. The precise mechanism of boundary lubrication is not the same from one bearing combination or for one mode of operation to another. According to Campbell (see Ling, Klaus and Fein (1969)), the boundary lubrication is defined as:

"…lubrication by a liquid under condition where the solid surfaces are so close together that appreciable contact between opposing asperities is possible. The friction and wear in boundary lubrication are determined predominantly by interaction between the solid and between the solid and liquid. The bulk flow properties of the liquid play little or no part in the friction and wear behavior."

Boundary lubrication usually occurs under high-load and low-speed conditions in machine components such as bearings, gears and traction drives. It is the regime, which controls the lifetime of the system.

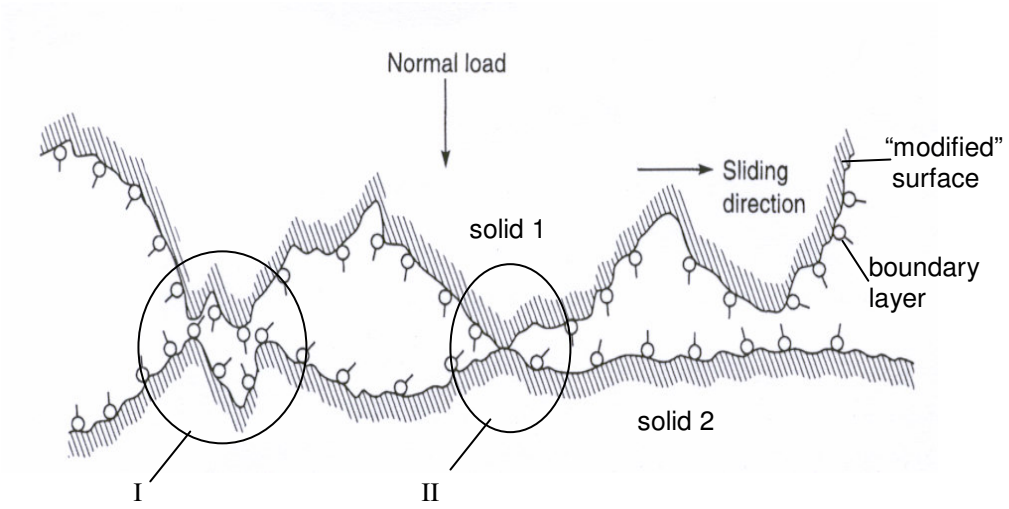

Fig.2.4: Schematic representation of two surfaces in contact. I local contact separated by a boundary layer and II direct contact between the opposing surfaces.

According to Godfrey (1968) the boundary films are formed by physical adsorption, chemical adsorption and chemical reaction Fig.2.5.

When the molecules of substances like fatty alcohols, fatty acids have a hydrocarbon with a functional polar group characterized by the presence of a dipole moment, this tends to attach to the metal surface by means of physical adsorption. The bonding between the dipole group and metal surface is a Van der Wals bond, which is relatively weak Fig.2.5[a].

Chemical adsorption or chemisorption is characterized by two stages. First, physical adsorption of the dipole group at the end of a molecule chain to the surface occurs. After physical adsorption, a chemical reaction occurs between the surface and the polar group. The chemical reaction depends on the chemical reactivity of the metal and environmental circumstances Fig.2.5[b].

Some combinations of fluids and substrates do not lead to physical adsorption of these substances to the surface. In some cases a direct chemical reaction between the surface and the lubricant occurs. For example in this way the so-called extreme pressure lubricants (EP-lubricants) work, which possess friction reducing qualities Fig.2.5[c].

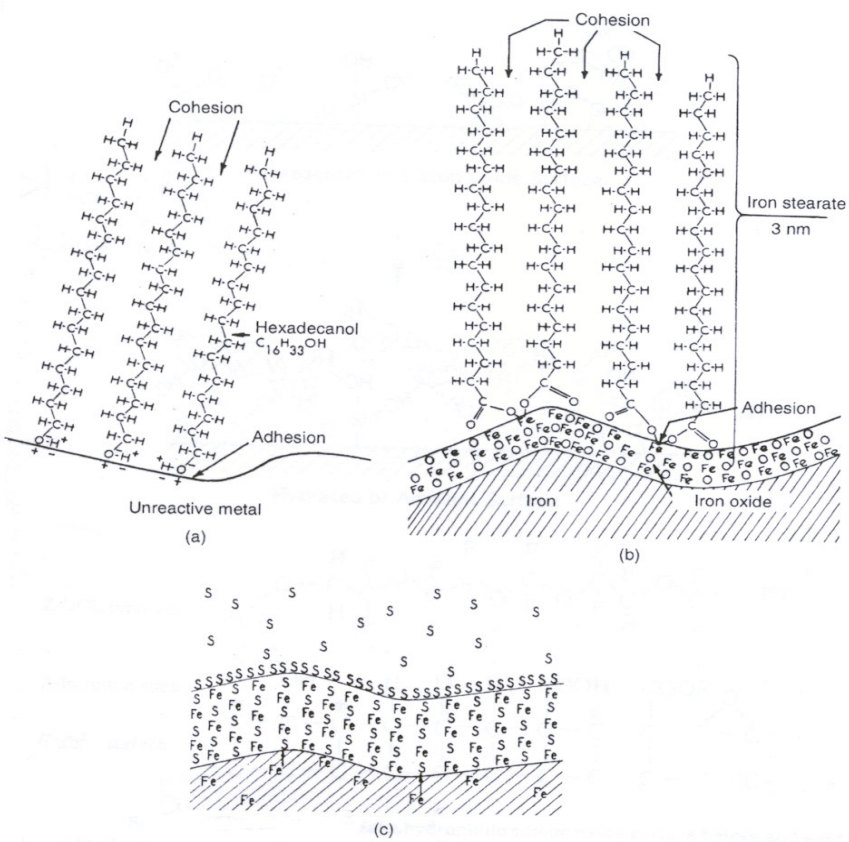

Fig 2.5: Different mechanisms of formation of boundary layers on steel surfaces. (a) physical adsorption, (b) chemical adsorption and (c) chemical reaction (Godfrey (1968)).

The physisorbed film can be either monomolecular (typically < 3nm) or polymolecular thick. The chemisorbed films are monomolecular, but layers formed by chemical reaction can have a larger layer thickness. In general, the stability and durability of surface film decreases in the following order: chemical reaction film, chemisorbed film and physisorbed layer.
From the literature (Zisman (1959) and Bowden (1950)) the following can be stated about the durability of the boundary layers:

- life of layer increases with thickness.

- durability increases with the increasing strength of dipole-metal interaction and with increasing lateral adhesion or closed packing of the hydrocarbon part of molecules.
- durability increases with increasing film chain length.

2.2.2 Factors influencing boundary lubrication

There is general agreement, that when the operating conditions lead to a sufficient small separation of the surfaces, high friction and wear occurs unless a film of some sort is present at the points of potential contact to prevent metallic adhesion. The critical distance of separation, the type of film whether solid or liquid and its mode of formation for a given situation are generally in dispute; but most of the factors that influence the situation are known and many have been evaluated comprehensively. In this section a literature review on the influence of the load (pressure), velocity, temperature and atmosphere on the boundary layer is presented.

2.2.2.1 Effect of load on friction

It is generally agreed that at very low loads (pressures) the coefficient of friction for boundary lubrication $f_{BL}=\tau/p$ rises with decreasing load. Campbell (1969) interpreted the result for a cetane solution, showing that at low loads the absorbed film is oriented approximately perpendicular to the surface with its active COOH end group attached to the metal. Slip is, therefore, largely between the CH_3 groups of the close-packed film. The reology of a suspension of calcium carbonate in n-dodecan (when the pressure is less than approximately 2 MPa) provide the same behaviour. Blancoe and Williams (1997) consider that at this pressure the liquid was able to flow relatively free in the interface gap so that the interfacial friction results largely from viscous flow. As the load (pressure) increases the chains of molecules deposited from cetane solution, are bent so that they lie almost parallel to the surfaces, allowing them to slip rather easily and friction is close to a constant value see Fig.2.6. The effect of load (pressure) will be discussed in more detail in Section 2.2.3.

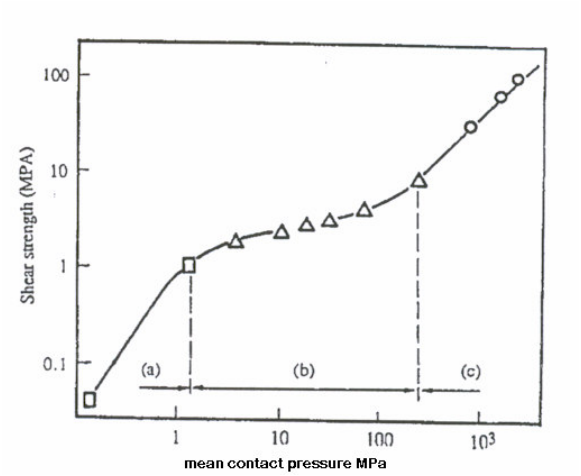

Fig.2.6: Pressure dependence on the shear rate of calcium carbonate film. Regions (a), (b) and (c) correspond with low pressure, intermediate pressure and high pressure region respectively (Georges and Mazuyer 1991).

2.2.2.2 Effect of velocity on friction

It is known that when viscosity effects appear to be negligible, friction changes very little with sliding velocity over a range from 0.005 to 1 cm/s. The friction may decrease with sliding velocity, increase or remain constant. There is general agreement that for the stick-slip situation a drop in friction with velocity is associated with low oiliness (the ability of a lubricant to perform well in reducing friction in boundary lubrication). For example a plot of friction at stick for dodecan on steel shows a drop in static friction from 0.28 to 0.24 from 0.005 to 2 cm/s. The kinetic coefficient of friction remains constant at 0.22 over the same velocity rage with pelargonic acid, a lubricant of high oiliness. At high velocity there is always a hydrodynamic contribution. In the mixed lubrication region friction tends to decrease.

When the viscosity effect is not negligible, the influence of the velocity has different results for different fluids. Fig.2.7 shows the results for BL monolayers of stearic acid and calcium stearate adsorbed on a mica surface. Stearic acid shows an increasing shear stress with increasing velocity while calcium stearate shows the opposite effect. According to Briscoe and Tabor (1978) two physical phenomena are responsible for the dependence of τ ($\tau = f_{BL} \cdot p$) on v. The first effect concerns the influence of the velocity on the strain rate in the boundary film, which leads to an

increasing of τ with increasing strain rate. The second effect of the velocity has to do with the visco-elastic effect. The time of contact between two monolayers is an important parameter which determines the importance of the visco-elastic behaviour. When a normal load is applied, the monolayer needs some time to respond to the applied normal load. The coefficient of friction is smaller when the visco-elastic effect is larger.

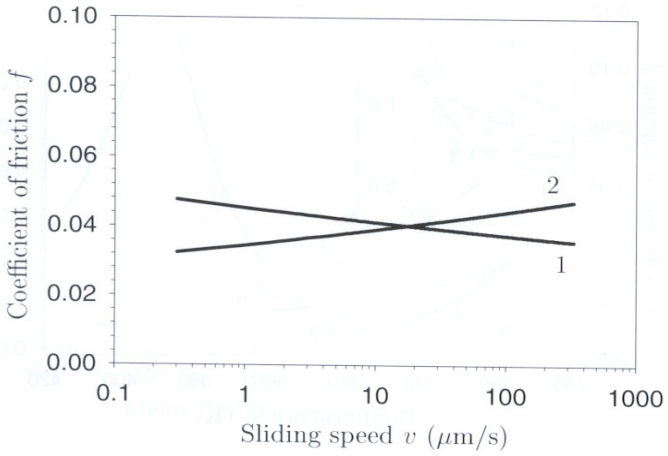

Fig.2.7: The coefficient of friction as a function of velocity (Briscoe and Evans (1982); 1 calcium stearate and 2 stearic acid).

2.2.2.3 Effect of temperature

In general it is shown in the literature that when the temperature increases, the shear stress of the boundary layer decreases (see Fig.2.8 Briscoe et al. (1973)) except when the melting temperature of the boundary layer is exceeded.
It is agreed that an increase in temperature of the conjunction formed by interacting asperities can change the situation critically from effective lubrication to high wear. It has been used successfully to explain the transition from effective to ineffective lubrication in machines, gears and cam-tappet mechanisms.

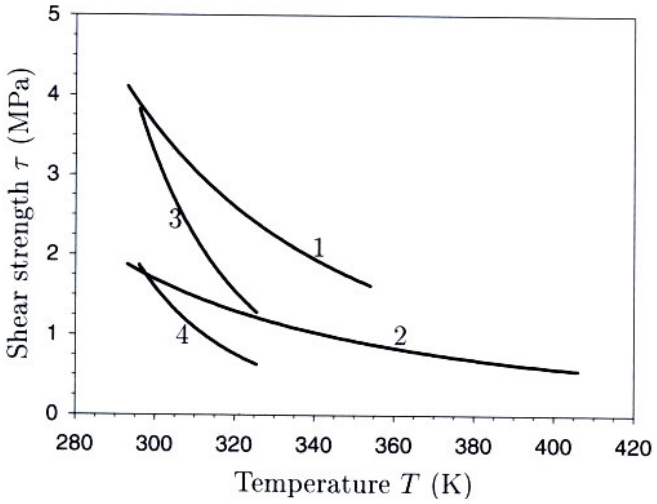

Fig.2.8: Shear stress as a function of temperature: 1 stearic acid, 2 three monolayers of calcium stearate, 3 Langmuir Blodgett (1920 and 1935) monolayer of behenic acid, 4 Langmuir Blodgett monolayer of Staric acid (Briscoe et al. (1973) and Briscoe and Evans (1982)).

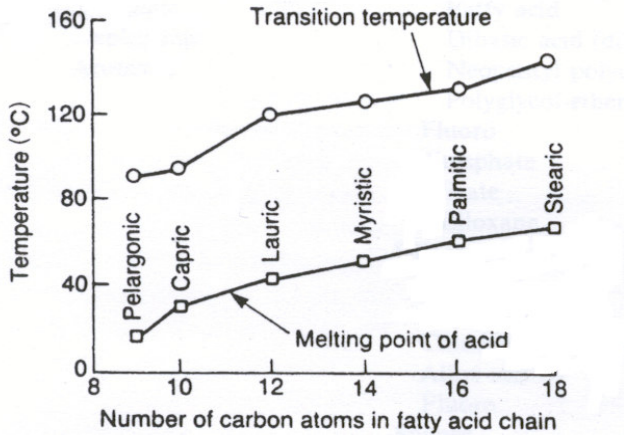

Fig.2.9: Breakdown or transition temperature of fatty acid on steel surface and their melting points as a function of chain length (Bowden and Tabor (1950)).

Essentially, it states that the load support breaks down in a contact when the temperature in the contact exceeds a characteristic temperature of the oil, called the transition temperature. Blok (1963) concluded that the transition temperature for dilute solutions of fatty acids in nonpolar oils is a function of the load and

velocity. Parraffins, alcohols, ketones, and amides became ineffective lubricants at the bulk melting point of the lubricant. When melting occurs, the adhesion between the molecules in the boundary layer is diminished and breakdown of the layer takes place. The increase of metallic contact leads to increase in friction and wear. With saturated fatty acids on reactive metals however, the breakdown does not occur at the melting point but at considerably higher temperatures. This is shown in Fig.2.9 for a series of fatty acids on a steel surface, from which it is clear that breakdown (transition temperature T_t) occurs at 50-70 °C above the melting point (T_m). The actual value of the breakdown temperature depends on the nature of the metals, as well as on the load and sliding velocity. Thus T_t-T_m is a measure of the strength of adsorption that is due to a dipole-metal interaction.

The chemical reactivity between polar molecules and the substrate is also temperature dependent. The coefficient of friction for octadecanoic acid provides a decrease in friction between 100 to 200 °C as shown in Fig.2.10 (the melting point of octdecanoic acid is at 75 °C). This material is expected to react with the metal surface to form an iron stearate film which would require more heat to be desorbed. With glass sliding on glass, no reaction is expected.

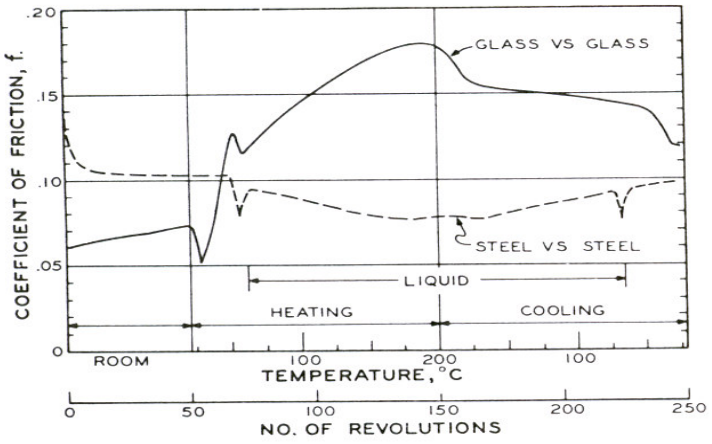

Fig.2.10: Friction of materials lubricated with octadecanoic (stearic) acid (load, 10 N; speed, 1 cm/s; room air) (Godfrey (1964)).

2.2.2.4 Effect of atmosphere

The two components of principal importance are water vapor and oxygen. Both enter into boundary lubrication, often supplementing each other. Studies noted that water vapor increases friction. Some results are shown in Tab.1 (Hardy and Bircumshaw (1925)). The friction is always larger at high humidity. Because water, due to its high dipole moment, exercises an initiating or accelerating effect on many reactions, it influences chemical reaction at the interface, which is important in boundary lubrication. Moisture is also an important factor in determining the type of film formed on a surface, whether physically or chemically adsorbed or a layer resulting from chemical reaction.

There is a great deal of evidence that oxygen exercises a key effect in boundary lubrication. Fig.2.11 shows the reduction in the coefficient of friction that is obtained by adsorption or chemical reaction of oxygen on clean iron surfaces in “vacuum” (roughly $1.31 \cdot 10^{-8}$ Pa). The coefficient of friction is markedly reduced by admission of oxygen gas though the pressure is very low (roughly $1.31 \cdot 10^{-6}$ Pa). As oxygen pressure is allowed to increase, the friction is reduced still more. Finally, if the pressure is allowed to stand for some period of time, the adsorbed oxygen film becomes more complete and the friction drops still further.

Effect of Moisture on Coefficient of Static Friction for 52000 Steel on Tool Steel

Lubricant	Steel		Glass	
	Dry	75% r.h.	Dry	75% r.h.
None	.76	1.05	.96	—
White oil	.35	0.56	.27	.95
Spindle oil	.27	0.46	.16	.70
Lard oil	.11	0.33	.16	.85
Oleic acid	.12	0.20	.16	.81

Table 1. (Hardy and Bircumshaw (1925)).

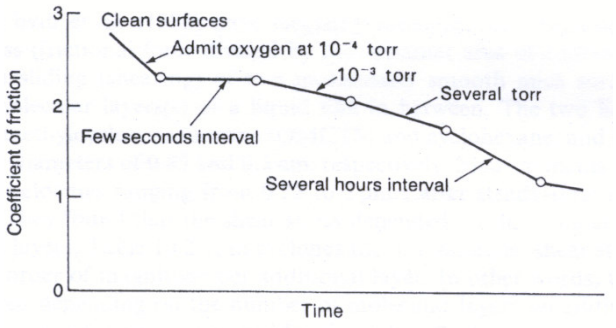

Fig.2.11: Effect of oxygen on the coefficient of friction of outgassed iron surface (Ling, Klaus and Fein (1969)).

2.2.3 Influence of the pressure on the shear stress in boundary lubrication

Many tribological contacts involve two surfaces which are in relative motion, consistent with the presence of a shear stress boundary film on one or both of the surfaces. A few authors as Briscoe et al. (1973), Thomas (1996) and Timsit et al. (1992) presented in their papers the effect of pressure on the shear stress of the boundary layer. The aim of this section is to give an overview of the influence of the pressure on the shear stress of boundary layers. This section discusses the coefficient of friction at asperity level.

2.2.3.1 Influence of pressure and boundary rheology

Bearing surfaces are generally 'smooth' by engineering standards, with a summit height of a few tenths of a μm. By contrast the molecular length of paraffinic hydrocarbon chains (characteristic for lubricant oils) for example, are of the order of 2.5 nm. Commercially available lubricating oils always contain some small additions of chemical compounds especially designed to enhance their boundary lubricating performance by forming protective surface films of much greater dimensions than would arise from the hydrocarbon base oil alone.
For practical frictional measurements a common approach is to use very smooth and geometrically simple surfaces, nearly always a sphere against a flat. Typical data for a variety of solid organic films, investigated in this way are shown in Fig.2.12 in which the shear stress τ is plotted against the mean contact pressure p.
The shear stress-pressure behaviour of layers like those from Fig.2.12 (curves 2, 3 and 4) can be described by the following equation in which and τ_*, n and α are constants:

$$\tau = \tau_* + \alpha p^n \tag{2.27}$$

The form of this dependence is for a wide range of materials, from metals, inorganic materials and fatty acid thin layers, to solid graphitic and polymer films.

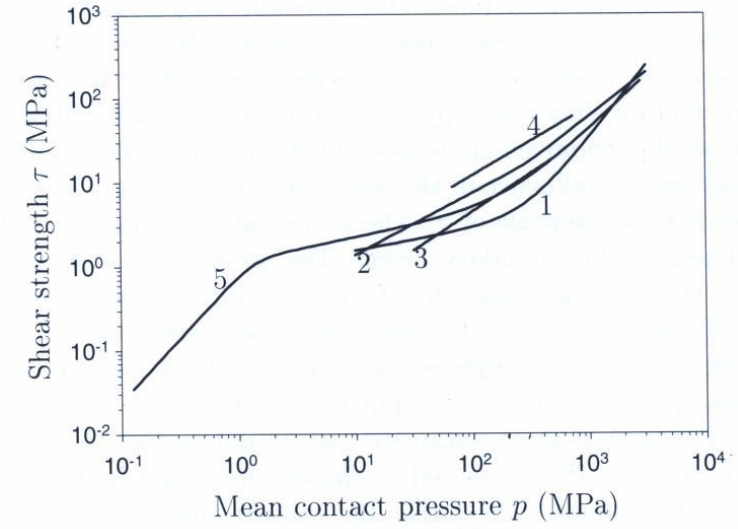

Fig.2.12: Shear stress as a function of pressure, 1 calcium stearate on glass (Briscoe et al. (1973)), 2 stearic acid on glass (Briscoe et al. (1973)), 3 stearic acid on mica (Briscoe and Evans (1982)), 4 stearic acid on aluminium (Timsit and Pelow (1992)), 5 calcium carbonate (Georges and Mazuyer (1991)).

Stearic acid is a classical boundary lubricant. When deposited in multiple films, there is some experimental evidence that these layers are more sensitive to pressure than a simple linear dependence (see Fig.2.12 (1, 5)). For these cases the boundary layers are more complex. In the contacts, particularly on steel lubricated by mineral oils whose performance has been enhanced by additives, the boundary layer is a rather thick “mushy” film. This structure is illustrated in Fig. 2.13.

Blancoe and Williams considered that a rather simple physical model of the complex structure as illustrated in Fig.2.13 can be provided by a colloidal suspension as presented in Fig.2.14. The rheological behaviour of a suspension of calcium carbonate in n-dodecan has been examined under hydrostatic pressure by George and Mazuyer (1990) using a sphere on flat geometry. These authors found that the behaviour of the suspension was very dependent on the applied pressure see Fig.2.12 (curve 1 and 5). At low pressures, if p was less than approximately 2 MPa, the liquid was able to flow relatively free in the interface gap, so that the interfacial friction resulted largely from viscous flow. The shear stress increases with the pressure. At higher pressure, within the range 2 MPa < p < 200 MPa the shear stress of the junction becomes much less dependent on the pressure. Compaction of colloidal film takes place as illustrated in Fig.2.14[b]. The ‘slab’ of material formed, appeared to slide at its interface with the solid substrate which remained coated with dodecan molecules. The effective shear stress was close to

constant. At a greater pressure, p > 200 MPa, the shear stress increases again with the pressure like in the low pressure case.

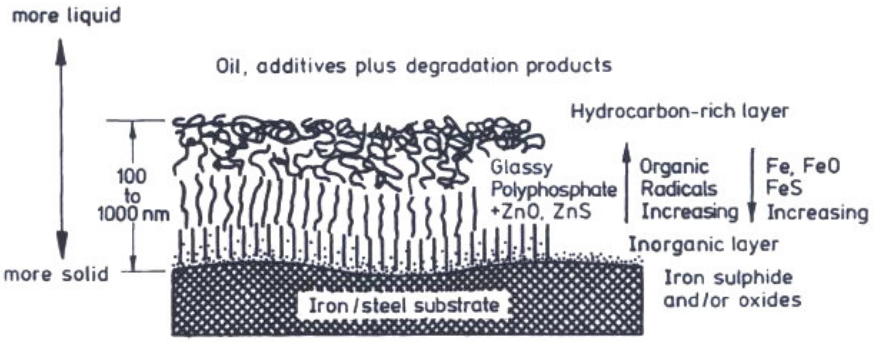

Fig.2.13: Schematic representation of layered ZDTP anti-wear film structure (Blencoe and Williams (1997)).

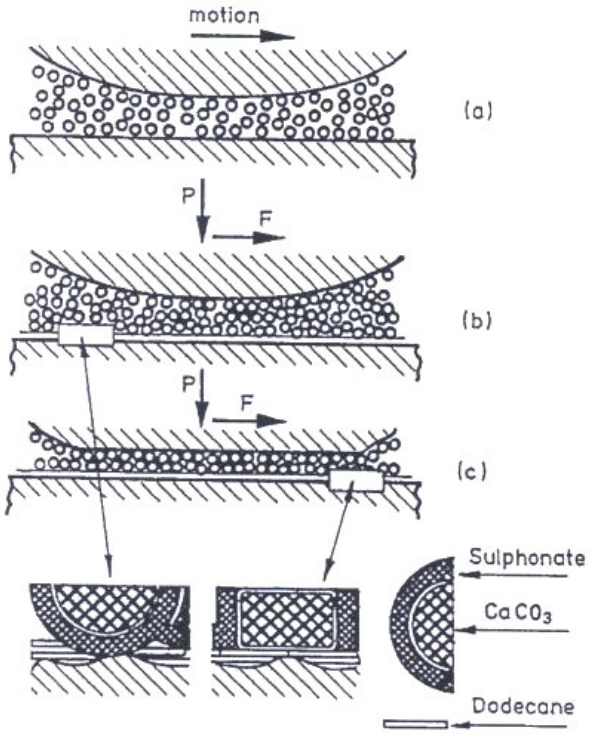

Fig.2.14: Pressure dependence of shear stress τ of a film of calcium carbonate (Blencoe and Williams (1997)).

Westeneng (2002) proposed function fits for the τ-p dependency of the curves presented in Fig.2.12. In the next chapter the τ-p relations proposed by Westeneng are implemented in the mixed lubrication model for a deterministic rough surface, in order to see the variation of the coefficient of friction with the macroscopic pressure in the BL regime.

2.3 Mixed Lubrication

The mixed lubrication regime is the transition regime between EHL and BL, and therefore it can be seen as a combination of these two, having the properties of both regimes. The coefficient of friction in the ML regime has a value situated between the coefficient of friction of the BL and EHL regime.
Many authors (i.e. Stribeck (1902), Hersey (1915), Lenning (1960) and Schipper (1988)) performed experimental research on mixed lubrication while in theoretical work only a few (Patir and Cheng (1978, 1979), Johnson, Greenwood and Poon (1972) and Gelinck and Schipper (1999)). Patir and Cheng investigated the effect of roughness on the hydrodynamic load by introducing the average Reynolds equation, however their analysis is valid for separations larger than three times the combined root mean square surface roughness (R_q). In 1972 Johnson, Greenwood and Poon developed a model in which the load carried by a contact in the mixed lubrication regime, is sheared between the asperity contact and the fluid film. In their model they combined the well-known Greenwood and Williamson (1966) theory of random rough surfaces in contact with the elasto hydrodynamic theory. This model was extended in 1999 by Gelinck and Schipper to calculate the Stribeck curve for line contacts.

2.3.1 Mixed lubrication model

According to Johnson the normal load (pressure) on the contact in the ML regime is carried by the BL and the EHL force component (Fig.2.15):

$$F_T = F_C + F_H \tag{2.28}$$

with F_C the load carried by asperities and F_H the load carried by hydrodynamic (EHL) component.

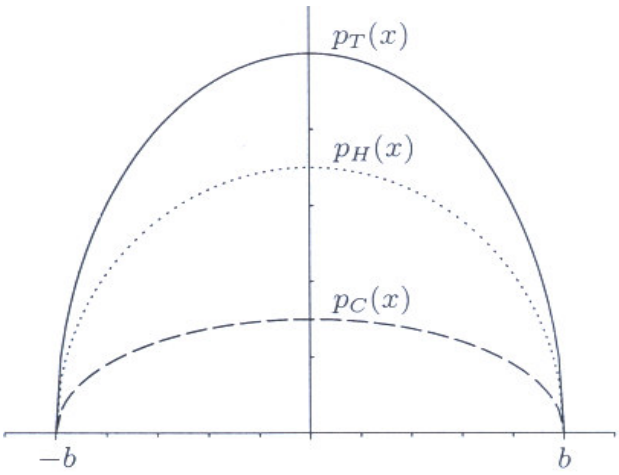

Fig.2.15: Pressure distribution in the mixed lubrication regime according to Johnson (1972).

Based on the Eq.2.28 two coefficients γ_1 and γ_2 are introduced:

$$\gamma_1 = \frac{F_T}{F_H},\ \gamma_2 = \frac{F_T}{F_C} \tag{2.29}$$

the two coefficients (γ_1 and γ_2) are mutually dependent through the equation:

$$1 = \frac{1}{\gamma_1} + \frac{1}{\gamma_2} \tag{3.30}$$

Using the two coefficients γ_1 and γ_2 and combining the well-known Greenwood and Williamson (1966) contact model of random rough surfaces with the EHL theory, the entire Stribeck curve can be calculated. In the next chapter a comprehensive description of the mixed lubrication model is given.

Summary

In this chapter the literature review on the EHL, BL and ML theory has been presented. Frictional models and rheology lubricant behaviour are discussed. It is shown that the friction of the boundary layers is strongly dependent on the operating factors (i.e. load (pressure), velocity, temperature and atmosphere). The friction of the boundary layer can increase or decrease with the sliding velocity depending on the type of lubricant. Generally the shear stress of the boundary

layer decreases with increasing temperature (except when the temperature exceeds its melting point, the boundary layer breaks down in the contact). In the case of steel the existence of the oxygen in the contact provides a reduction in friction due to adsorption or chemical reaction of the oxygen with the clean steel surface. The presence of water vapor in the contact leads to a higher coefficient of friction (a higher humidity results in a higher coefficient of friction). In the last part of this chapter the influence of the pressure on the shear stress of the boundary layer is presented. It is shown that in general an increase in pressure leads to an increase in shear stress but the relation between τ and p depends on the type of boundary layer.

Section 2.3 attempts to give a brief literature review on the mixed lubrication regime. A short description of a mixed lubrication model is also made.

In the first part of the next chapter an extension of the isothermal mixed lubrication model of Gelinck and Schipper (1999) is presented. The extension consists of the modification of the separation model, and incorporating in the model different effects such as shear thinning, two rough surfaces in contact and starvation. In the second part of the next chapter, a Stribeck curve model for deterministic rough surfaces is presented. The variation of the macroscopic coefficient of friction in BL regime is investigated by incorporating the τ-p relation (coefficient of friction at asperity level) in the deterministic mixed lubrication model.

References

Bair, S. and Winer, W.O. (1979 a), “A rheological model for elasto hydrodynamic contacts based on primary laboratory data”, ASME, Journal of Lubrication Technology, Vol. 101, 258-265.

Bair, S. and Winer, W.O. (1979 b), “Shear strength measurements of lubricants at high pressure”, ASME, Journal of Lubrication Technology, Vol. 101, 251-257.

Barus, C. (1893), “Isothermals, isopiestics and isometrics relative to viscosity”, Am. J. of Science, Vol. 45, 87-96.

Bell, J.C., Kannel, J.W. and Allen, C.M. (1964), “The rheological behaviour of the lubricant in the contact zone of a rolling contact system”, ASME, Journal of Basic Eng., Vol. 86, 423.

Blencoe, K.A., Roper, G.W. and Williams, J.A. (1997), “The influence of lubricant rheology and surface topography in modeling friction at concentrate contacts”, Proc. Instn. Mech. Engrs., Vol. 212(J), 391-400.

Blencoe, K.A. and Williams, J.A. (1997), “Friction of sliding surfaces carrying boundary films”, Wear, Vol. 203-204, 722-729.

Blodgett, K.B. (1935), “Film built by depositing successive monomolecular layers on a solid surface”, Journal American Chemical Society, Vol. 57, 1007-1022.

Blok, H. (1963), “The flash temperature concept”, Wear, Vol. 6, 94-483.

Bowden, F.P. and Tabor, D (1950), “Friction and lubrication of solids”, Part I, Clarendon Press, Oxford, UK.

Bowden, F.P. and Tabor, D. (1964), “Friction and lubrication of solids”, Part II- ed., Clarendon Press, Oxford, UK.

Briscoe, B.A., and Tabor, D. (1973), ”Rheology of thin organic films”, ASLE Transaction, Vol. 17(3), 158-165.

Briscoe, B.J. and Tabor, D. (1978), “Shear properties of thin polymeric films”, Journal of adhesion, Vol. 9, 145-155.

Dowson, D. and Higginson, G.R. (1966), “Elasto-hydrodynamic lubrication-The fundamentals of roller and gear lubrication”, Pergamon Press, Oxford, UK.

Evans, C.R. (1983), “Measurements and mapping of the rheological properties of elasto hydrodynamic lubricants”, PhD thesis, University of Cambridge, UK.

Gecim, B. and Winer, W.O. (1980), “Lubricant limiting shear stress effect on EHD film thickness”, ASME, Journal of Lubrication Technology, Vol. 102, 303-312.

Gelinck, E.R.M (1999), “Mixed lubrication of line contacts”, PhD thesis, University of Twente Enschede, The Netherlands.

Gelinck, E.R.M and Schipper, D.J. (1999), “Friction model for mixed contact including slip”, Technical report, University of Twente Enschede, The Netherlands.

George, J-M. and Mazurey, D.M. (1990), “Pressure effects on the shearing of a colloidal layer”, J. Phys. Condensed Matter, Vol. 2, SA399- SA403.

Greenwood, J.A. and Williamson, J.B.P. (1966), “Contact of nominally flat surfaces”, Phil. Trans. R. Soc. London Series A, Vol. 295, 300-319.

Hamrock, B.J. (1994), “Fundamentals of fluid film lubrication”, Mc. Graw-Hill Series in Mechanical Engineering, Mc. Graw-Hill, Inc, New York.

Hardy, W. and Doubleday, I. (1922), “Boundary lubrication-the paraffin series”, Proc. Roy. Soc. A, Vol. 102, 550-74.

Hardy, W. and Bircumshaw I. (1925), “Boundary lubrication of plane surfaces and the limitations of Amonton’s law”, Proc. Roy. Soc. A, Vol. 168, 1-72.

Hardy, W. (1931), “Problems of boundary state”, Phil. Trans. Roy. Soc. A., vol. 230, 1-37.

Hersey, M.D. (1915), “On the laws of lubrication of journal bearings”, ASME Transaction, Vol. 37, 156-171.

Johnson, K.L., Greenwood, J.A. and Poon, S.Y. (1972), “A simple theory of asperity contact in elasto-hydrodynamic lubrication”, Wear, Vol. 19, 91-108.

Johnson, K.L. and Tevaarwerk, J.L. (1977), “Shear behaviour of EHD oil films”, Phil. Trans. R. Soc. London, Series A, Vol. 365, 215.

Langmuir, I. (1920), “The mechanism of the surface phenomena of flotation”, Trans. Farad. Soc., Vol. 15, 62-74.

Larsen, R.G. and Perry, G.L. (1950), “Chemical aspects of wear and friction”, in J. T. Burwell (ed.): Mechanical Wear, Am. Soc. Metals, 73-79.

Lenning, R.L. (1960), “The transition from boundary to mixed friction”, Lubrication Engineering, Vol. 16(12), 575-582.

Ling, F.F., Klaus, E.E. and Fein, R.S. (1969), “Boundary lubrication-an appraisal of world literature”, ASME, New York.

Moes, H. (1992), “Optimum similarity analysis with applications to Elasto-hydrodynamic lubrication”, Wear, Vol. 159, 57-66.

Moes, H. (1997), “Lubrication and Beyond”, lecture notes 115531, University of Twente, Enschede, The Netherlands.

Owens, D.K. (1964), “Friction of polymers I. lubrication”, J. Appl. Poly. Sci., Vol. 8, 1465-1475.

Patir, N. and Cheng, H.S. (1978), “An average flow model for determining effects of three-dimensional roughness on partial hydrodynamic lubrication”, ASME, Journal of Lubrication Technology, Vol. 100, 12-17.

Patir, N. and Cheng, H.S. (1979), “Application of average flow model to lubrication between rough sliding surfaces”, ASME, Journal of Lubrication Technology, Vol. 101, 220-230.

Roelands, C.J.R. (1966), “Correlation aspects of the viscosity-temperature-pressure relationship of lubricating oils”, PhD thesis, Technical University of Delft, The Netherlands.

Schipper, D.J. (1988), “Transitions in the lubrication of concentrated contacts”, PhD thesis, University of Twente, Enschede, The Netherlands.

Stribeck, R. (1902), “Die wesentlichen Eigenschaften der Gleit- und Rollenlager”, VDI-Zeitschrift, Vol. 46, 1341-1348, 1432-1438 and 1463-1470.

Thomas, P.S. (1996), “Dependence of the friction process on the molecular structure and architecture of thin polymer films”, Tribology international, Vol. 29(8), 631-637.

Timsit, R.S. and Pelow, C.V. (1992a), ”Shear strength and tribological proprieties of stearic acid films – Part II: On gold-coated glass”, Transactions of the ASME, Vol. 114, 159-166.

Timsit, R.S. and Pelow, C.V. (1992b), “Shear strength and tribological proprieties of stearic acid films – Part I: On glass and aluminum – coated glass”, Transactions of the ASME, Vol. 114, 150-158.

Timoschenko, S.P. and Goodier, J.N (1982), “Theory of Elasticity”, 3 edn MC Graw-Hill, New York.

Westeneng, A. (2002), “Modeling of contact and friction in deep drawing processes”, PhD thesis, University of Twente, Enschede, the Netherlands.

Zisman, W.A. (1959), “Durability and wettability proprieties of monomolecular films on solids”, in R. Davies (ed.): Friction and Wear, Elsevier Publishing Co., 110-48.

Chapter 3

Stribeck curve for statistical rough surfaces

3.1 Introduction

Due to manufacturing processes, surfaces may have a Gaussian distribution of surface heights. The asperity contact model of Greenwood and Williamson is used in the Gelinck and Schipper (1999) friction model to describe the asperity contact component in the mixed lubrication (ML) regime. The model of Greenwood and Williamson is restricted to a Gaussian distribution of the summits heights in which the asperities have the same parabolic radius of curvature. It is known that the model of Greenwood and Williamson is quite accurate as long as certain conditions are obeyed. The main disadvantage of this model is the assumed Gaussian distribution of equal summits.
When the surfaces have a Gaussian distribution of the summits, a statistical contact model can be successfully used. A statistical contact model like for instance Greenwood and Williamson's model can be implemented rather easily in a mathematical program and the time needed for calculations is very short compared to a deterministic contact model.

In this chapter at first the mixed lubrication model introduced by Gelinck and Schipper is reviewed. Then, in sections 3.3 to 3.5 extensions of the deterministic mixed lubrication model for two rough surfaces, shear thinning lubricants and starved lubrication are made. In the last section, conclusions concerning this chapter are pointed out.

3.2 Mixed lubrication model for statistical rough surfaces

As was mentioned in section 2.3 Gelinck and Schipper developed a mixed lubrication model for statistical rough surfaces in 1999. Based on the idea of Johnson et al. they combined the Greenwood and Williamson contact model with EHL theory in a mixed lubrication model for line contacts. By using this model, the Stribeck curve can be predicted.
In this section the mixed lubrication model is introduced and some results of calculations are presented. In section 3.2.2 a summary concerning this subchapter is given.

3.2.1 Mixed lubrication model

The mixed lubrication (ML) regime is the transition regime between the boundary and the elasto-hydrodynamic lubrication regime, having the characteristics of both regimes. As pointed out in Section 2.3.1 (see Eq. 2.29) the total normal load (pressure) in ML regime is sheared between the load carried by the contacting asperities and the load carried by the EHL fluid film. The two coefficients defined in Eq. 2.30 can also be written in terms of pressure as:

$$\gamma_1 = \frac{p_T}{p_H},\ \gamma_2 = \frac{p_T}{p_C} \tag{3.1}$$

where p_T, p_C and p_H are the total pressure carried by the contact, the pressure carried by the asperities and the pressure carried by the fluid respectively. The two coefficients γ_1 and γ_2 are mutually dependent as in Eq. 2.31 and refer to the BL component and the EHL component respectively. In order to calculate the pressure carried by the asperities, Greenwood and Williamson's contact model and a function fit introduced by Gelinck (1999) are used. To describe the pressure carried by the EHL film, the film thickness formula of Moes (1997) is used.
In order to simplify the equations, all the parameters in the Greenwood and Williamson model are made dimensionless in terms of Hertzian parameters for line contacts (i.e. half width of the contact b and the Hertzian maximum pressure p_h). These parameters read as:

$$\bar{p} = \frac{p}{p_h},\ X = \frac{x}{b},\ H_h = \frac{hR}{b^2} = \frac{\pi}{8}\frac{hBE'}{F_N},$$

$$\overline{\sigma}_s = \frac{\sigma_s R}{b^2} = \frac{\pi \sigma_s BE'}{8F_N},\ \overline{n} = 4nb^2\sqrt{\frac{\beta}{R}} = \frac{32}{\pi}\frac{nF_N}{BE'}\sqrt{\beta R}$$

A summary of the Hertzian theory for line contacts is given in Appendix B.
For the EHL dimensionless numbers the reader is referred to section 2.1.4.
In the next two sections the two components (EHL and BL) which describe the mixed lubrication model, will be presented.

3.2.1.1 The hydrodynamic component

The EHL component in mixed lubrication regime can be adapted by using the following relation:

$$p_T = \gamma_1 \cdot p_H \tag{3.2}$$

where γ_1 is a constant. Now the Reynold equation (Eq. 2.1) can be written for the line contact case as:

$$\frac{\partial}{\partial x}\left(\frac{\rho h^3}{\eta}\frac{\partial p_H}{\partial x}\right) = 6(v^+)\frac{\partial(\rho h)}{\partial x} \tag{3.3}$$

in which the pressure is replaced by the hydrodynamic component p_H. In the film shape equation (Eq. 2.10) the pressure p which gives the deformation (Eq. 2.8) is replaced by $\gamma_1 \cdot p_H$:

$$h(x) = h_\infty + \frac{x^2}{2R} - \frac{4\gamma_1}{\pi E'}\int_{-\infty}^{\infty} p_H(s)\ln|x-s|ds \tag{3.4}$$

The last equation which has to be adapted, is the force balance equation (Eq. 2.4) in which the pressure p is again replaced by the product $\gamma_1 \cdot p_H$:

$$F_N = B\gamma_1\int_{-\infty}^{\infty} p_H(x)dx \tag{3.5}$$

The following substitutions are used for the EHL calculations in the mixed lubrication regime:

$$F_N \rightarrow \frac{F_N}{\gamma_1} \tag{3.6}$$

$$E' \rightarrow \frac{E'}{\gamma_1} \tag{3.7}$$

By considering the substitutions from Eq. 3.6 and 3.7, the film thickness relation (Eq. 2.14) becomes:

$$H_C = \left[\gamma_1^{\,s} \left(H_{RI}^{\frac{7}{3}} + \gamma_1^{-\frac{14}{15}} H_{EI}^{\frac{7}{3}} \right)^{\frac{3}{7}s} + \left(H_{RP}^{-\frac{7}{2}} + H_{EP}^{-\frac{7}{2}} \right)^{-\frac{2}{7}s} \right]^{s^{-1}} \tag{3.8}$$

where s is defined as:

$$s = \frac{1}{5}\left(7 + 8e^{-2\frac{H_{EI}}{H_{RI}}\gamma_1^{-\frac{2}{5}}} \right) \tag{3.9}$$

3.2.1.2 The asperity contact or BL component

In order to calculate the pressure carried by the asperities in the mixed lubrication regime, Greenwood and Williamson's model is used. In their calculations Greenwood and Williamson assume a normal distribution of the summits in which the probability that a random summit is in contact with the opposite surface is:

$$P(s > h) = \int_h^{\infty} f(s)ds \tag{3.10}$$

with h the separation and f(s) the Gaussian distribution defined as:

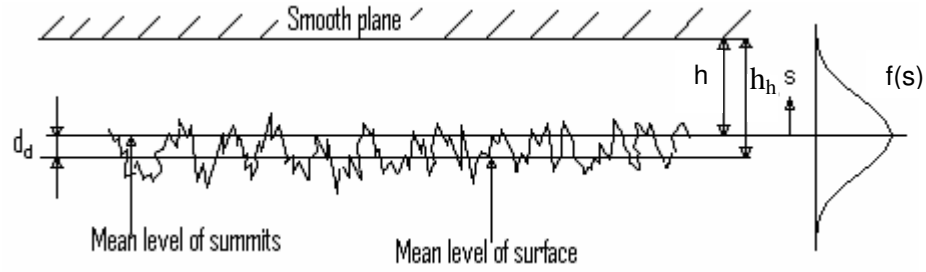

Fig.3.1: The contact between a smooth surface and a rough surface with the corresponding Gaussian distribution of the summits.

$$f(s) = \frac{1}{\sigma_s \sqrt{2\pi}} \exp\left\{\frac{-s^2}{2\sigma_s^2}\right\} \tag{3.11}$$

In the theory of Greenwood and Williamson the summits are considered paraboloids, having the same radius β. The asperities are uniformly distributed on the surface with a density of asperities n per unit area. In Appendix A the definition of a summit and how to calculate n, β and σ_s (standard deviation of the summits) from a measured surface is presented.

In the Greenwood and Williamson model the contact between two rough surfaces is replaced by a contact between a rough deformable and a smooth rigid flat surface (Fig.3.1), where the rough surface combines the roughness and the properties of the two initial rough surfaces (for more details see Appendix A).

Two mean lines and a Gaussian height distribution of the summits heights are depicted in Fig.3.1. The mean line through the surface heights is the reference plane for the EHL component and the mean line for the summits heights is used to calculate the asperity contact component. The distance between the two mean lines d_d is defined by Whitehouse and Archard (1970) as:

$$d_d = 0.82\sigma \tag{3.12}$$

where σ is the standard deviation of the surface heights ($\sigma = 1.4\sigma_s$).

In Greenwood and Williamson's theory the summits deform independently from each other, and elastically according to the Hertzian theory.

Greenwood and Williamson derived expressions for the number of summits in contact, N:

$$N = nA_{nom} \int_h^\infty f(s)ds = nA_{nom} F_0\left(\frac{h}{\sigma_s}\right) \tag{3.13}$$

the total real contact area, A_r:

$$A_r = \pi n \beta A_{nom} \int_h^\infty (s-h) f(s) ds = \pi n \beta \sigma_s A_{nom} F_1\left(\frac{h}{\sigma_s}\right) \tag{3.14}$$

and the applied normal load, F_N:

$$F_N = \frac{2}{3} n \sqrt{\beta} E' A_{nom} \int_h^\infty (s-h)^{\frac{3}{2}} f(s) = \frac{2}{3} n \beta \sigma_s \sqrt{\frac{\sigma_s}{\beta}} E' A_{nom} F_{\frac{3}{2}}\left(\frac{h}{\sigma_s}\right), \tag{3.15}$$

with A_{nom} the nominal contact area. It should be mentioned that the product of the surface parameters $n\beta\sigma_s$ should be in the range of 0.03 to 0.05, Johnson et al. (1972).
In Eq. 3.13, 3.14 and 3.15 the integral identity is used:

$$F_j = \int_h^\infty (\bar{s} - h/\sigma_s)^j \phi(\bar{s}) ds \tag{3.16}$$

where j is a real number, $\bar{s} = s/\sigma_s$ and $\phi(\bar{s})$ is the normalized Gaussian distribution function:

$$\phi(\bar{s}) = \frac{1}{\sqrt{2\pi}} \exp\left(\frac{-\bar{s}^2}{2}\right) \tag{3.17}$$

If in Eq. 3.15 the nominal contact area A_{nom} is omitted, the remaining relation describes the average contact pressure carried by asperities which can be written by using the dimensionless parameters, section 3.2.1, as:

$$\bar{p} = \frac{F_N}{A_{nom}} = \frac{2}{3} \bar{n} \bar{\sigma}_s \sqrt{\bar{\sigma}_s} F_{\frac{3}{2}}\left(\frac{H_h - D_d}{\bar{\sigma}_s}\right) \tag{3.18}$$

where D_d is defined as:

$$D_d = \frac{\pi}{8} \frac{d_d B E'}{F_N} \tag{3.19}$$

In Eq. 3.18 the definition of the film thickness according to Johnson et al. (1992) is used. The film thickness is defined as the average fluid volume between the two rough surfaces divided by the nominal contact area, or:

$$h' = \int_{-\infty}^{h} (h - s) f(s) ds \tag{3.20}$$

Using the definition of Johnson et al. (Eq. 3.20) the film thickness (separation) does not become negative. This film thickness definition is different from that used by Gelinck and Schipper and can be used for the high loading situation.
The following substitutions are used for the asperity contact or BL component calculations in the mixed lubrication regime:

$$F_N \rightarrow \frac{F_N}{\gamma_2} \tag{3.21}$$

$$E' \rightarrow \frac{E'}{\gamma_2} \tag{3.22}$$

$$n \rightarrow n\gamma_2 \tag{3.23}$$

For the central pressure in a rough line contact, Gelinck and Schipper introduced a function fit which reads as:

$$\frac{p_c}{p_h} = (1 + (a_1 \bar{n}^{a_2} \bar{\sigma}_s^{\,a_3})^{a_4})^{\frac{1}{a_4}} \tag{3.24}$$

with a_i as fit parameters:

$$a_1 = 0.953,\ a_2 = 0.0337,\ a_3 = -0.442 \text{ and } a_4 = -1.70$$

Eq. 3.24 can be adapted to the ML regime by using the substitutions defined in Eq. 3.21, 3.22 and 3.23. The modified relation for the central pressure reads as:

$$\frac{p_c}{p_h} = (1 + (a_1 \bar{n}^{a_2} \bar{\sigma}_s^{\,a_3} \gamma_2^{a_2})^{a_4})^{\frac{1}{a_4}} \frac{1}{\gamma_2} \tag{3.25}$$

Eq. 3.18 and 3.25 are equaled and used together with the film thickness equation in an iterative algorithm in order to find the right ratio between the load carried by the asperities and the load carried by the fluid.
Gelinck and Schipper developed a function fit for the real contact area A_r which will be used in the next section to calculate the hydrodynamic contact area in the ML regime. This relation reads:

$$\frac{A_r}{Bb} = (a_1 + (a_2 \bar{n}^{a_3} \bar{\sigma}_s^{a_4})^{a_5})^{\frac{1}{a_5}} \tag{3.26}$$

with a_i:

$$a_1 = 0.292,\ \ a_2 = 0.477,\ \ a_3 = -0.992,\ \ a_4 = -1.470 \text{ and } a_5 = -0.463$$

In the next section the way how the coefficient of friction is calculated, and the corresponding solution scheme is presented.

3.2.1.3 Calculating the coefficient of friction

In order to calculate the coefficient of friction for a mixed lubricated line contact, the load carried by the asperities, the load carried by the fluid and the film thickness must be determined. Three equations are used to calculate the values of the three parameters mentioned:

- The first equation is Eq. 2.29, but written in dimensionless form (similar to W, see section 2.1.4):

$$W_N = W_C + W_H \tag{3.27}$$

  with W_N, W_C and W_H the dimensionless total normal load, the dimensionless load carried by the asperities and the dimensionless load carried by the fluid respectively.

- The second equation is the film thickness relation, Eq. 3.8 in which the definition of Johnson (Eq. 3.20) is used to calculate H_C.

- The third equation is the equality of Eq. 3.18 and Eq. 3.25:

$$\frac{2}{3}\overline{n}\overline{\sigma}_s\sqrt{\overline{\sigma}_s}F_{\frac{3}{2}}\left(\frac{H_h - D_d}{\overline{\sigma}_s}\right) = \left(1 + \left(a_1\overline{n}^{a_2}\overline{\sigma}_s^{a_3}\gamma_2^{a_2}\right)^{a_4}\right)^{\frac{1}{a_4}}\frac{1}{\gamma_2} \tag{3.28}$$

By solving this system of three equations, the load carried by the asperities, the load carried by the fluid, and the separation are obtained and therefore the coefficient of friction in ML regime can be calculated as explained below.
The total friction force in the ML regime is the sum of the friction force of the contacting asperities and shear force of the lubricant:

$$F_f = \sum_{i=1}^{N}\iint_{A_{Ci}}\tau_{Ci}(\dot{\gamma})dA_{Ci} + \iint_{A_H}\tau_H(\dot{\gamma})dA_H \tag{3.29}$$

where N is the number of contacting asperities, A_{Ci} the area of contact of a single asperity i, τ_{Ci} the shear stress at the asperity contact, A_H the contact area of the hydrodynamic component and τ_H the shear stress of the lubricant.
For the contacting asperities the friction is assumed to be of the Coulomb type, i.e.:

$$f_{Ci} = \frac{\tau_{Ci}}{p_{Ci}} \tag{3.30}$$

with p_{Ci} the normal pressure on the current asperity. The coefficient of friction f_{Ci} is assumed to be constant for all asperities, therefore the first term of the Eq. 3.29 can be written as:

$$\sum_{i=1}^{N}\iint_{A_{Ci}} f_C p_{Ci} dA_{Ci} = f_C F_C \tag{3.31}$$

where the value of f_C is experimentally determined.
The shear stress in the film is determined according to the Eyring model:

$$\tau_H = \tau_0 \operatorname{arcsinh}\left(\frac{\eta\dot{\gamma}}{\tau_0}\right) \tag{3.32}$$

where η is calculated according to Roelands.
Now the coefficient of friction can be written as:

$$f = \frac{F_f}{F_N} = \frac{f_C \cdot F_C + \tau_0 \operatorname{arcsinh}\left\{\frac{\eta v^{dif}}{h\tau_0}\right\} A_H}{F_N} \tag{3.31}$$

with v^{dif} the sliding velocity and A_H the hydrodynamic contact area defined as:

$$A_H = A_{nom} - A_r \tag{3.32}$$

In Fig.3.2 the solution scheme of the Stribeck curve calculation is presented.

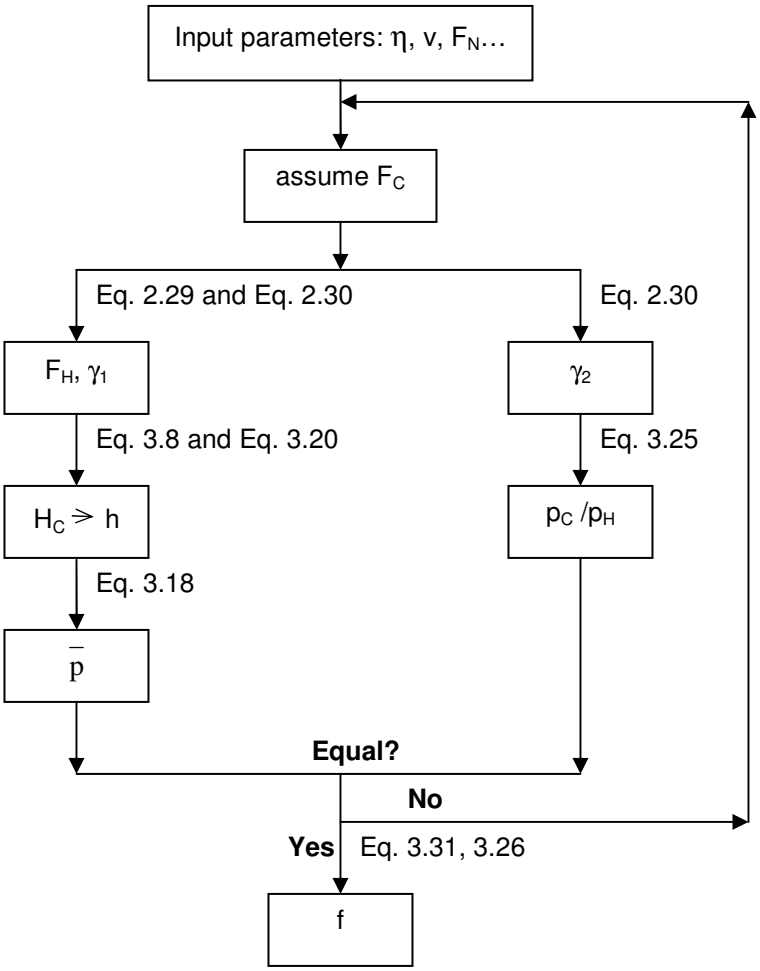

Fig.3.2: Solution scheme of the coefficient of friction calculation.

3.2.1.4 Stribeck curve calculations

In this section some Stribeck curve calculations, based on the model presented in the previous section, are presented. The influence of a few parameters, i.e. load (F_N) and roughness parameters (σ_s, β and n) is investigated. In table 3.1 the values of the input parameters for the reference case are given.

Table 3.1: Input parameters for the reference case.

property	value	unit	description
n	$1.0 \cdot 10^{11}$	m^{-2}	density of asperities
β	$1.0 \cdot 10^{-5}$	m	radius of asperities
σ_s	$0.05 \cdot 10^{-6}$	m	standard deviation of asperities
B	$10 \cdot 10^{-3}$	m	length of the contact
E'	231	GPa	combined elasticity modulus
R	$20 \cdot 10^{-3}$	m	reduced radius of cylinder
η_0	0.0202	Pa·s	viscosity
α	$2 \cdot 10^{-8}$	Pa^{-1}	viscosity pressure coefficient
τ_0	2.5	MPa	Eyring shear stress
f_c	0.13	-	coefficient of friction in BL
F_N	500	N	normal load

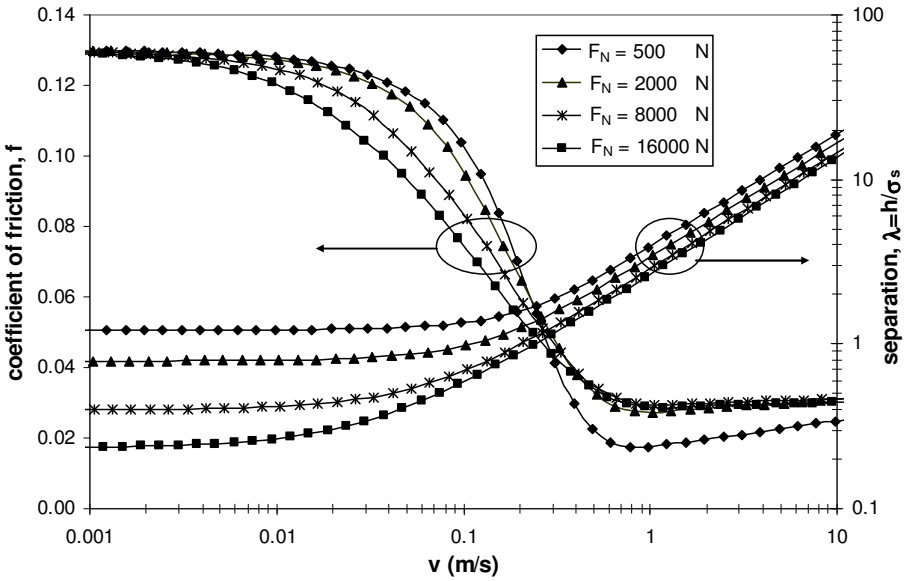

Fig.3.3: Influence of the load on the Stribeck curve and the separation.

In Fig.3.3 the Stribeck curve calculations as a function of velocity for different normal loads are presented. In this figure, the three lubrication regimes are clearly visible, i.e. boundary lubrication at low velocity (≈ 0.001-0.01 m/s) in which the load is carried by asperities, mixed lubrication (≈ 0.01-1 m/s) in which the normal load is sheared between the asperities and the fluid and elasto hydrodynamic lubrication regime (≈ 1-10 m/s) where the normal load is carried by the lubricant.
As can be noticed in Fig.3.3, the transition from ML to EHL is hardly influenced by the load (the transition ML to EHL takes place at almost the same velocity). With increasing normal load the transition region BL to ML is extended and shifts to the left while the ML lubrication regime extends over a larger velocity range as observed by experiments for point contacts, Schipper (1988).
On the right side of Fig.3.3, the separation λ is plotted on a logarithmic scale. As can be seen, the separation in BL regime decreases with increasing load. In the EHL regime the contact operates in the Koets area (Fig.2.3) and the separation is proportional to $(v^+)^{0.7}$.

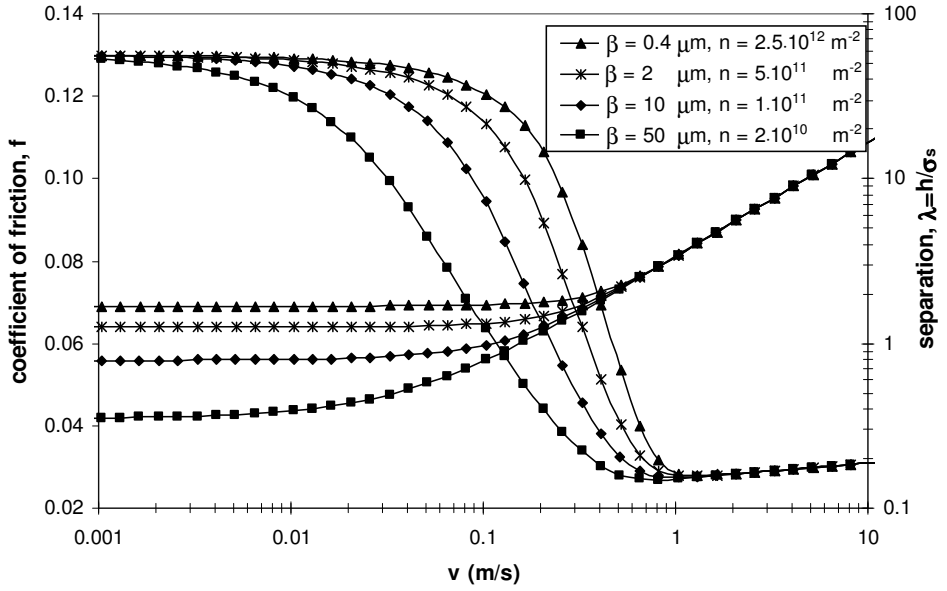

Fig.3.4: Effect of the statistical roughness parameters β and n on the Stribeck curve for F_N = 2000 N and σ_s = 0.05 μm.

In Fig.3.4 the influence of the statistical roughness parameters β and n on the Stribeck curve is presented. The product $n\beta\sigma_s$ is kept constant i.e. 0.05. It can be seen in Fig.3.4 that the separation in the BL and ML region decreases with increasing β and decreasing n and as a consequence the transitions from BL to ML and from ML to EHL shift to the left (low velocity region). The decrease in

separation, by increasing β and decreasing n is caused by the fact that the surface becomes less stiff. The load carried by asperities is proportional to $\beta^{-0.5}$(see Eq. 3.15) and by increasing β the contact deforms more in order to carry the same load. In Fig.3.5 the influence of σ_s and respectively n on the Stribeck curve is depicted.

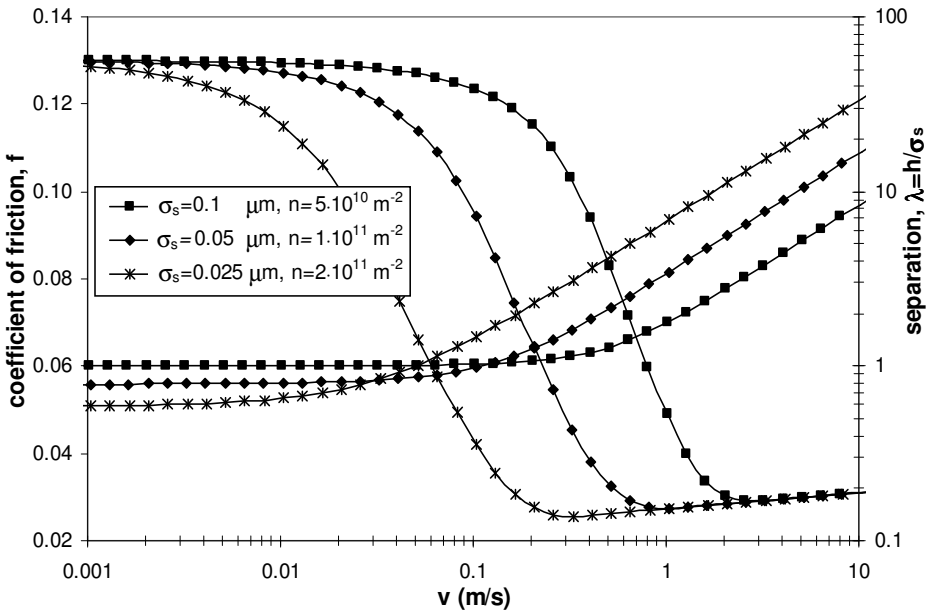

Fig.3.5: Effect of the statistical roughness parameters σ_s and n on the Stribeck curve for F_N = 2000 N and β = 10 μm.

The product $n\beta\sigma_s$ is again kept constant having the value of 0.05. It can be noticed, that by increasing the value of σ_s, the Stribeck curve shifts to the right. In this case the shift of the Stribeck curve is caused by a higher separation between the surfaces which increases with σ_s.

In Fig.3.6 the influence of viscosity η_0 on the Stribeck curve is depicted. The viscosity η_0 is varied between 0.06 to 0.006 Pa·s and the other input parameters are given table 3.1. As expected, by increasing the viscosity η_0 the film thickness is higher for the same velocity $h \approx (\eta_0)^{0.7}$ and as a consequence the ML regime shifts to the left whilst the friction in the EHL regime increases (friction ≈ $\text{arcsinh}(\eta v^{dif}/(h\tau_0))$.

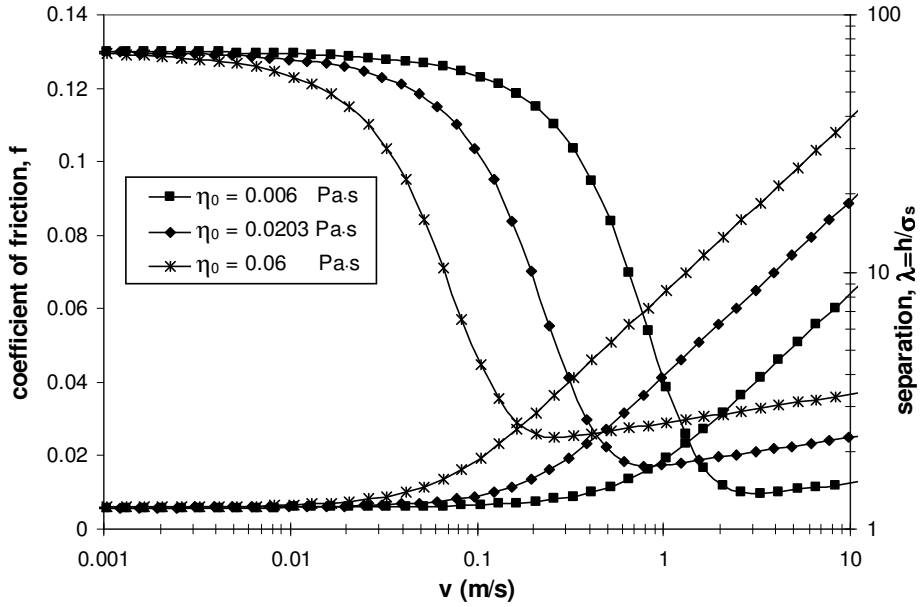

Fig.3.6: Effect of the viscosity η_0 on the Stribeck curve and the separation for F_N = 500 N.

3.2.2 Summary

The statistical mixed lubrication model has been described and Stribeck curve calculations have been presented using this model.

The presented mixed lubrication model for line contacts is a combination of the Greenwood and Williamson contact model and the EHL theory. Stribeck curve calculations for different normal loads have been performed (Fig.3.3). It is shown that the load has an influence on the transition from BL to ML. In this section, the influence of the roughness parameters on the Stribeck curve is also studied. The results show that the Stribeck curve predictions strongly depend on the roughness parameters σ_s, β and n if friction is depicted as a function of velocity. By increasing σ_s, the transitions from BL to ML and from ML to EHL, shift to the right (higher velocities) while by increasing β the opposite effect is obtained. It has been shown that the viscosity η_0 has a strong influence on the ML transition regime and also on the friction in the EHL regime.

In the next section an improved statistical Stribeck model for two rough surfaces is presented. The contact model of Greenwood and Tripp (1970) for two rough surfaces is extended and implemented in the statistical Stribeck curve model.

3.3 Stribeck curve for two rough surfaces

3.3.1 Introduction

In this section the mixed lubrication model for statistical rough surfaces is extended, in order to predict the Stribeck curve, when both surfaces are considered to be rough. In the Greenwood and Williamson model, which describes the asperity component in the BL regime, the contact between two rough surfaces is reduced to a contact between a smooth flat surface and a rough surface which combines the roughness of the two initial surfaces (for more details the reader is referred to Appendix A). In order to combine the roughness of the two contacting surfaces as used by Greenwood and Williamson, the central axes of the interacting roughness summits must coincide. The assumption that the asperity pairs are not aligned is more realistic and the probability that their central axes coincide is very small. In the case of contact with aligned asperity pairs, the separation between the two contacting surfaces is larger compared to the case of misaligned asperity pairs where overlap between the summits is possible. The same result has been found by Greenwood and Tripp (1970) who studied the misalignment of the roughness summit pairs for a contact between two identical flat rough surfaces. Greenwood and Tripp showed that the relation which describes the load with real contact area remains the same as in Greenwood and Williamson's model, only the separation between the surfaces is smaller for the same nominal contact pressure. The difference found in the separation of the two contacting surfaces by the two models (GW and GT) depends on the difference in the roughness parameters of the two contacting surfaces. When one of the contacting surfaces is very smooth compared to the other, the separation calculated with the Greenwood and Williamson and Greenwood and Trip model is almost the same while for two surfaces with comparable roughness the separation is significantly different for the two models, as expected.

In the Stribeck curve calculations, the separation influences the transitions between the three lubrication regimes, i.e. the transition from BL to ML and ML to EHL regime. Therefore, it is more appropriate to implement in the Stribeck curve model an asperity contact model in which both contacting surfaces are rough. In section 3.3.2 an extension of Greenwood and Tripp's model for two contacting rough surfaces (having different roughness parameters) is described and implemented in the mixed lubrication model as presented in the previous section. The difference of the two models (Greenwood and Williamson and the new contact model) on the Stribeck curve is studied in section 3.3.3. In the last subsection of this section, a summary concerning the new approach is given.

3.3.2 Two rough surfaces contact model

In 1970, Greenwood and Tripp published a paper in which they presented a deterministic contact model between two identical rough surfaces (n, β and σ_s of the two surfaces are the same). In the Appendix C the model of Greenwood and Tripp is summarized. In this section the Greenwood and Tripp contact model is extended to a contact between two rough surfaces when the radii of asperities are not equal ($\beta_1 \neq \beta_2$). For simplicity, the asperity shape is considered to be parabolic.

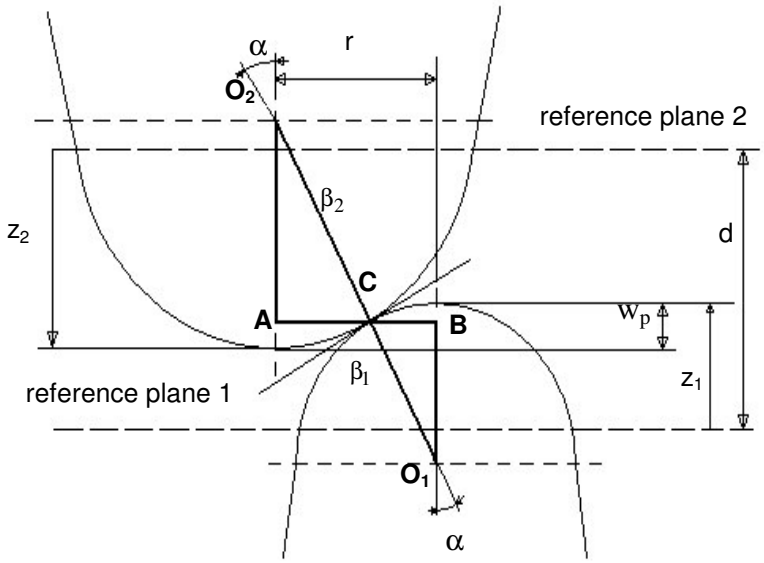

Fig.3.7: The misaligned contact between two particular asperities.

In Fig.3.7 the contact between two asperities is schematically presented.
In analogy with the Greenwood and Tripp model (Appendix C) from the triangles O_2AC and O_1BC, the parameter r becomes:

$$r = (\beta_1 + \beta_2)\sin\alpha \tag{3.51}$$

and

$$dr = (\beta_1 + \beta_2)\cos\alpha d\alpha \tag{3.52}$$

The following assumption is made and is used throughout this section: the angle α is small (in section 3.3.3 will be shown that the angle is smaller than 11 degrees) and therefore the tangential load and tangential deformation are neglected.

Now by considering the asperity z_1 from surface 1 in contact with the asperities of the opposite surface 2, the number of asperities with heights between z_2 and z_2+dz_2 situated between r and r+dr from asperity z_1 is:

$$N = n_2 \cdot 2 \cdot \pi \cdot r \cdot dr \cdot \phi\{z_2\} \cdot dz_2 \tag{3.53}$$

with r and dr according to Eq. 3.51 and 3.52 and n_2 is the density of asperities of the second surface.
The force on an asperity of surface 1 due to the action of the second surface is:

$$F = \int_{z_2}\int_{r} 2\pi n_2 F\{w_p - f\{\beta_1 \sin\alpha\} - f\{\beta_2 \sin\alpha\}, r\}\phi\{z_2\} r dr dz_2 \tag{3.54}$$

If we take into account all the asperities of the first surface in contact with the asperities of the second surface, then the force reads:

$$F\{d\} = 2\pi n_1 n_2 A_{nom} \int_{d}^{\infty}\int_{r} F\{w_p - f\{\beta_1 \sin\alpha\} - f\{\beta_2 \sin\alpha\}, r\}\phi_0\{z\} r dr dz \tag{3.55}$$

where n_1 is the density of asperities of the first surface, $z = z_1 + z_2$ and $\phi_0\{z\}$ is the combined Gaussian distribution of asperities defined as:

$$\phi_0\{z\} = \phi\{z_1\} \cdot \phi\{z_2\} \tag{3.56}$$

We write the r-integral as:

$$F_0\{w_p\} = 2\pi n_2 \int_{0}^{\infty} F\{w_p - f\{\beta_1 \sin\alpha\} - f\{\beta_2 \sin\alpha), r\} r dr \tag{3.57}$$

Implementing the deformation law relation (Appendix C) in Eq. 3.57, this reads:

$$F_0\{w_p\} = \frac{4}{3}\pi n_2 E' \beta^{1/2} \int_{0}^{\infty} (w_p - c)^{3/2} (\beta_1 + \beta_2)^2 \sin\alpha \cos\alpha d\alpha \tag{3.58}$$

where $c = (\beta_1 + \beta_2)(1 - \cos\alpha)$. Taking into consideration, that the bracket $(w_p\text{-}c)$ should be positive, then the angle α varies between 0 and $\arccos(1\text{-}w_p/(\beta_1+ \beta_2))$ and as a result Eq. 3.58 becomes:

$$F_0\{w_p\} = \frac{8}{15}\pi n_2 E' \beta^{1/2} (\beta_1 + \beta_2) w_p^{5/2} \tag{3.59}$$

where $1/\beta = 1/\beta_1 + 1/\beta_2$.
Writing $z = s\sigma_s$ and using Eq. 3.59, Eq. 3.55 becomes:

$$F\{d\} = \frac{8}{15}\pi n_1 n_2 E' \beta^{1/2} (\beta_1 + \beta_2) \sigma_s{}^{5/2} A_{nom} F_{5/2}\left\{\frac{d}{\sigma_s}\right\} \tag{3.60}$$

with $F_{5/2}\left\{\frac{d}{\sigma_s}\right\} = \int_h^\infty (s-h)^{5/2}\phi(s)ds$, where $s = z/\sigma_s$.
The total real area of contact is:

$$A_r\{d\} = \pi^2 n_1 n_2 \beta(\beta_1 + \beta_2)\sigma_s{}^2 A_{nom} F_2\left\{\frac{d}{\sigma_s}\right\} \tag{3.61}$$

and the number of asperity contacts is:

$$N\{d\} = 4\pi n_1 n_2 \sigma_s (\beta_1 + \beta_2) A_{nom} F_1\left\{\frac{d}{\sigma_s}\right\} \tag{3.62}$$

If the total force (Eq. 3.60) is divided by the real contact area Eq. 3.61, the average real contact pressure is obtained by:

$$p\{d\} = \frac{8}{15\pi} E' \sqrt{\frac{\sigma_s}{\beta}} \frac{F_{5/2}\left\{\frac{d}{\sigma_s}\right\}}{F_2\left\{\frac{d}{\sigma_s}\right\}} \tag{3.63}$$

With Eq. 3.60 to 3.63 F, A_r, N and p is expressed as a function of roughness parameters for the contact between two rough surfaces. The new concept can now be implemented in the Stribeck curve model for line contacts (Eq. 3.15, 3.14 and 3.13 are replaced repetitively by Eq. 3.60, 3.61 and 3.62).
A comparison between the new contact model, two rough surfaces in contact and the Greenwood and Williamson contact model is made in the next section.

3.3.3 Comparison on Stribeck curve between new contact model and Greenwood and Williamson model

In order to make a comparison between the two models on the Stribeck curve two different combinations of roughness parameters for the two contacting surfaces are chosen (table 3.3). In order to see the influence of the two models on the Stribeck curve, the roughness parameters of each surface are chosen in a such way that in the first case the standard deviation of the summits of one surface is eight times larger than the other (table 3.3 case a) and in the second case the roughness of the two contacting surface are comparable (table 3.3 case b), whilst the combined standard deviation of the summits σ_s of the two reference cases is almost the same (see table 3.3 case a, b).
In table 3.2 the input parameters for the calculations of the Stribeck curve in the two roughness parameters cases are presented.

Table 3.2: Input parameters used for Stribeck curve calculations.

property	value	unit	description
B	$10 \cdot 10^{-3}$	m	length of the contact
E'	231	GPa	combined elasticity modulus
R	$20 \cdot 10^{-3}$	m	reduced radius of cylinder
η_0	0.0202	Pa·s	viscosity
α	$2 \cdot 10^{-8}$	Pa^{-1}	viscosity pressure coefficient
τ_o	2.5	MPa	Eyring shear stress
f_c	0.13	-	coefficient of friction in BL
F	500	N	normal load

Table 3.3: Roughness parameters used for Stribeck curve calculations (de Rooij (1998)).

property	value (case a)	value (case b)	unit	description
σ_{s1}	0.49	0.31	µm	standard deviation of asperities
β_1	2.6	8.8	µm	radius of asperities
n_1	$13 \cdot 10^9$	$12.5 \cdot 10^9$	$1/m^2$	density of asperities
σ_{s2}	0.064	0.4	µm	-
β_2	40.8	9	µm	-
n_2	$13 \cdot 10^9$	$10 \cdot 10^9$	$1/m^2$	-
$\sigma_s=(\sigma_{s1}+\sigma_{s2})^{0.5}$	0.49	0.51	µm	-
β	2.5	4.5	µm	-
n	$13 \cdot 10^9$	$10 \cdot 10^9$	$1/m^2$	-

The main difference between the two models is that in the new model, due to the misalignment of the roughness summit pairs, results into a smaller separation between the opposing surfaces under BL conditions compared to the Greenwood and Williamson model (see Fig.3.8 and Fig.3.9).

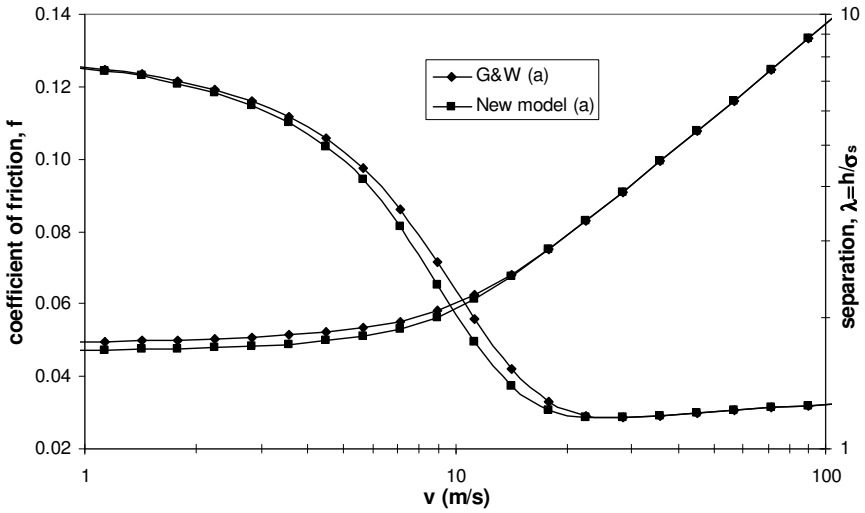

Fig.3.8: Stribeck curve and corresponding separation, calculated using the new and Greenwood and Williamson's model for reference case a.

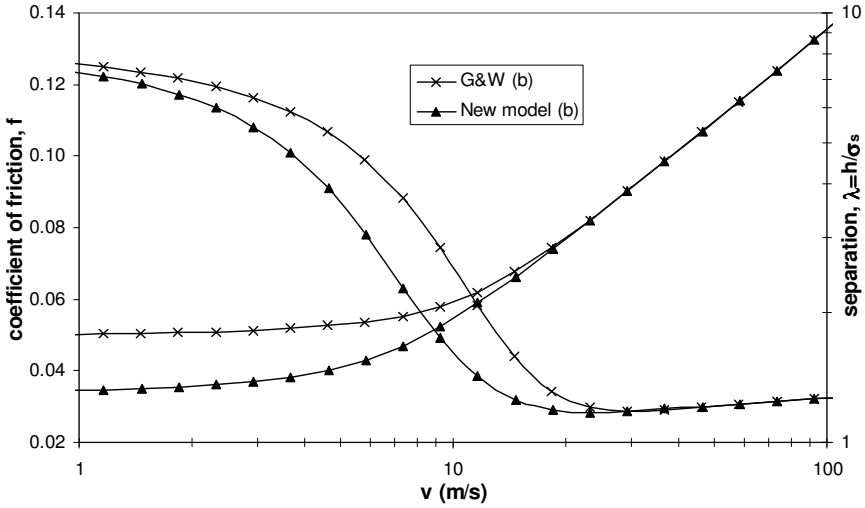

Fig.3.9: Stribeck curve and corresponding separation, calculated using the new model and Greenwood and Williamson's model for reference case b.

In Fig.3.8 the Stribeck curve and separation for the two models for the reference case a are given. In this case, one surface is smooth compared to the other surface and the new contact model in this case gives nearly the same separation as in the Greenwood and Williamson model. Therefore, the Stribeck curves for the two models are almost identical.
For reference case b, where the roughness parameters of the two surfaces are almost the same, the misalignment effect is significantly and the separation under BL conditions given by the new contact model is significant smaller than for the Greenwood and Williamson model (Fig.3.9). As a result, the Stribeck curve shifts to lower velocities with a factor of approximately 1.5. The overlap between the two surfaces in reference case b is actually the difference between the two separations given by the two models in the BL regime and it has a value of 0.235 μm. This value of overlap is almost maximum for the considered combined standard deviation of the summits ($\sigma_s \approx 0.5$ μm).
Based on the overlap, the angle α between the summits (see Fig.3.7) can be calculated (see Eq. 3.58). For the reference case b, α varies between 0 and 10.35 degrees. In this situation the tangential displacement and tangential force are negligible compared to their normal component and therefore are not considered in the calculations.

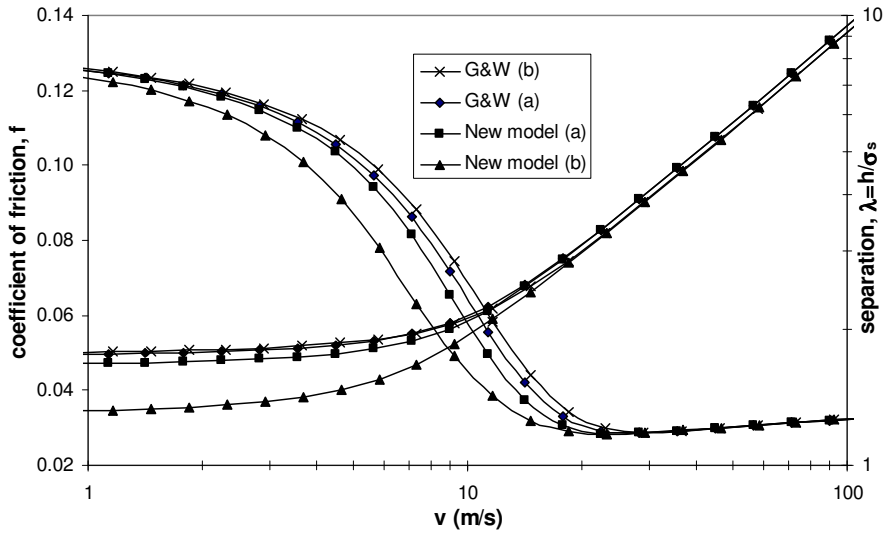

Fig.3.10: Stribeck curve and corresponding separation, using the new model and the Greenwood and Williamson model for the two reference cases a and b.

In Fig.3.10 the Stribeck curves for the two reference cases and the two models (Greenwood and Williamson and the new model) are drawn in order to see the

difference. It can be seen that Greenwood and Williamson's model gives almost identical Stribeck curves because this model does make no difference whether the two surfaces have the same or different roughness parameters as long as the combined standard deviation of the summits is nearly the same. Whereas the new model does account for different roughness parameters and gives a significant shift to lower velocities of the ML regime when the roughness parameters of both surfaces are almost identical (Fig.3.10 new model b).

3.3.4 Summary

A new asperity elastic contact model has been implemented in the ML model in order to predict the Stribeck curve when two rough surfaces are in contact. The contact model is an extension of Greenwood and Tripp's contact model. The difference between the new model and the model of Greenwood and Williamson is that the new contact model takes into account the misalignment of the asperity couples resulting in a smaller separation under BL conditions, whereas the model of Greenwood and Williamson does not consider this effect and therefore the resulting separation in the BL regime is larger. The two models are compared in the Stribeck curve and the results show that if the two contacting surfaces have comparable roughness parameters, the Mixed Lubrication regime shifts to lower velocities when using the new model compared to Greenwood and Williamson's model. Whereas one of the contacting surfaces is smooth compared to the other surface, the difference between the two models on the Stribeck curve is insignificant.
In the next section the shear thinning effect of the lubricants on the Stribeck curve is investigated.

3.4 Stribeck curve for shear thinning lubricants

3.3.1 Introduction

One of the phenomena that lubricants possess is that they get a lower viscosity when the shear rate exceeds a critical value, this is called shear thinning. As a consequence the film thickness may decreases due to a reduction in viscosity in the inlet of an EHL contact. Next, due to the viscosity change in the contact the overall friction in the ML and BL changes.
The reduction in film thickness has an influence on the Stribeck curve by shifting the mixed lubrication regime to the right. The friction in the EHL regime shifts to a higher or lower level. The magnitude of these shifts depends on the properties of the lubricant.
In the section 3.4.2 the shear thinning effect is incorporated in the film thickness formula for the simple sliding situation for line contacts. Section 3.4.3 discusses the influence of the shear thinning effect on the Stribeck curve by incorporating the new film thickness relation in the mixed lubrication model. Comparison of the shear thinning effect on the Stribeck curve between a shear thinning independent lubricant and a shear thinning lubricant respectively is made. In the last section a summary concerning this topic is given.

3.4.2 The influence of high shear rate on reduced pressure and film thickness for line contacts

In recent years there has been an increased interest in the shear thinning effect on the film thickness and in literature two different approaches are given to this phenomenon. On one hand some authors like Bair and Khonsari (1996) and Bair (1998) considered the influence of the shear rate on the lubricant shear stress and on the other hand authors like Taylor (1998) and Chynoweth et al. (1995) considered the decrease of viscosity with increasing shear rate. The aim of the two approaches is to determine the influence of the shear thinning on the film thickness. Due to its simplicity the second approach is used in this section.
When the shear rate exceeds a certain value, the viscosity decreases and therefore the film thickness may reduce. In Fig.3.11 the general trend of the viscosity -shear rate dependency for a shear rate independent (dotted line) and a shear thinning lubricant (solid line) is depicted.

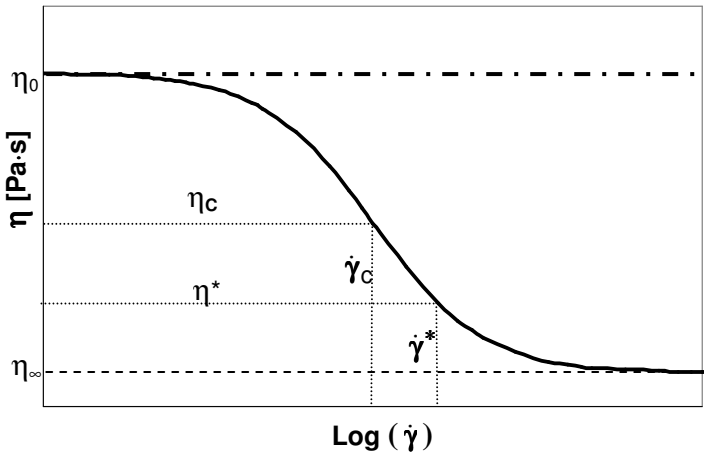

Fig.3.11: Viscosity as a function of the shear rate, for a shear rate independent (dotted line) and a shear thinning lubricant (solid line).

The Cross (1965) equation (typical for mineral oils) is chosen to describe the variation of the inlet viscosity with the shear rate, as follows:

$$\eta = \eta_\infty + \frac{\eta_0 - \eta_\infty}{1 + \left(\frac{\dot{\gamma}}{\dot{\gamma}_c} \right)^m} \tag{3.64}$$

where η_∞ is the viscosity at high shear rate values, η_0 is the viscosity at low shear rate, $\dot{\gamma}$ is the shear rate, $\dot{\gamma}_c$ is the critical shear rate at which the lubricant viscosity is half away between η_0 and η_∞ and m is an exponent (in the calculations presented, m is considered to be one). The inlet shear rate is expressed as:

$$\dot{\gamma} = \frac{v^{dif}}{h} \tag{3.65}$$

where v^{dif} is the sliding velocity and h is the film thickness.

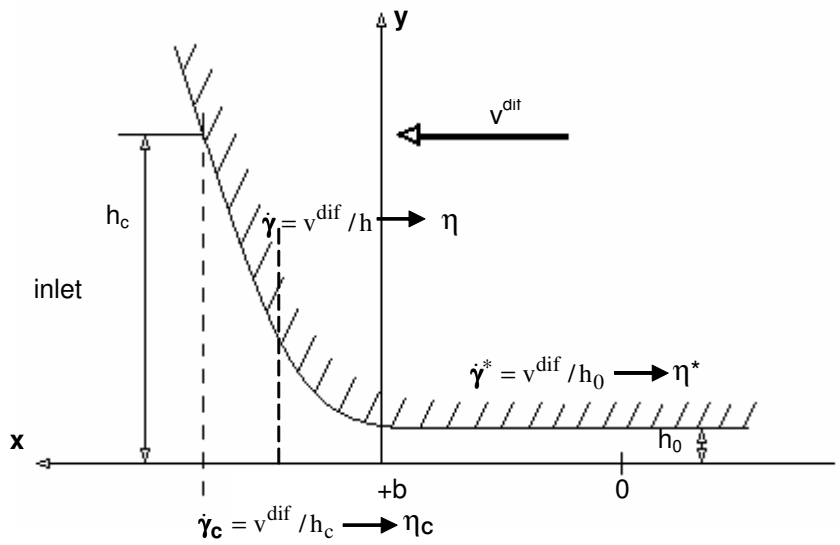

Fig.3.12: Schematic representation of the inlet of a line contact.

The shear rate stays the same in the contact gap for highly loaded contacts and therefore the influence of the shear rate on the viscosity in the inlet zone is of interest. In Fig.3.12 a schematic representation of the inlet of an EHL contact, with respect to the shear thinning situation for a shear thinning lubricant, is presented. In the inlet, the shear rate increases and as a result the viscosity reduces ($\eta < \eta_0$, see Fig.3.11). The shear rate of the lubricant increases towards the contact gap (x = b) where it stays constant ($\dot{\gamma} = \dot{\gamma}^*$ = constant). Consequently, the viscosity decreases (see Fig.3.11) according to Eq. 3.64 and stays the same ($\eta = \eta^*$= constant) in the contact gap.
The shear thinning effect as described above will be incorporated in the film thickness formula for line contacts. In order to do this, Crook's (1966) approximation for the inlet zone is used:

$$h = h_0 + C\left\{ |\bar{x}|\sqrt{\bar{x}^2 - 1} - \ln(|\bar{x}| + \sqrt{\bar{x}^2 - 1}) \right\} \qquad (3.66)$$

with $C = 2F_N/(B \cdot E')$ and $\bar{x} = x / b$ where F_N is the load, B is the contact length, E' is the combined elasticity modulus, x is the inlet coordinate and b is the Hertzian half contact width. This equation has the advantage that the inlet shape is described only by a function of the inlet coordinate.
Grubin (1966) defined the reduced pressure q in the inlet zone as:

$$q = \frac{1 - e^{-\alpha p}}{\alpha} \tag{3.67}$$

The integrated Reynolds equation Eq. 3.2 becomes:

$$\frac{dq}{dx} = 6v^{+}\eta\left(\frac{h - h_0}{h^3}\right) \tag{3.68}$$

where $v^{+} = v^{dif}$ (for simple sliding, the sum velocity is equal with sliding velocity), α is the viscosity-pressure coefficient and q is the local reduced pressure.
If the expression of inlet viscosity (Eq. 3.64) is substituted in Eq. 3.68, the Reynolds equation becomes:

$$\frac{dq}{dx} = \frac{6v^{+}\eta_\infty}{h_0^2}\frac{\Delta/\overline{H}_0}{(\Delta/\overline{H}_0+1)^3} + \frac{6v^{+}}{h_0^2}\frac{\eta_0-\eta_\infty}{\left[1+\frac{1}{(1+\Delta/\overline{H}_0)}\frac{h_c}{h_0}\right]}\frac{\Delta/\overline{H}_0}{(\Delta/\overline{H}_0+1)^3} \tag{3.69}$$

where $\overline{H}_0$ and Δ are dimensionless numbers expressed as:

$$\overline{H}_0 = \frac{BE'h_0}{F_N}, \quad \Delta = 2\left\{|\overline{x}|\sqrt{\overline{x}^2-1} - \ln(|\overline{x}| + \sqrt{\overline{x}^2-1})\right\} \tag{3.70}$$

and:

$$\frac{\dot{\gamma}}{\dot{\gamma}_c} = \frac{h_c}{h} = \frac{h_c}{h_0}\cdot\frac{h_0}{h} = \frac{h_c}{h_0}\cdot\frac{1}{1+\frac{\Delta}{\overline{H}_0}} \tag{3.71}$$

in which h_c is the critical value of the film thickness for $\dot{\gamma} = \dot{\gamma}_c$.
Eq. 3.69 is numerically solved and the results are approximated by an analytical expression. In order to do this, the value of $\overline{H}_0$ has been taken in the range of 0.1 to 1.3 (Cameron (1966) pp. 207) and the ratio h_c/h_0 between 0.1 and 50.
After integration, the reduced pressure for shear thinning lubricants in $\overline{x} = 1$ is:

$$q_{HS(\overline{x}=1)} = 0.099\left\{\overline{H}_0^{-11/8}\cdot\frac{6v^{+}\eta_\infty\overline{H}_0^2 b}{h_0^2} + \left[\frac{2}{3} - \frac{3}{17}\ln\left(\frac{h_c}{h_0}\right)\right]\cdot\overline{H}_0^{0.624}\cdot\frac{6v^{+}(\eta_0-\eta_\infty)b}{h_0^2}\right\} \tag{3.72}$$

The reduced pressure for a Newtonian lubricant reads as (Gohar (2001)):

$$q_{c(\bar{x}=1)} = 0.099\bar{H}_0^{-11/8} \cdot \frac{6v^+\eta_0\bar{H}_0^2 b}{h_0^2} \tag{3.73}$$

It is known that the reduced pressure for classic (q_c) as well as for the high shear rate situation (q_{HS}) in $\bar{x}=1$ is 1/α. Now the ratio between the two reduced pressures in $\bar{x}=1$, reads as:

$$1 = \frac{q_{HS}(\bar{x}=1)}{q_c(\bar{x}=1)} = \frac{\bar{H}_{0HS}^{-11/8} \cdot \frac{6v^+\eta_\infty \bar{H}_{0HS}^2 b}{h_{0HS}^2} + \left[\frac{2}{3} - \frac{3}{17}\ln\left(\frac{h_c}{h_{0HS}}\right)\right] \cdot \bar{H}_{0HS}^{0.624} \cdot \frac{6v^+(\eta_0-\eta_\infty)b}{h_{0HS}^2}}{\bar{H}_{0c}^{-11/8} \cdot \frac{6v^+\eta_0\bar{H}_{0c}^2 b}{h_{0c}^2}} \tag{3.74}$$

where $\bar{H}_{0HS} = BE'h_{0HS}/F_N$, $\bar{H}_{0c} = BE'h_{0c}/F_N$ and h_{0HS}, h_{0c} are the film thickness for shear thinning and classical situation respectively. Rewriting Eq. 3.74 gives:

$$h_{0HS} = h_{0c} \cdot \left[\frac{\eta_\infty}{\eta_0} + \frac{2}{3}\frac{\eta_0-\eta_\infty}{\eta_0} - \frac{3}{17}\frac{\eta_0-\eta_\infty}{\eta_0}\ln\left(\frac{h_c}{h_{0HS}}\right)\right]^{\frac{8}{11}} \tag{3.75}$$

The ratio h_c/h_{0HS} can be approximated as $h_c/h_{0HS} \cong h_c/h_{0c} = \dot{\gamma}_{0c}/\dot{\gamma}_c$ and thus Eq. 3.75 becomes:

$$h_{0HS} = h_{0c} \cdot \left[\frac{\eta_\infty}{\eta_0} + \frac{2}{3}\frac{\eta_0-\eta_\infty}{\eta_0} - \frac{3}{17}\frac{\eta_0-\eta_\infty}{\eta_0}\ln\left(\frac{\dot{\gamma}_{0c}}{\dot{\gamma}_c}\right)\right]^{\frac{8}{11}} \tag{3.76}$$

Eq. 3.76 is accurate up to 10%.

The decrease of the film thickness due to shear thinning of the lubricant is proportional to $(\eta_\infty/\eta_0)^{8/11}$ and the film thickness decreases as the critical shear rate $\dot{\gamma}_c$ decreases.

The film thickness relation for shear thinning lubricants is ready to be implemented in the mixed lubrication model for statistical rough surfaces in order to study the shear thinning effect on the Stribeck curve. Eq. 3.76 can be written in dimensionless form and h_{0HS} becomes H_{HS} and h_{0c} becomes H_C respectively. The film thickness equation for line contacts including shear thinning reads as:

$$H_{HS} = H_c \cdot \left[\frac{\eta_\infty}{\eta_0} + \frac{2}{3}\frac{\eta_0 - \eta_\infty}{\eta_0} - \frac{3}{17}\frac{\eta_0 - \eta_\infty}{\eta_0} \ln\left(\frac{\dot{\gamma}_{0c}}{\dot{\gamma}_c}\right) \right]^{\frac{8}{11}} \qquad (3.77)$$

Eq. 3.77 is used to calculate the separation for the EHL component in the ML regime. The shear thinning effect may influence the film formation and in the same time the shear stress of the lubricant.
The friction in the EHL regime is proportional to $\text{arcsinh}(\eta v^{dif}/(h\tau_0))$ (see Eq. 2.23) and therefore a competition between the viscosity and the film thickness (for a certain velocity) influences the coefficient of friction.
In the next section the influence of the shear thinning effect on the Stribeck curve is discussed.

3.4.3 Results

The influence of shear thinning of the lubricant on the film thickness depends on the low shear rate viscosity over high shear rate viscosity ratio η_0/η_∞ and the critical value of the shear rate $\dot{\gamma}_c$. Therefore, Stribeck curve calculations are performed for different values of the ratio η_0/η_∞ (Fig.3.13) and different values of the critical shear rate $\dot{\gamma}_c$ (Fig.3.14). The values of the other parameters used in the calculations are presented in table 3.4.

Table 3.4: Input parameters for the Stribeck curve calculations.

property	value	unit	description
σ_s	0.487	μm	standard deviation of asperities
β	2.6	μm	radius of asperities
n	$13 \cdot 10^9$	$1/m^2$	density of asperities
B	$20 \cdot 10^{-3}$	m	length of the contact
R	$20 \cdot 10^{-3}$	m	reduced radius of cylinder
F	300	N	normal load
E	231	GPa	combined elasticity modulus
η_0	0.1	Pa·s	viscosity
α	$2 \cdot 10^{-8}$	Pa^{-1}	viscosity pressure coefficient
τ_o	2.5	MPa	Eyring shear stress
f_c	0.13	-	coefficient of friction in BL

In Fig.3.13 the effect of the viscosity ratio η_0/η_∞ on the Stribeck curve is presented. The value of the critical shear rate $\dot{\gamma}_c$ and viscosity at ambient pressure are kept constant i.e. $\dot{\gamma}_c = 1 \cdot 10^6$ 1/s and $\eta_0 = 0.1$ Pa·s, whilst the value of the viscosity at

high shear rates is varied. It can be noticed that by increasing the ratio η_0/η_∞ the transition from the ML to EHL regime shifts to the higher velocity region and the separation in the EHL regime decreases. By increasing the ratio η_0/η_∞ the friction in the EHL regime decreases as well. This is caused by the fact that for a certain velocity by decreasing the viscosity, the film thickness decreases less.

In Fig.3.14 the effect of the critical shear rate $\dot{\gamma}_c$ on the Stribeck curve and separation is presented. The value of the ratio η_0/η_∞ is kept constant i.e. $\eta_0/\eta_\infty = 3$ while the critical shear rate is varied. It can be seen that by decreasing the critical shear rate the separation in the EHL regime decreases and as a consequence the transition from the ML to EHL regime shifts to the right. The friction in the EHL regime decreases when the critical shear rate $\dot{\gamma}_c$ decreases from 10^7 to 10^6 s^{-1} whilst for $\dot{\gamma}_c = 10^5$ s^{-1} the friction in the EHL regime increases. In order to explain this effect, Fig.3.15 shows the influence of the critical shear rate on the Stribeck curve and viscosity plotted as a function of the shear rate. As it can be noticed for $\dot{\gamma}_c = 10^7$ s^{-1} and $\dot{\gamma}_c = 10^6$ s^{-1} the curves which describe the viscosity-shear rate dependency have the same slopes when the shear rate $\dot{\gamma}$ is between 10^6 s^{-1} and 10^7 s^{-1} while for $\dot{\gamma}_c = 10^5$ s^{-1} the viscosity is almost constant when the shear rate $\dot{\gamma}$ is between 10^6 s^{-1} and 10^7 s^{-1}.

Friction in the EHL regime is proportional to $\text{arcsinh}(\eta\dot{\gamma}/\tau_0)$ and therefore the friction due to the viscous shear for $\dot{\gamma}_c = 10^5$ increases faster with the shear rate than in the other two cases, resulting in a higher friction in the EHL regime for $\dot{\gamma}_c = 10^5$ s^{-1}.

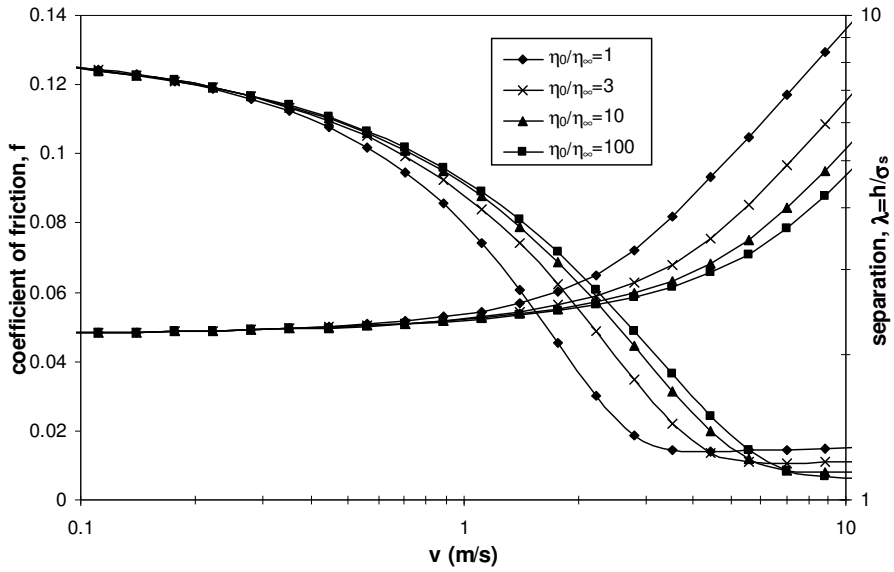

Fig.3.13: Generalized Stribeck curve and corresponding separation, by varying the ratio η_0/η_∞, $\dot{\gamma}_c = 10^6$ s^{-1}.

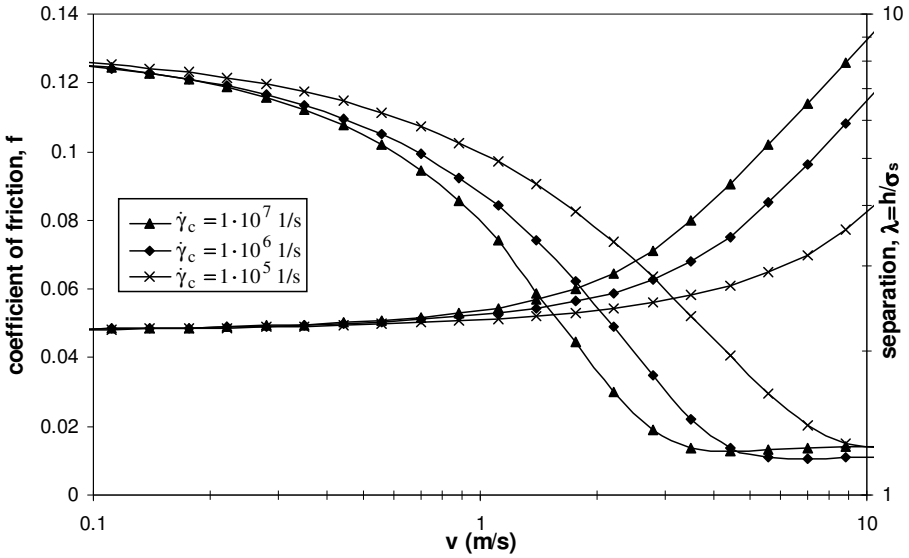

Fig.3.14: Generalized Stribeck curve and corresponding separation by varying the critical shear rate $\dot{\gamma}_c$, $\eta_0/\eta_\infty = 3$.

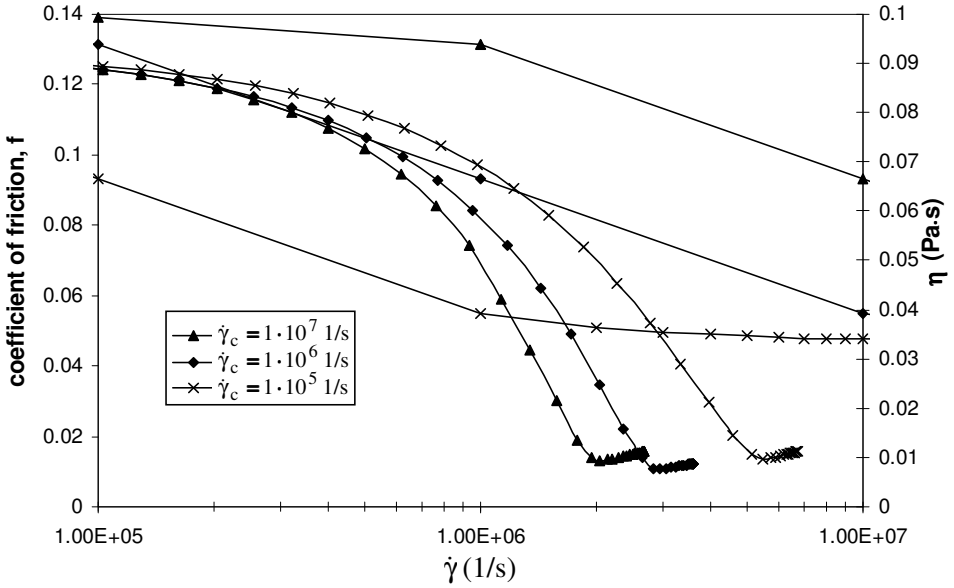

Fig.3.15: Stribeck curve and viscosity as a function of the shear rate.

3.4.3 Summary

A film thickness formula has been developed in order to predict the Stribeck curve for shear thinning lubricants. The influence of shear thinning lubricants on the Stribeck curve is investigated by varying two parameters. On one hand the low shear rate viscosity over high shear rate viscosity ratio η_0/η_∞ was varied while the critical shear rate $\dot{\gamma}_c$ was kept constant and on the other hand the critical shear rate $\dot{\gamma}_c$ was varied while the viscosity ratio η_0/η_∞ was kept the same.
By increasing the viscosity ratio η_0/η_∞ the transition from the ML to EHL regime shifts to the higher velocity region while the friction in the EHL regime decreases.
When the value of the critical shear rate $\dot{\gamma}_c$ decreases, the transition from the ML to EHL regime shifts to the high velocity region while the friction in the EHL regime is controlled by the viscosity-shear rate dependency.
In the next section the Stribeck curve model will be improved by taking into account starvation of lubricated line contacts.

3.5 Stribeck curve for starved line contacts

3.5.1 Introduction

In literature a lot of attention is paid to starvation, however, the investigations were solely conducted for the full-film situation (i.e. no contact takes place between the opposing surfaces) with the emphasis on the inlet boundary conditions and cavitation. Most of these investigations were applied to the circular contact situation. For the starved line contact situation, only a few papers were published, for instance Wolveridge et al. (1971). In the work of Wolveridge et al. a correction on the film thickness formula for line contacts due to starvation is presented. Combining this modified film thickness relation for starved line contacts with the mixed lubrication model as presented in section 3.2, this will result into a mixed lubrication model for starved line contacts. In this chapter the consequences of starvation on friction depicted in the generalised Stribeck curve due to change in film formation is discussed. In section 3.5.2 the starved film thickness relation for smooth line contacts is presented and implemented in the mixed lubrication model for statistical rough surfaces. In the section 3.5.3 results of calculations are presented and discussed. The last section gives a summary concerning this section.

3.5.2 The starved model

In 1971 Wolveridge et al. published an article in which they presented the influence of starved conditions on the film thickness of a smooth line contact. In Fig.3.16 a two dimensional representation of the starved contact situation is presented in which h_{oil} is the supplied oil layer thickness and h'_{oil} is the oil layer thickness when surface tension is taken into account; x_i and x'_i are the lubricant inlet lengths belonging to the aforementioned lubricant layer thicknesses; h^*, b and v^{dif} are the starved film thickness, half contact width and the sliding velocity respectively. The surface tensions depend on the properties of the lubricant and the surface, see for instance Tian and Bhushan (1996). In this model h_{oil} and h'_{oil} are taken as equals.
According to Crook (1958) the oil layer thickness in the converging entry is given with good approximation by:

$$h_{oil} = h^*[1 + \frac{4\sqrt{2}}{3}\phi^{\frac{3}{2}}] \tag{3.78}$$

where ϕ is a non dimensionless coordinate:

$$\phi = b^{\frac{1}{3}} x_i / (2Rh^*)^{\frac{2}{3}} \tag{3.79}$$

in which R is the reduced radius.

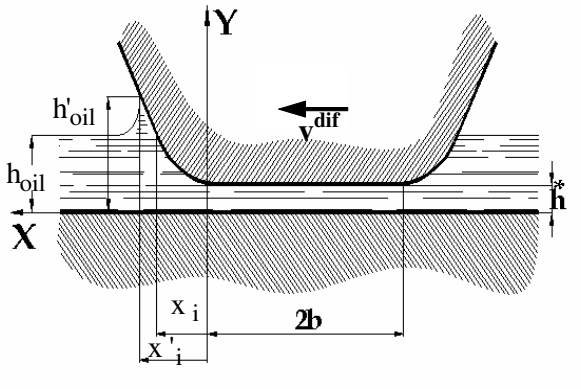

Fig.3.16: Schematic representation of starved situation.

The ratio between the film thickness for the starved (h^*) and fully flooded condition (h) is derived by Wolveridge et al., based on computational solutions of Occurt and Cheng (1966), as a function of dimensionless lubricant inlet length ψ_i :

$$\frac{h^*}{h} = \frac{H_C^*}{H_C} = \theta = f(\psi_i) \tag{3.80}$$

where:

$$\psi_i = b^{\frac{1}{3}} x_i / (2Rh)^{\frac{2}{3}} \tag{3.81}$$

In order to implement the numerical solution of Wolveridge et al. in the mixed lubrication mode,l an analitical solution is needed.
The numerical solutions are fitted well by the following equation:

$$\theta = \frac{h^*}{h} = \frac{H_C^*}{H_C} = \frac{2}{\pi} \arctan(2.7 \cdot \psi_i) \tag{3.82}$$

as can be noticed in Fig.3.17. If in the EHL component of the mixed lubrication model, the film thickness formula is replaced by the fitted starved film thickness formula (Eq. 3.82), the starved mixed lubrication model is completed.

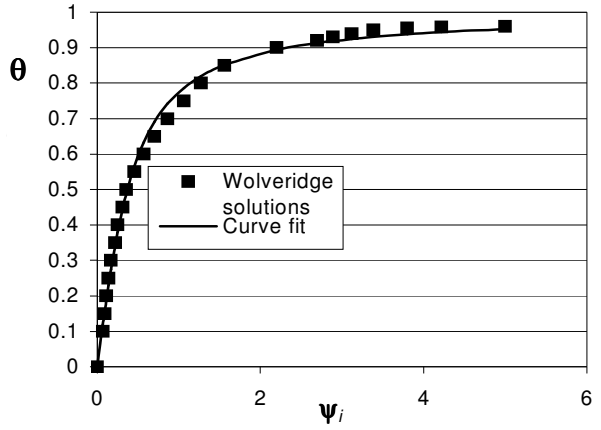

Fig.3.17: The approximation of numerical solutions of Wolveridge et al. (1971).

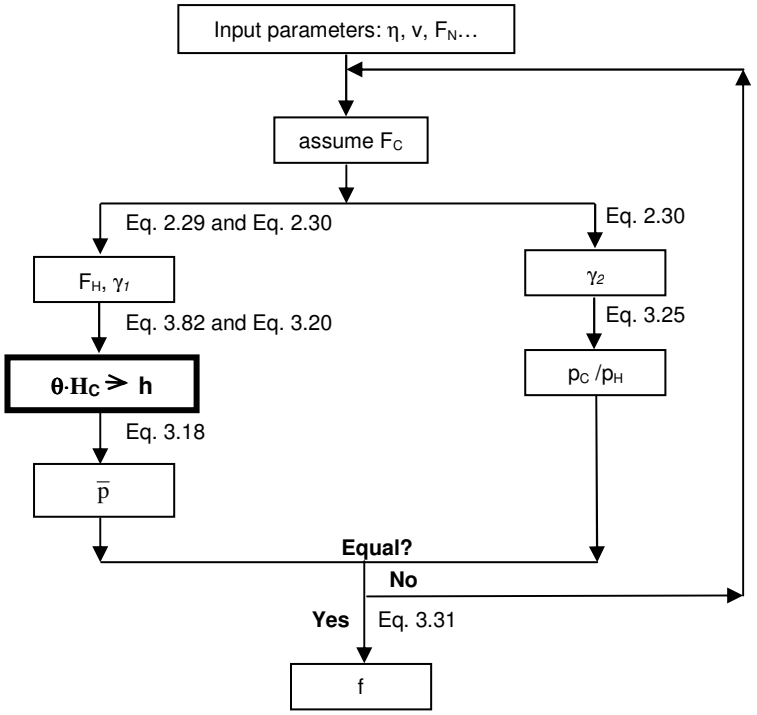

Fig.3.18: Solution scheme of the coefficient of friction calculation.

In Fig.3.18 the solution scheme for the starved Stribeck curve calculations is presented.
In the next section, results of the presented starved Stribeck model for two different sets of roughness parameters are presented.

3.5.3 Results of starved Stribeck curve calculations

The Stribeck curve for starved lubrication conditions can now be calculated. Two sets of surface parameters in combination with the supplied oil layer thickness h_{oil} are used to see their influence on friction under starved conditions. The parameters used for the calculations are presented in table 3.5.
The surface parameters of reference case 1 are of a spur gear transmission and the parameters of reference case 2 are taken from Johnson and Spence (1991).

Table 3.5: Input parameters used for Stribeck curve calculations.

property	value reference case 1	value reference case 2	unit	description
n	$1 \cdot 10^{11}$	$13 \cdot 10^{9}$	m^{-2}	density of asperities
β	10	2.6	μm	radius of asperities
σ_s	0.05	0.49	μm	standard deviation of asperities
B	$10 \cdot 10^{-3}$	$12.7 \cdot 10^{-3}$	m	length of the contact
E'	231	231	GPa	combined elasticity modulus
R	$20 \cdot 10^{-3}$	$19 \cdot 10^{-3}$	m	reduced radius of cylinder
η_0	0.0202	0.038	Pa·s	viscosity
α	$2 \cdot 10^{-8}$	$2 \cdot 10^{-8}$	Pa^{-1}	viscosity pressure coefficient
τ_0	2.5	2.5	MPa	Eyring shear stress
f_c	0.13	0.13	-	coefficient of friction in
F_N	1000	1000	N	BL normal load

The results of the calculation of the Stribeck curve and the separation for the two reference cases performed for different oil layer thickness over roughness ratios, h_{oil}/σ_s are given in Fig.3.19 and 3.20.
The tendency of the starved Stribeck curve and the corresponding separation as a function of oil layer thickness ratio h_{oil}/σ_s can be described as follows:

- When the oil layer thickness (h_{oil}) is larger than, say, 6 times standard deviation of summit heights (σ_s), the Stribeck curve and separation do not change compared to the fully flooded condition.

- If the oil layer thickness ratio (h_{oil}/σ_s) varies between 6 and, say, 0.7 the friction level in the EHL and ML regimes starts to increase and the separation decreases, Fig.3.19 and Fig.3.20. The mixed lubrication regime becomes less steep in this range of oil layer thickness over roughness ratio. The transition from BL to ML and from ML to EHL respectively stays approximately at the same transition velocity, only the friction level changes. The Stribeck curve for starved lubricated contact "pivots" at the transition ML/BL as the ratio of h_{oil}/σ_s decreases.

- For values of oil layer thickness over roughness ratio's (h_{oil}/σ_s) less than ≈ 0.7 the Stribeck curve tends to transform into a straight line and the separation stays on the same level as in the BL regime, Fig.3.19 and Fig.3.20.

Similar results have been found for point contacts by Q. Liu (2002).

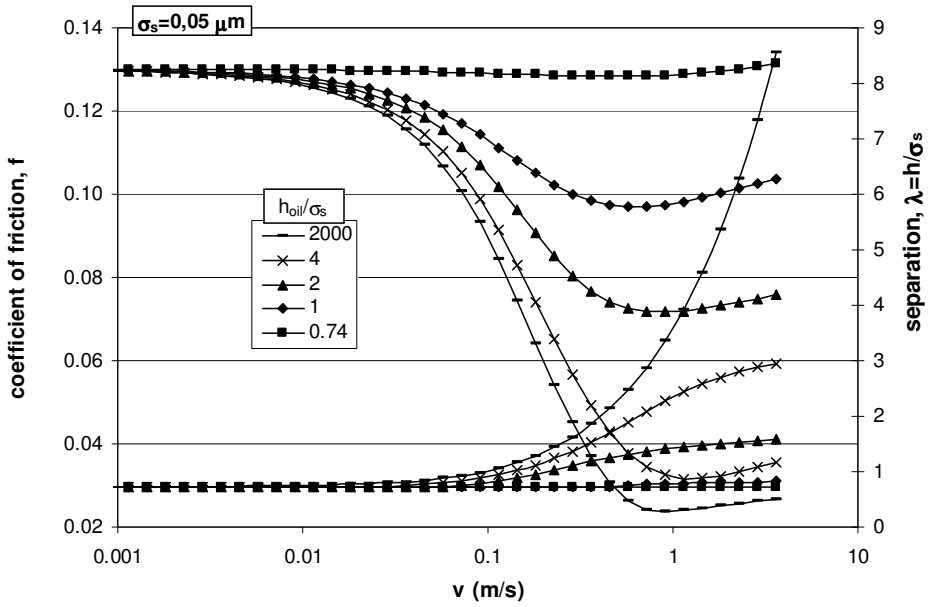

Fig.3.19: Influence of starvation on the Stribeck curve and the separation reference case 1, see table 3.5.

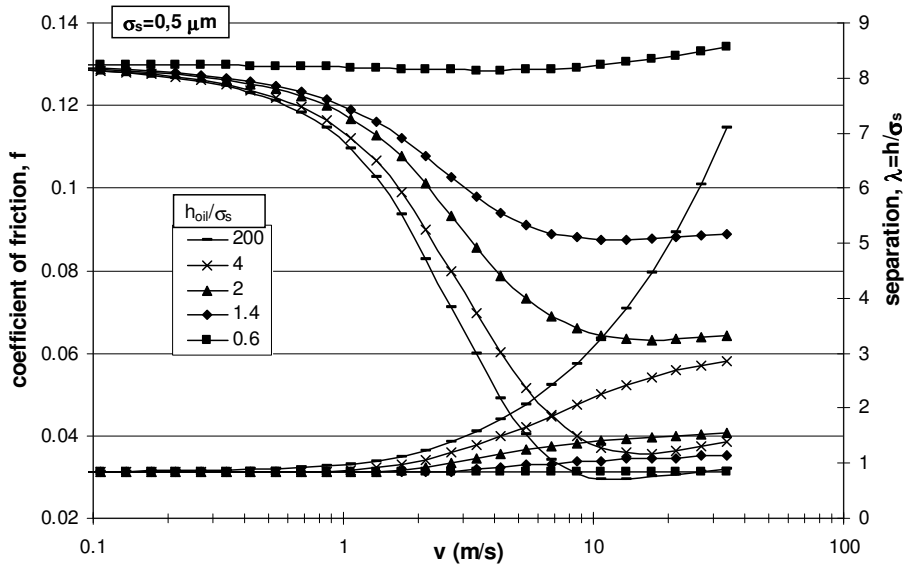

Fig.3.20: Influence of starvation on the Stribeck curve and the separation for the reference case 2, see table 3.5.

3.5.4 Summary

A model has been developed in order to calculate the starved Stribeck curve and separations in the mixed lubrication regime. The model is a combination of the mixed lubrication model and numerical calculations for starved smooth lubricated line contacts of Wolveridge et al. (1971). Due to surface tensions h_{oil} increases which results in an increase of the film thickness and due to heat development in the contact, reduces the inlet viscosity which reduces the film thickness. Both these effects are neglected, however in real contacts these two main effects may compensate each other.

The calculations have been performed for two sets of roughness parameters. In terms of oil layer thickness over roughness ratio (h_{oil}/σ_s) the results show the same trend for the two reference cases. For values of oil layer thickness over roughness ratio (h_{oil}/σ_s) larger than approximately 6, the Stribeck curve and separation do not change. If oil layer thickness over roughness ratio is in the range of 6 to 0.7, the friction starts to increase and the film thickness decreases. When oil layer thickness over roughness ratio is less than approximately 0.7, the Stribeck curve tends to transform into a straight line (constant friction level) and separation stays on the same value as in the BL regime.

In order to be able to predict the Stribeck curve for real rough surfaces in the next chapter the mixed lubrication model will be adapted by taking into consideration the deterministic contact model for rough surfaces.

3.6 Conclusions

Deterministic contact models for two rough surfaces, shear thinning lubricants and starved lubrication have been developed. When the manufactured surfaces have a Gaussian distribution of summits, the statistical contact model is recommended due to its applicability.

In section 3.2 a statistical mixed lubrication model for highly loaded line contacts was presented. It was shown that the load and viscosity have an influence on the transition from BL to ML regime. The influence of the roughness parameters on the stribeck curve was also studied. The results show that the Stribeck curve predictions strongly depend on the roughness parameters. By increasing σ_s the transitions from BL to ML and from ML to EHL shift to the right (higher velocities) while by increasing β the opposite effect is obtained.

Next, the effect of two rough surfaces on the Stribeck curve was investigated by extending the contact model of Greenwood and Tripp. The difference between the new contact model and the model of Greenwood and Williamson is that the new contact model takes into account the misalignment of the asperity couples resulting in a smaller separation under BL conditions, whereas the model of Greenwood and Williamson does not consider this effect and therefore the resulting separation in the BL regime is larger. It was shown that the difference in separation between the two models is significant when the two contacting surfaces have comparable roughness parameters.

In section 3.4 the shear thinning effect was incorporated in the film thickness relation. The influence of the shear thinning effect on the Stribeck curve was investigated by varying two parameters, i.e. the low shear rate viscosity over high shear rate viscosity ratio η_0/η_∞ and critical shear rate $\dot{\gamma}_c$. It was found that by increasing the viscosity ratio η_0/η_∞ the transition from the ML to EHL regime shifts to the higher velocity region while the friction in the EHL regime decreases. When the value of the critical shear rate $\dot{\gamma}_c$ decreases, the transition from the ML to EHL regime shifts to the high velocity region while the friction in the EHL regime is controlled by the viscosity-shear rate dependency.

In section 3.5 a model is presented which is able to predict the influence of starvation on the Stribeck curve. It was shown that for values of oil layer thickness over roughness ratio (h_{oil}/σ_s) larger than approximately 6, the Stribeck curve and separation do not change. If oil layer thickness over roughness ratio is on the range of 6 to 0.7, the friction starts to increase and the film thickness decreases.

When oil layer thickness over roughness ratio is less than approximately 0.7, the Stribeck curve tends to transform into a straight line (constant friction level) and separation stays on the same value as in BL regime.
In the next chapter a mixed lubrication model for deterministic rough surfaces will be presented.

References

Bair, S. and Khonsari, M. (1996), “An EHD inlet zone analysis Incorporating the second Newtonian”, Journal of Tribology, Vol. 118, 341-343.

Bair, S. and Winer, W.O. (1996), “A simple formula for EHD film thickness of non-Newtonian liquids”, In proceeding of 23rd Leeds-Lyon Symposium EHD-96, 235-241.

Bair, S. (1998), “Elasto-hydrodynamic film forming with shear thinning liquids”, Journal of Tribology, Vol. 120, 173-178.

Briscoe, B.J. (1981), “Friction and wear of organic solids and the adhesion model of friction”, Philosophical Magazine, Vol. A 43(3), 511-527.

Cameron, A. (1966), “The principles of lubrication”, Imperial College Press, London UK, 207.

Chynoweth, S., Coy, R.C., Michopoulos, Y. and Scales, L.E. (1995), “Simulated lubricant non-Newtonian behaviour under elasto-hydrodynamic conditions”, In Proceeding of the International Tribology Conference, Yokohama, 663-668.

Crook, A.W. (1958), “The lubrication of rollers-I”, Phil. Trans. R. Soc. London Series A., Vol. 250, 387.

Cross, M.M. (1965), “Rheology of non-Newtonian fluids: a new flow equation for pseudo plastic systems”, J. Colloid Sci., Vol. 20, 417-437.

Gelinck, E.R.M. (1999), “Mixed lubrication of line contacts”, PhD thesis, University of Twente, Enschede, The Netherlands.

Gohar, R. (2001), “Elasto-hydrodynamics”, Imperial College Press, London UK, 108-112.

Greenwood, J.A. and Williamson, J.B.P. (1966), “Contact of nominally flat surfaces”, Phil. Trans. R. Soc. London Series A, Vol. 295, 300-319.

Greenwood, J.A. and Tripp, J.H. (1970), “The contact of two nominal flat rough surfaces”, Proc. Inst. Mech. Engrs., Vol. 185, 625-633.

Greenwood, J.A. (1984), “A unified theory of surface roughness”, Phil. Trans. R. Soc. London Series A, Vol. 393, 133-157.

Greenwood, J.A. and Kauzlarich, J.J. (1997), “Elasto-hydrodynamic film thickness for shear-thinning lubricants”, Proc. Instn. Mech. Engrs., Vol. 212 Part J, 179-191.

Grubin, A.N. and Vinogradova, I.E. (1949), Central Scientific Research Institute for Technology and Mechanical Engineering Book 30 (Moscow), D.S.I. R. Trans. No. 337.

Hertz, H. (1881), “Über die berührung fester elastischer körper”, Journal für die reine und angewandte Mathematik, Vol. 92, 156-171.

Johnson, K.L., Greenoowd, J.A. and Poon, S.Y. (1972), “A simple theory of asperity contact in elasto-hydrodynamic lubrication”, Wear, Vol. 19, 91-108.

Johnson, K.L. (1985), “Contact mechanics”, Cambridge University Press, Cambridge, UK.

Johnson, K.L. and Spence, D.I. (1991), “Determination of gear tooth friction by disc machine”, Tribology International, Vol. 24(5), 269-275.

Liu, Q. (2002), “Friction in mixed and elasto-hydrodynamic lubricated contacts Including thermal effects”, PhD. Thesis, University of Twente, Enschede, The Netherlands.

Moes, H. (1997), “Lubrication and beyond”, lecture notes 115531, University of Twente, Enschede, The Netherlands.

Orcutt, F.K. and Cheng, H.S. (1966), “Lubrication of rolling contact instrument bearings, giro spin axis”, Hydrodynimic Bearing Symposium, Vol. 2, USA (M.I.T. Instrument Lab., Cambridge, Mass.).

Schipper, D.J. (1988), “Transitions in the lubrication of concentrated contacts”, PhD thesis, University of Twente, Enschede, The Netherlands.

Taylor, R.I. (1998), “The inclusion of lubricant shear thinning in the short bearing approximation”, Proc. Instn. Mech. Engrs., Vol. 213 Part J, 35-46.

Tian, X. and Bhushan, B. (1996), “The micro-meniscus effect of a thin liquid film on the static friction of rough surface contact”, J. Phys. D: Appl. Phys., Vol. 29, 163-178.

Whitehouse, D.J. and Archard, J.F. (1970), “The properties of random surfaces of significance in their contact”, Phil. Trans. R. Soc. London Series A, Vol. 316, 97-121.

Wolveridge, P.E., Baglin, K.P. and Archard, J.F. (1971), “The starved lubrication of cylinders in line contact”, Proc. Instn. Mech. Engrs., Vol. 181, 1159-1169.

Chapter 4

Stribeck curve for deterministic rough surfaces

4.1 Introduction

In the previous chapter the Stribeck curve model for statistical rough surfaces was extended by taking into consideration different aspects, i.e. two rough surfaces, shear thinning lubricants and starved lubrication. The contact model of Greenwood and Williamson for statistical rough surfaces was used to model the BL component of the mixed lubrication model of Gelinck and Schipper (see section 3.2.1.2) which is extended for high load (i.e. high contact pressure) situations by incorporating Eq. 3.20. Greenwood and Williamson's model assumed that the asperities are spheres with the same radius and the model is restricted to a Gaussian distribution of the summit heights. In reality the asperities do not have the same radius, being spheres or ellipsoids and most of the surfaces have a distribution of the asperity which is not Gaussain. It is known that the model of Greenwood and Williamson is quite accurate as long as aforementioned conditions are obeyed. The main disadvantage of this model is the assumed Gaussian distribution of equal summits.
Recently, a lot of three dimensional surface topography measurement equipment has been developed. As a consequence, in order to avoid Greenwood and Williamson's assumptions, a deterministic contact model for rough surfaces is developed. In section 4.2 the deterministic contact model is described and in section 4.3 a comparison between the deterministic and the statistic contact model on the Stribeck curve is made. In section 4.4 the effect of the circular versus the elliptical asperity contact model on the Stribeck curve is investigated. In section 4.5 the effect of elastic versus elastic - plastic contact on the Stribeck curve is studied and in section 4.6 the shear stress - pressure dependency effect on the boundary lubrication regime is investigated. In the last section conclusions concerning this chapter are drawn.

4.2 Deterministic contact model

In the last years many three dimensional surface topography measurement devices have been developed, for example the interference microscope. The interference microscope provides digital data of the measured surface topography which can be used for different purposes (e.g. to calculate the load carried by the asperities of the measured surface when it is deformed by a flat surface, see Fig.4.1).

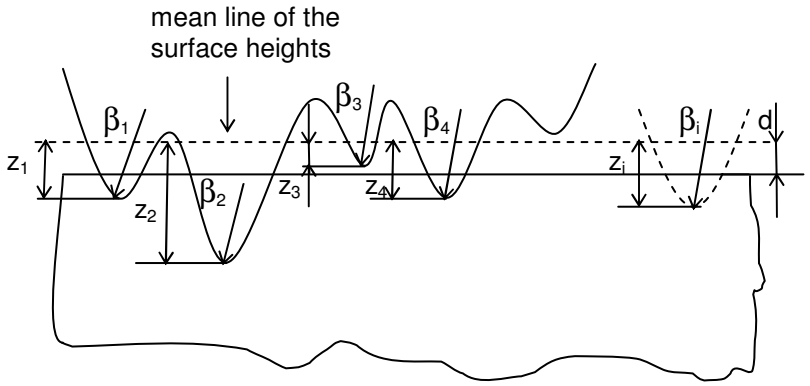

Fig.4.1: The contact between a rough surface and a flat surface.

In Fig.4.1 the contact between a rigid flat surface against a rough one is presented. For a given separation d between the two surfaces, the number of asperities, the real contact area, and the total force carried by the contact can be calculated deterministically by summing up their local components. The asperities are considered to be ellipsoids with different radii (the asperity radii are measured in sliding and in perpendicular direction β_{xi}, β_{yi}) and it is assumed that they deform independently from each other.
The compliance of an asperity is defined as:

$$w_i = z_i - d \tag{4.1}$$

where d is the separation and z_i the individual summit height (Fig.4.1).
By knowing the indentation w_i of each deformed asperity, the total real contact area and total normal force acting on the surface can be calculated by adding the individual components of each asperity, see Appendix B. The parameters which govern the BL component of the ML model are the pressure (force) acting on the surface, separation and the real contact area (see section 3.2.1.2). Therefore, the deterministic method can be used to model the BL component of the ML model. By

implementing the deterministic contact model in the ML model, the Stribeck curve for real rough surfaces can be predicted.
In the next section a comparison between the statistical and the deterministic contact model on the Stribeck curve is made.

4.3 Comparison between deterministic and statistic contact model on Stribeck curve

The Stribeck curve for deterministic rough surfaces can be calculated by varying the velocity. In order to compare the deterministic and the statistic contact model on the Stribeck curve, two different surfaces are used (see Fig.4.2). The measured surface height distribution of one surface is Gaussian (Fig.4.2[a]) and for the other surface, the surface height distribution is typically non-Gaussian (Fig.4.2[b]). The roughness parameters of the two surfaces are presented in table 4.2.
In Fig.4.3 and Fig.4.4 comparison between the deterministic and the statistic contact model on the Stribeck curve and the separation, for the Gaussian and non Gaussian surface are presented. The input parameters used for the Stribeck curve calculations are presented in the table 4.1. It should be mentioned that the asperities deform elastically according to the Hertzian theory (see Appendix B).
When the measured surface height distribution is Gaussian, the difference between the two contact models (deterministic and statistic) on the Stribeck curve is insignificant (Fig.4.3[a] and 4.3[b]); e.g. for a normal force of 1000 N the two models show almost the same Stribeck curve and for a normal force of 5000 N there is an insignificant difference between the two models on the Stribeck curve. The deviation of the value of the measured radius of each asperity from the average value β_{avg} (Fig.4.2[a]) is in this case not that large, and as it can be noticed in Fig.4.3[a] and 4.3[b] it is not affecting the result of the "deterministic Stribeck" curve compared to the "statistic Stribeck curve".

Table 4.1: The input parameters for Stribeck curve calculations.

property	value	unit	description
B	$10 \cdot 10^{-3}$	m	length of the contact
R	$20 \cdot 10^{-3}$	m	reduced radius of cylinder
E'	231	GPa	combined elasticity modulus
η_0	0.0202	Pa·s	viscosity
α	$2 \cdot 10^{-8}$	Pa^{-1}	viscosity pressure coefficient
f_c	0.13	-	coefficient of friction in BL
τ_0	2.5	MPa	Eyring shear stress

Table 4.2: The statistical roughness parameters of the two surfaces.

description	σ_s [µm]	β [µm]	n [1/m^2]
case 1	0.05	10	$1.15 \cdot 10^{11}$
case 2	0.16	10	$1.8 \cdot 10^{10}$

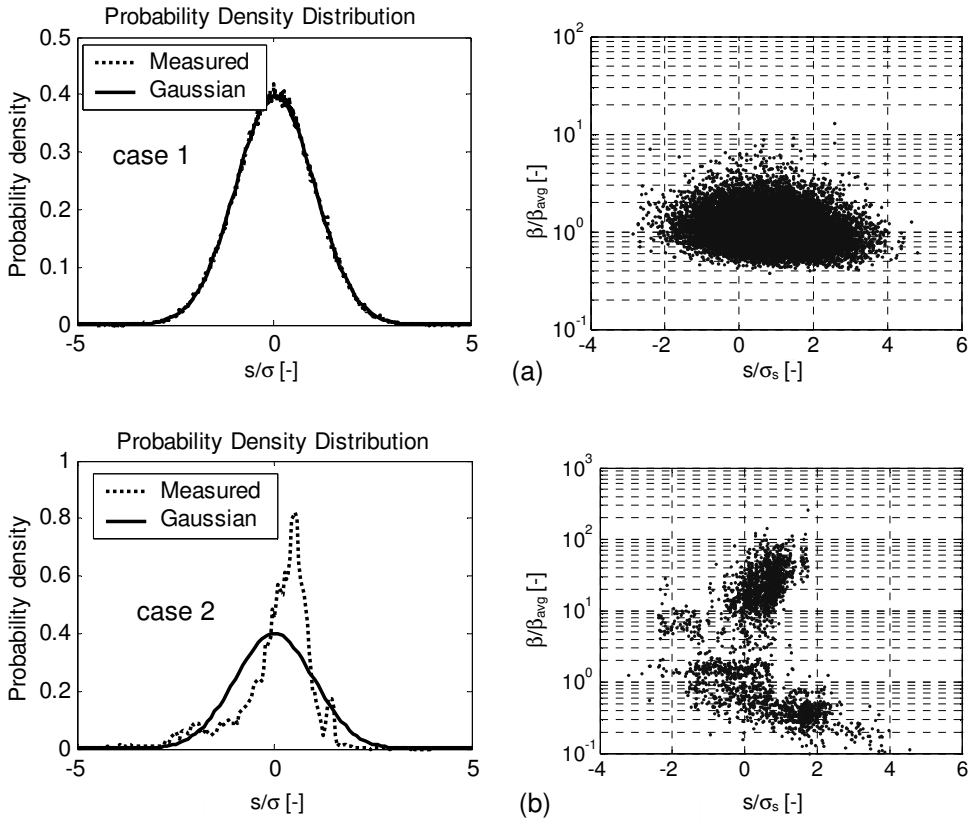

Fig.4.2: Distribution of surface heights and the radii of each asperity as a function of the dimensionless asperity height (s/σ, s/σ_s) for a Gaussian (a) and a non-Gaussian surface height distribution (b).

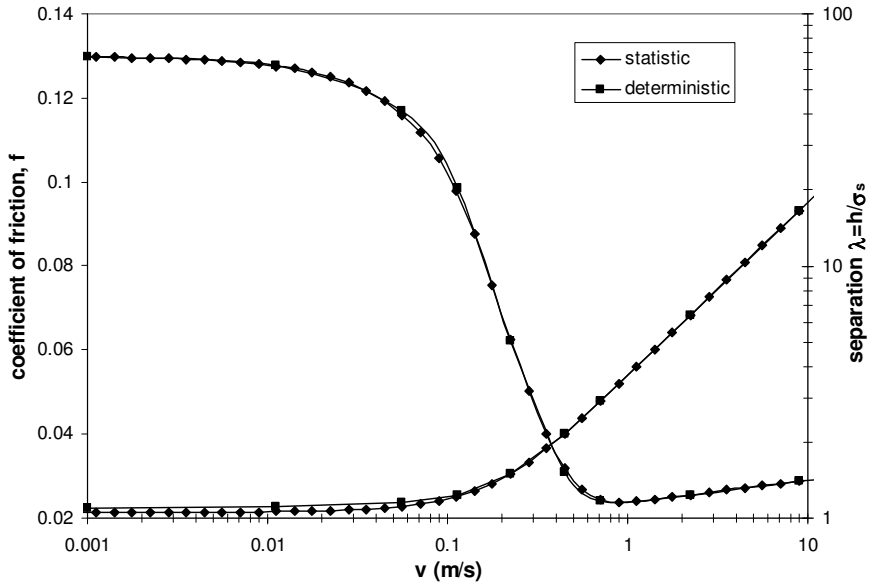

(a)

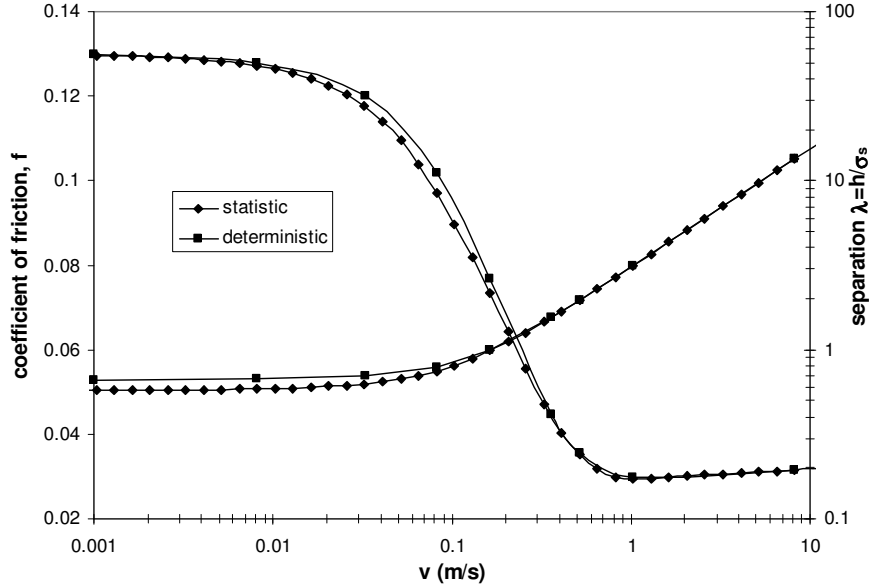

(b)

Fig.4.3: Comparison between the deterministic and the statistic contact model with respect to the Stribeck curve and separation for a surface with a Gaussian height distribution (reference case 1) for different normal forces.
a) F_N = 1000 N, $\overline{p}_H = 0.35$ GPa and b) F_N = 5000 N, $\overline{p}_H = 0.77$ GPa.

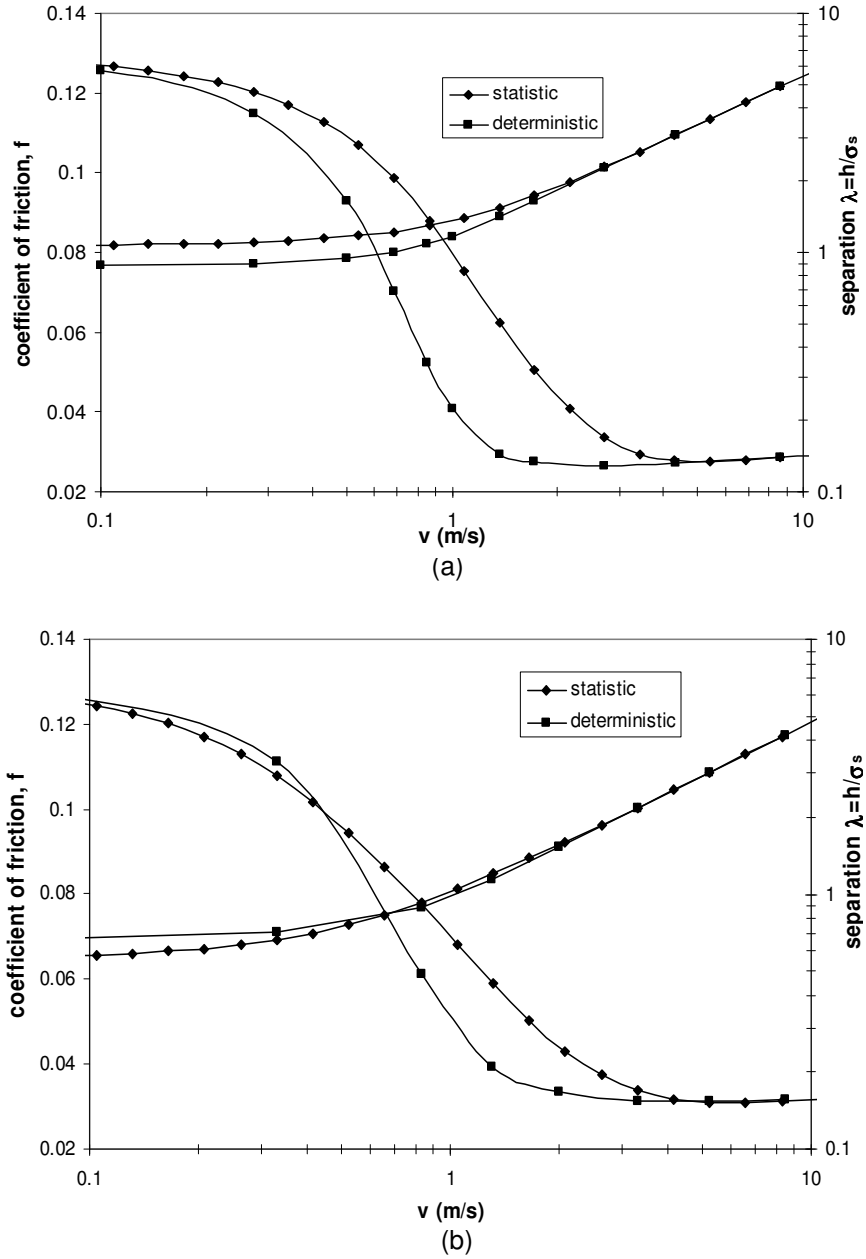

Fig.4.4: Comparison between the deterministic and the statistic contact model with respect to the Stribeck curve and separation for a surface with a non Gaussian height distribution (reference case 2) for different normal forces a) F_N = 1000 N, $\overline{p}_H = 0.35$ GPa and b) F_N = 5000 N, $\overline{p}_H = 0.77$ GPa.

In Fig.4.4 a comparison between the statistic and the deterministic contact model for two different normal loads on the Stribeck curve for a non Gaussian surface height distribution (Fig.4.2[b]) is presented. As can be noticed, in this case, there is a significant difference between the two models on the Stribeck curve. The difference between the two models on the Stribeck curve is caused mainly due to the difference between the measured and the equivalent Gaussian surface height distribution (see Fig.4.2[b]). For example when the normal load F_N is 1000 N (Fig.4.4[a]) the separation λ between the two contacting surfaces in the BL regime for the deterministic contact model case (λ = 0.88) is smaller compared to the statistic case (λ = 1.1), due to the difference between the measured and the Gaussian surface heights distribution (see Fig.4.2[b]). As a consequence, the ML regime for the deterministic contact model shifts to the lower velocity region compared to the statistical contact model (Fig.4.4[a]).
For the 5000 N normal load (Fig.4.4[b]) situation the separation λ in the BL regime for the deterministic case (λ = 0.67) is a bit larger than for the statistic case (λ = 0.58) which can be explained by looking at the surface height distribution diagram (Fig.4.2[b]). When the dimensionless asperity height s/σ_s decreases from about 1 to 0.6 (Fig.4.2[b]) the number of the asperities in contact for the measured surface increases much more than for the equivalent Gaussian surface. Therefore, the contacting surface in this region is stiffer for the deterministic contact model compared to the statistic one and as consequence deforms less. Due to the small difference in the separation in the BL regime given by the two models, the friction level at the transition from BL to ML regime (v = 0.1 - 0.4 m/s) is almost the same (see Fig.4.4[b]). As the velocity increases (v = 0.6 - 2 m/s) the separation also increases (λ = 0.9 - 1.8) (Fig.4.4[b]) and due to the difference in the density distribution of the asperities (see Fig.4.2[b], $s/\sigma \approx$ 0.9 - 1.8) between the two considered surfaces, the equivalent Gaussian surface becomes stiffer. As a consequence, the load carried by the asperities in the statistic contact model case for this velocity range (v = 0.6 - 2 m/s) is larger compared to the deterministic contact model and therefore the Stribeck curve is more gradually (see Fig.4.4[b]).
The deviation of the value of measured radius of the asperities from the average value β_{avg} (Fig.4.2[b]) in this case is large and it is expected that it has an influence on the deterministic Stribeck curve compared to the statistic one. This effect cannot be separated from the effect of the surface heights distribution and therefore cannot be quantified.
It is clear for the two cases presented before that the Stribeck curve results obtained with the statistic and deterministic contact models are different when the distribution of the surface heights deviates from the Gaussian type. In the next section the effect of circular versus elliptical contact models on the Stribeck curve will be investigated.

4.4 Influence of the elliptical versus circular asperity contact model on the Stribeck curve

Many models assume the summit being a paraboloid or a sphere. In reality most of the summits are ellipsoids and the probability that they are paraboloids or spheres is rather small.
The influence on the Stribeck curve, considering the asperity being an ellipsoid (β_{xi}, β_{yi}) or its equivalent sphere β_{ei} is studied in this section by using the deterministic method described in the section 4.2.
From geometrical considerations (volume conservation) for the equivalent spherical asperity, the effective radius is taken as the square root of the product of the two principal radii (i.e. in sliding direction and perpendicular to this direction) of the considered ellipsoid:

$$\beta_{ei} = \sqrt{\beta_{xi} \cdot \beta_{yi}} \tag{4.2}$$

In Fig.4.5 two generated surfaces with different ellipticity ratios are presented. In order to characterise the ellipticity ratio of the surface, the following relation is considered:

$$\varphi = \frac{\beta_{x1} + \beta_{x2} + ...\beta_{xi} + ...\beta_{xn}}{\beta_{y1} + \beta_{y2} + ...\beta_{yi} + ...\beta_{yn}} \tag{4.3}$$

where β_{xi} and β_{yi} are the local summit radii in x and y direction (Fig.4.5).
The statistical roughness and the input parameters used to calculate the Stribeck curve are presented in table 4.3. In these calculations the asperities deform elastically according to the Hertzian theory (see Appendix B).
The influence on the Stribeck curve and separation of circular versus elliptical asperity contact for the two surfaces considered is investigated by varying the normal load (Fig.4.6 and 4.7).
For an ellipticity ratio of 0.995 (Fig.4.6[a] and 4.6[b]), as it is expected, there is almost no difference in the Stribeck curve between the elliptical and circular asperity contact.

Table 4.3: The statistical roughness and the input parameters for Stribeck curve calculations.

property	value	unit	description
σ_s (φ=0.995)	0.05	μm	standard deviation of asperities
β(φ=0.995)	10	μm	radius of asperities
n (φ=0.995)	$1 \cdot 10^{11}$	m^{-2}	density of asperities
σ_s (φ=0.15)	0.043	μm	standard deviation of asperities
β (φ=0.15)	7.17	μm	radius of asperities
n (φ=0.15)	$1.13 \cdot 10^{11}$	m^{-2}	density of asperities
B	$10 \cdot 10^{-3}$	m	length of the contact
R	$20 \cdot 10^{-3}$	m	reduced radius of cylinder
E'	231	GPa	combined elasticity modulus
η_0	0.0202	Pa·s	viscosity
α	$2.0 \cdot 10^{-8}$	Pa^{-1}	viscosity pressure coefficient
τ_0	2.5	MPa	Eyring shear stress
f_c	0.13	-	coefficient of friction

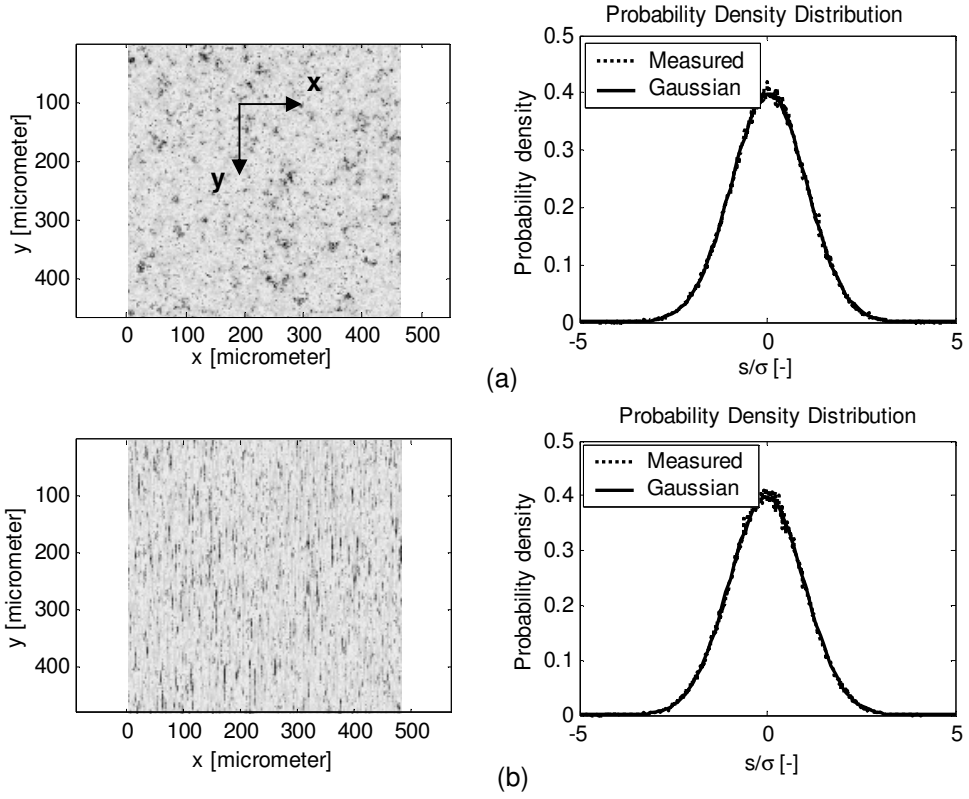

Fig.4.5: Generated surfaces and their histograms with different ellipticity ratios, a) φ = 0.995 and b) φ = 0.15.

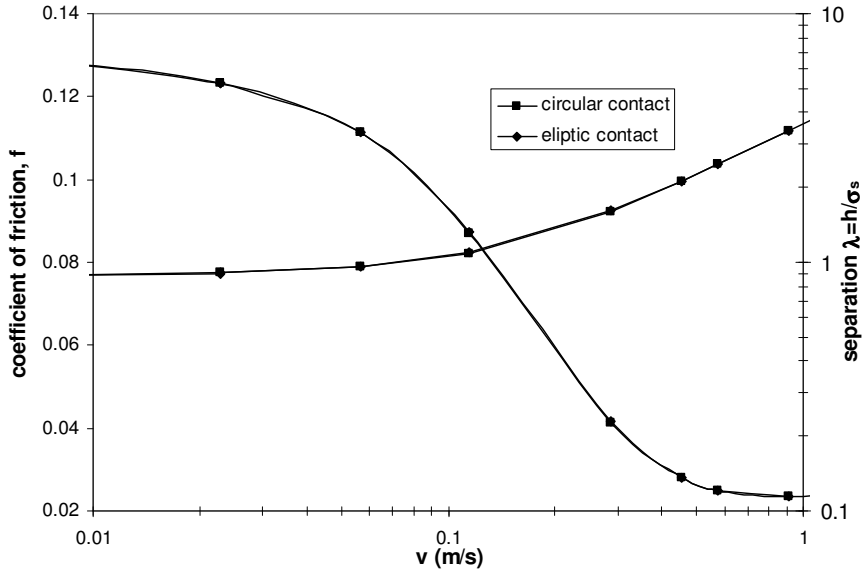

(a)

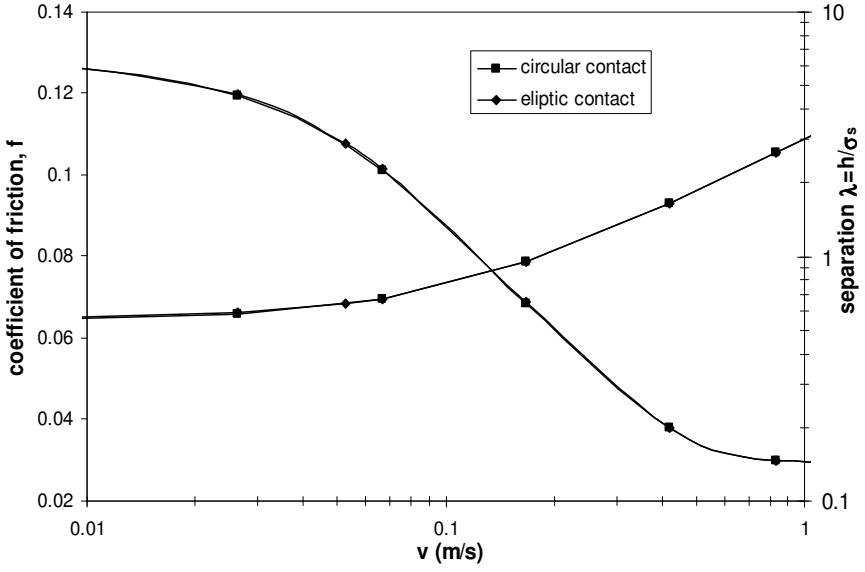

(b)

Fig.4.6: Stribeck curve and corresponding separation for a surface with an ellipticity ratio φ of 0.995, a) F_N = 1000 N, $\overline{p}_H = 0.35$ GPa and b) F_N = 5000 N, $\overline{p}_H = 0.77$ GPa.

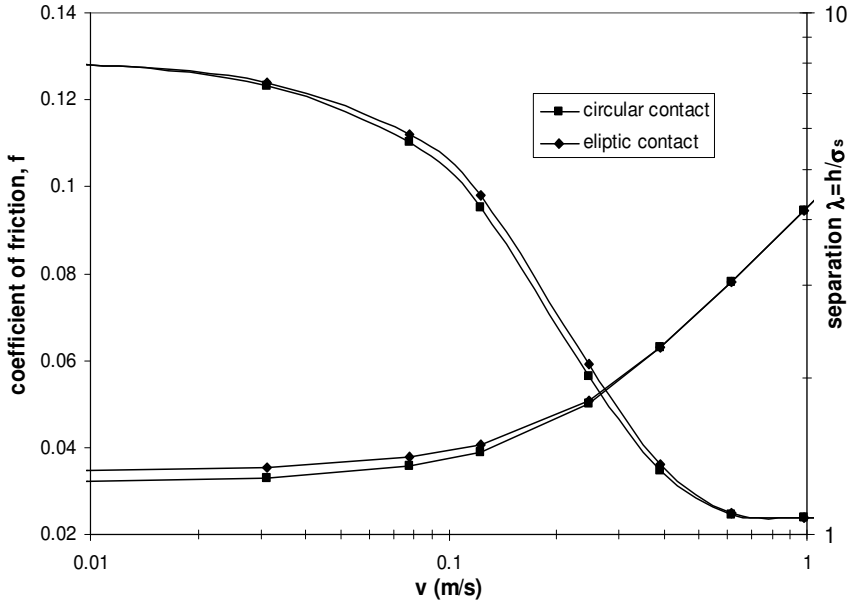

(a)

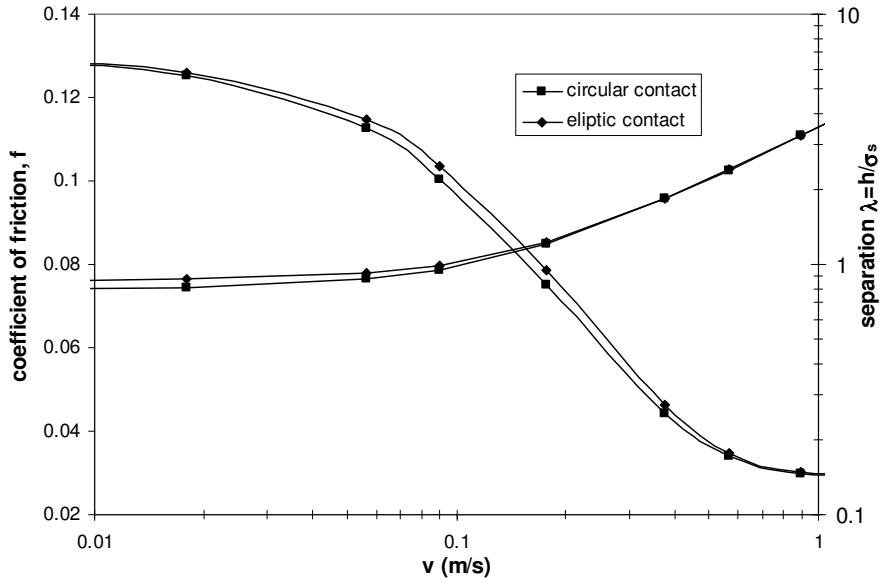

(b)

Fig.4.7: Stribeck curve and corresponding separation for a surface with an ellipticity ratio φ of 0.15, a) F_N = 1000 N, $\overline{p}_H = 0.35$ GPa and b) F_N = 5000 N, $\overline{p}_H = 0.77$ GPa.

As the ellipticity ratio decreases (φ = 0.15) there is an insignificant difference on the Stribeck curve between the two types of contacts (Fig.4.7[a] and 4.7[b]). This difference in the coefficient of friction is caused by the difference in separation which is slightly smaller in the circular contact case (for the circular contact the equivalent radius is defined by $\beta_{ei} = (\beta_{xi} \cdot \beta_{yi})^{1/2}$). When the local elliptical ratio (β_{xi}/β_{yi}) decreases, the circular contact becomes less stiff compared to the elliptical one and therefore the separation is smaller. The difference in determining the coefficient of friction in the ML regime by using a sphere instead of ellipsoid is up to 5%.

It can be concluded that the difference in the Stribeck curve by using a sphere for the asperity shape instead of ellipsoid is negligible and therefore the circular contact is recommended due to its simplicity and applicability in the asperity contact modeling.

In the next section, the influence of an elastic-plastic versus elastic deforming asperity contact on the Stribeck curve is investigated.

4.5 Influence of the elastic versus elastic-plastic asperity contact model on the Stribeck curve

4.5.1 Introduction

In this section the influence of the elastic versus elastic-plastic asperity contact model on the Stribeck curve is investigated by using the deterministic contact model described in section 4.2.

In section 4.5.2 the elastic-plastic asperity contact model is described and in section 4.5.3 the results of the Stribeck curve calculations are discussed.

4.5.2 The elastic-plastic asperity contact model

The contact model for rough surfaces introduced by Greenwood and Williamson (1966) assumes that the asperities deform elastically, however, in reality when the contact pressure exceeds the yield strength of the material, elastic-plastic deformation occurs. Tabor (1951) observed for metals that when the maximum Hertzian pressure reaches 0.6 the hardness of the metal, the first yield occurs. Based on Tabor's (1951) observation, Greenwood and Williamson introduced the critical indentation of an asperity. This reads:

$$w_e = \left(0.94 \frac{H}{E'} \right)^2 \beta \qquad (4.4)$$

where H is the hardness of the material and β is the radius of the asperity.
For $w > w_e$ elastic-plastic deformation occurs. Johnson (1985) stated that for metals the fully plastic regime occurs when the deformation of the asperity is about 54 times the value of the critical indentation ($w_p \cong 54 \cdot w_e$). Therefore, there is a large transition regime between the elastic and the fully plastic deformation situation. Based on the work of Johnson (1985), $w_p \cong 54 \cdot w_e$ and Abbott and Firestone (1933), $A_p = 2\pi\beta\omega$, Zhao (2000) introduced a solution for the contact area in the elastic-plastic transition regime of a spherical asperity. By using a cubic polynomial function, Zhao (2000) defined a smooth transition between the elastic and fully plastic deformation regime for the contact area (see Fig.4.8) as:

$$A_{iep} = \pi\beta_i w_i \left(1 - 2\left(\frac{w_i - w_e}{w_p - w_e} \right)^3 + 3\left(\frac{w_i - w_e}{w_p - w_e} \right)^2 \right) \tag{4.5}$$

where w_i is the asperity indentation depth.

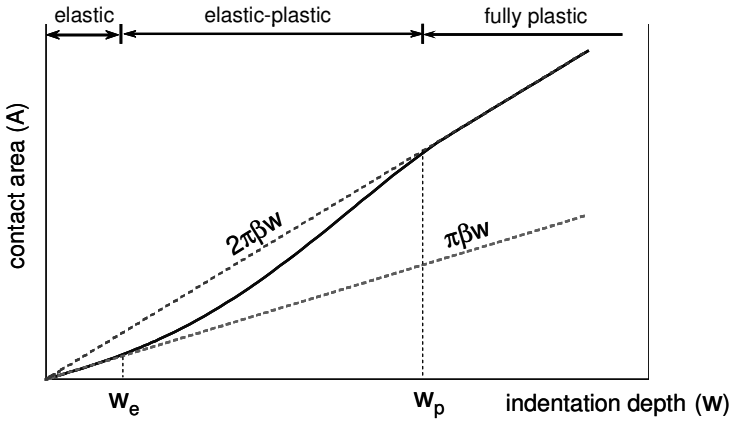

Fig.4.8: Contact area as a function of the indentation depth (Zhao (2000)).

Based on Francis' work (1976), Zhao assumed for the mean pressure evolution in the elasto-plastic regime the following relation:

$$p_{iep} = H - 0.6H \frac{\ln w_p - \ln w_i}{\ln w_p - \ln w_e} \tag{4.6}$$

By supposing that there is contact between the opposing surfaces, then a number of asperities are elastically deformed, some elastic-plastically and the other plastically depending on the asperity indentation value (w_i). The asperity contact area can be calculated according to the following scheme:

$$A_i(w_i) = \begin{cases} A_{ie}(w_i) & \text{if} \quad w_i \le w_e \\ A_{iep}(w_i) & \text{if} \quad w_e < w_i \le w_p \\ A_{ip}(w_i) & \text{if} \quad w_i > w_p \end{cases} \tag{4.7}$$

where

$$A_{ie} = \pi \beta_i w_i \tag{4.8}$$

is the elastic contact area when the asperity is elastically deformed,

$$A_{ip} = 2\pi \beta_i w_i \tag{4.9}$$

is the plastic contact area when the asperity is plastically deformed and A_{iep} is the elastic-plastic contact area given by Eq. 4.5.
By using the same scheme, the load carried by each asperity can be calculated as:

$$F_i(w_i) = \begin{cases} F_{ie}(w_i) & \text{if} \quad w_i \le w_e \\ F_{iep}(w_i) & \text{if} \quad w_e < w_i \le w_p \\ F_{ip}(w_i) & \text{if} \quad w_i > w_p \end{cases} \tag{4.10}$$

where

$$F_{ie} = \frac{4}{3} E' \beta_i^{0.5} w_i^{1.5} \tag{4.11}$$

is the load carried by an elastically deformed asperity,

$$F_{iep} = (H - 0.6H \frac{\ln w_p - \ln w_i}{\ln w_p - \ln w_e}) A_{iep} \tag{4.12}$$

is the load carried by an elasto-plastically deformed asperity, and

$$F_{ie} = H A_{ip} \tag{4.13}$$

is the load carried by a plastic deformed asperity.
The total contact area and the total contact load carried by the contacting asperities can be found, by summing up the individual components of each contacting asperity couple, as follows:

$$A_r = \sum_{1}^{n} A_i(w_{i)} \quad \text{and} \tag{4.14}$$

$$F_N = \sum_{1}^{n} F_i(w_{i)} \tag{4.15}$$

The presented deterministic elastic-plastic contact model can be implemented in the deterministic mixed lubrication friction model and in the next subsection the influence of the elastic versus elastic-plastic deterministic contact model on the Stribeck curve is investigated.

4.5.3 Results

In order to study the influence of the elastic versus elastic-plastic contact on the Stribeck curve, a non run-in and a run-in surface are considered. The equivalent statistical roughness parameters of the two surfaces used, are presented in table 4.5 and the measured versus equivalent Gaussian standard height distributions of the asperities are depicted in Fig.4.9. The input parameters for the Stribeck curve calculations are defined in table 4.4.
In Fig.4.10 and 4.11 the results of the calculations for the Stribeck curve and the corresponding separation, when the contacting asperities deform elastically and when elastic-plastic regime is taken into account respectively for the two surfaces, are presented. In order to see the influence of the elastic-plastic effect on the Stribeck curve, the calculations are performed for two different normal forces. In Fig.4.12 the percentages of the elastic, elastic-plastic and plastic deformed asperities in the BL regime when the elastic-plastic regime is taken into account for the two surfaces, are depicted.

Table 4.4: The input parameters for Stribeck curve calculations.

property	value	unit	description
B	$5 \cdot 10^{-3}$	m	length of the contact
R	$3 \cdot 10^{-3}$	m	reduced radius of cylinder
E'	231	GPa	combined elasticity modulus
η_0	0.0202	Pa·s	viscosity
α	$2.0 \cdot 10^{-8}$	Pa^{-1}	viscosity pressure coefficient
τ_0	2.5	MPa	Eyring shear stress
f_c	0.13	-	coefficient of friction
H	6.6	GPa	hardness

Table 4.5: The statistical roughness parameters of the two used surfaces.

description	σ_s [μm]	β [μm]	n [1/m^2]
case 1	0.049	9.5	$1.15 \cdot 10^{11}$
case 2	0.15	13.2	$1.6 \cdot 10^{10}$

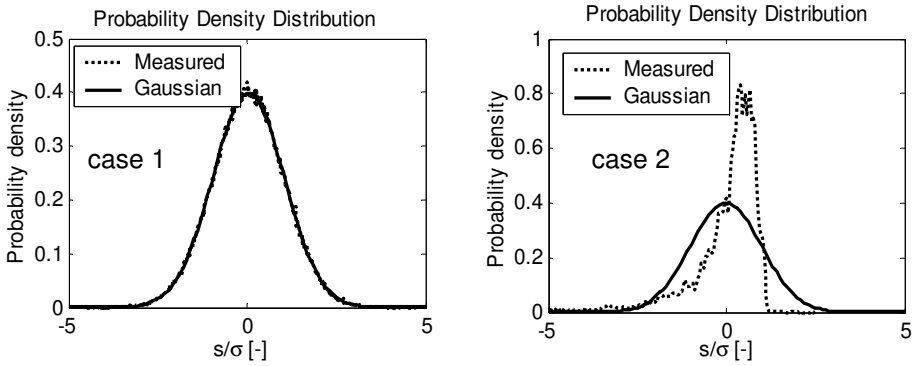

Fig.4.9: The distribution of surface heights as a function of the dimensionless asperity height (s/σ). Case 1 non run-in surface and case 2 run-in surface.

As it can be observed in Fig.4.10[a], the difference in the calculated Stribeck curves, when the elastic or the elastic-plastic contact is considered, are small for a macroscopic mean contact pressure of 0.39 GPa. The amount of the elasto-plastically deformed asperities in this case is 64% and there are no plastic deformed asperities (Fig.4.12[a]). As the macroscopic mean contact pressure increases (1.23 GPa), the difference in Stribeck curve also increases (Fig.4.10[b]). The amount of elastic-plastic deformed asperities in this case increases to 87 % (Fig.4.12[b]).

By taking in the calculation, plasticity into account, the amount of load carried by a single asperity is smaller compared to the ideally elastic situation (for the same indentation value). Therefore, in order to carry the same load, the asperities deform more in the elastic-plastic regime and as a consequence the ML lubrication regime shifts to the left. The magnitude of the translation of the ML regime increases as the macroscopic mean contact pressure increases due to the fact that the number of elastic-plastic deformed asperities becomes larger. This phenomenon takes place during the running-in process of new contacting surfaces and is attenuated as soon as the asperities are able to carry the load in the elastic regime. This consequence can be observed in Fig.4.11[a] and 4.11[b] where the Stribeck curve is calculated for the same mean contact pressure, but the considered surface is run-

in. In this case, the amount of the elastic-plastic and plastic deformed asperities is small compared to those elastically deformed (see Fig.4.12[b]) and therefore the difference is insignificant between the Stribeck curves where the elastic or the elastic-plastic contact is considered.

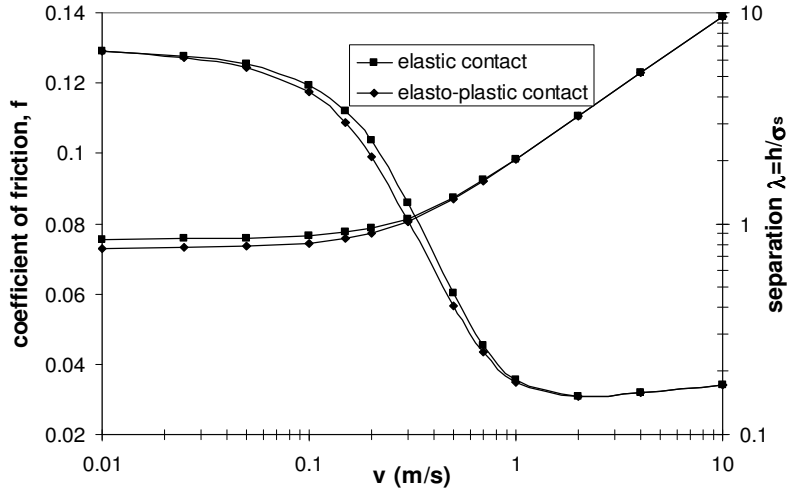

(a)

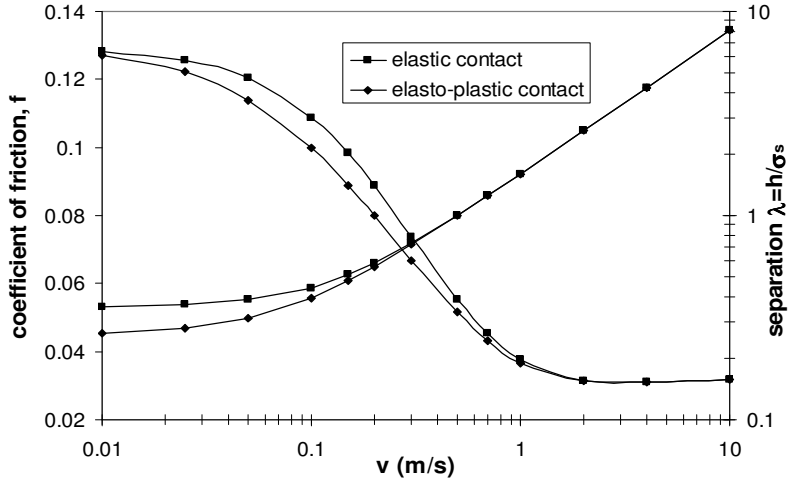

(b)

Fig.4.10: Comparison between the Stribeck curve and corresponding separation for the non run-in surface (case 1), when the contacting asperities deform elastically or elastic-plastically, a) F_N = 100 N ($\overline{p}_H$ = 0.39 GPa) and b) F_N = 1000 N ($\overline{p}_H$ = 1.23 GPa).

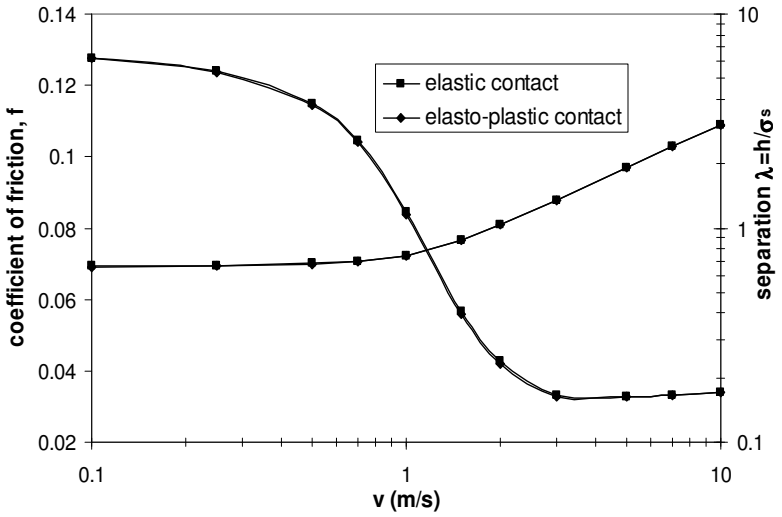

(a)

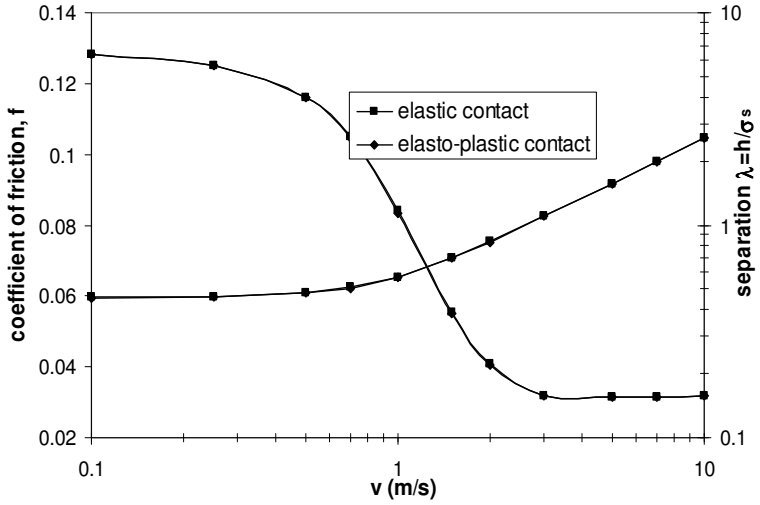

(b)

Fig.4.11: Comparison between the Stribeck curve and corresponding separation for the run-in surface (case 2), when the contacting asperities deform elastically or elastic-plastically, a) F_N = 100 N ($\overline{p}_H$ = 0.39 GPa) and b) F_N = 1000 N ($\overline{p}_H$ = 1.23 GPa).

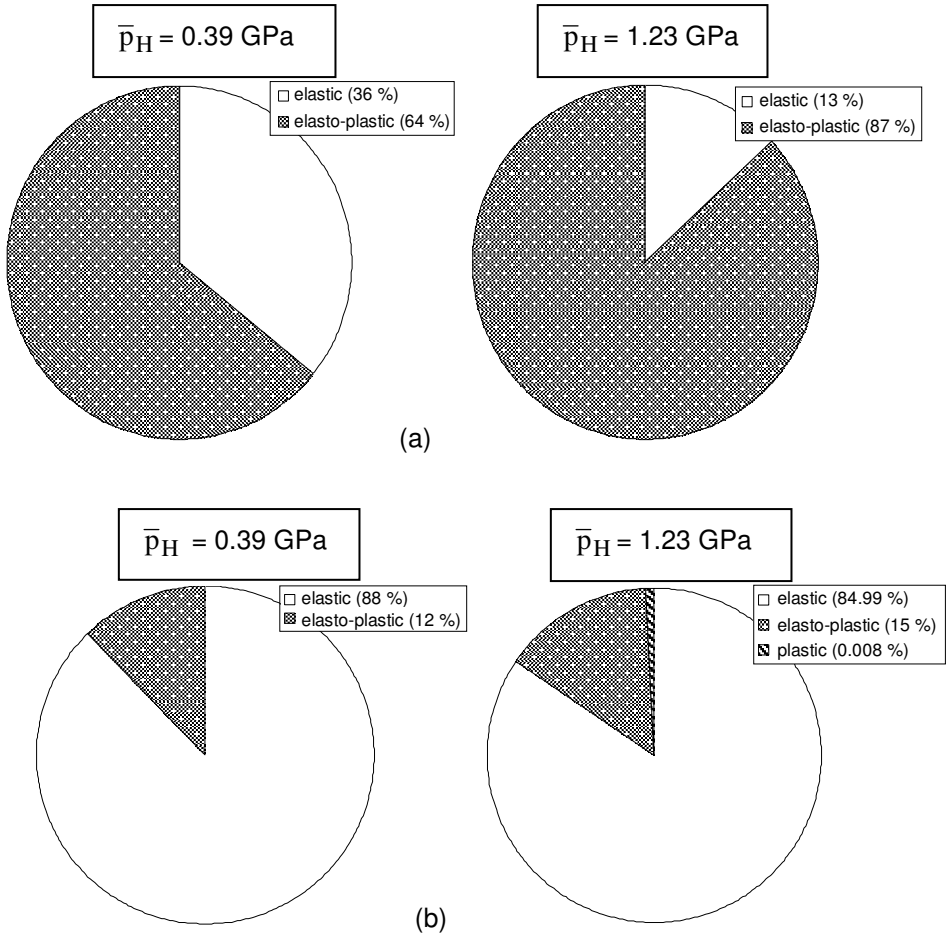

Fig.4.12: Percentage of elastic, elasto-plastic and plastic deformed asperities in the BL regime when elasto-plasticity is taken into account. a) non run-in surface (case1) and b) run-in surface (case 2).

In conclusion, the influence of the elastic versus elastic-plastic contact on the Stribeck curve is significant when the contacting surfaces are not run-in and is negligible when the contacting surfaces are run-in.

4.6 Influence of the shear stress-pressure dependency on the Stribeck curve

4.6.1 Introduction

In section 2.2.3 the influence of the pressure on the shear stress at asperity level in the boundary lubrication regime was discussed. For most of the boundary layers the shear stress increases linear with the pressure, but there are lubricants like calcium carbonate for which the shear stress of the boundary layer is not linear with the pressure. The variation of the coefficient of friction ($f = \tau/p$) at asperity level may give a variation in the macroscopic coefficient of friction in the BL regime when the normal load acting on the macroscopic contact varies. In order to study the influence of the shear stress - pressure dependency on the Stribeck curve, a boundary layer of calcium carbonate is considered in this section.
In section 4.6.2 the relation which describes the shear stress - pressure dependency for a calcium carbonate boundary layer and the calculation method of the macroscopic coefficient of friction are presented. In section 4.6.3 the results of the Stribeck curve calculations are discussed.

4.6.2 Influence of the pressure on the shear stress and the calculation method of the macroscopic coefficient of friction

In 1991, Georges and Mazuyer published a paper in which they presented the shear stress - pressure dependency in the boundary lubrication regime for a few lubricants (see Fig.2.12). In this section the shear stress-pressure (coefficient of friction-pressure) dependency, for in this case, calcium carbonate (Fig.4.13) on the Stribeck curve is studied. A function fit which describes the shear stress-pressure dependency for calcium carbonate was introduced by Westeneng (2001). This relation is used in this section to calculate the coefficient of friction at asperity level. The relation reads:

$$\tau(p) = \{(7.8 \cdot 10^{-4} p^{1.5})^{-4} + [(2.39 \cdot 10^{4} p^{0.28})^{1.5} + (6.31 \cdot 10^{-5} p^{1.31})^{1.5}]^{-2.67}\}^{-0.25} \quad (4.16)$$

with p the mean asperity contact pressure. The asperity coefficient of friction (f_i) is calculated as the ratio between the shear stress (τ) and the asperity mean contact pressure (p).
By using the deterministic contact model described in section 4.2, the mean contact pressure on each deformed asperity can be calculated and by implementing Eq. 4.16 in the deterministic contact model makes it possible to calculate the coefficient of friction (f_i) for each contacting asperity. Only elastic deformations are considered in this section.
By knowing the microscopic coefficient of friction (f_i) and the normal load acting on the deformed asperity (F_i) the following relation is used to calculate the macroscopic coefficient of friction:

$$f_c = \frac{f_1 \cdot F_1 + f_2 \cdot F_2 + ...f_i \cdot F_i + ...f_n \cdot F_n}{F_1 + F_2 + ...F_i + ...F_n} \qquad (4.17)$$

where f_1, f_2, f_i and f_n are the coefficients of frictions of the deformed asperities and F_1, F_2, F_i and F_n are the normal forces acting on these asperities respectively.
In the next section results of the Stribeck curve calculations for a calcium carbonate lubricant are presented.

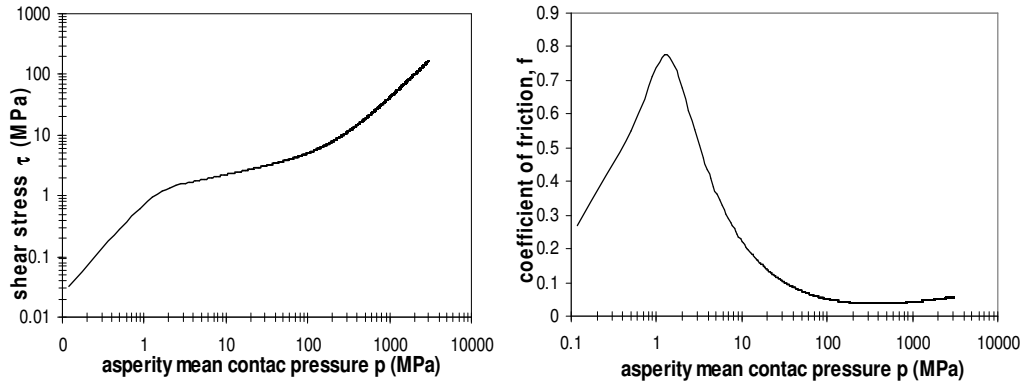

(a) (b)

Fig.4.13: Shear stress (a) and coefficient of friction (b) as a function of the pressure for a calcium carbonate boundary layer, Georges and Mazuyer (1991).

4.6.3 Results

In order to perform the Stribeck curve calculations, the input parameters are defined in table 4.6. A measured surface is used to study the influence of the shear stress-pressure dependency of calcium carbonate on the Stribeck curve. In Fig.4.14 the measured and the equivalent Gaussian height distribution of the surface heights for the surface considered, is presented.

Table 4.6: Input parameters for the Stribeck curve calculations.

property	value	unit	description
σ_s	0.24	µm	standard deviation of asperities
β	9.3	µm	radius of asperities
n	$1.4 \cdot 10^{10}$	$1/m^2$	density of asperities
B	$10 \cdot 10^{-3}$	m	length of the contact
R	$20 \cdot 10^{-3}$	m	reduced radius of cylinder
E'	231	GPa	combined elasticity modulus
η_0	0.0202	Pa·s	viscosity
α	$2 \cdot 10^{-8}$	Pa^{-1}	viscosity pressure coefficient
τ_o	2.5	MPa	Eyring shear stress

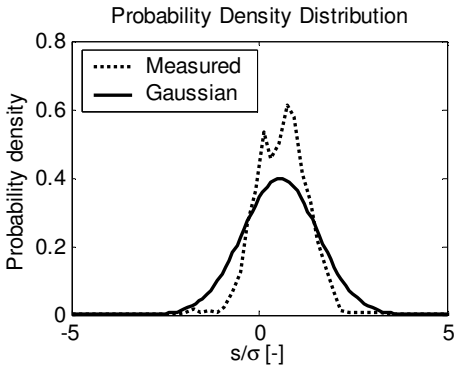

Fig.4.14: Distribution of the surface heights as a function of the dimensionless asperity height (s/σ).

In Fig.4.15 the influence of the load on the Stribeck curve for a calcium carbonate lubricant is presented for three different normal loads. As it can be seen, the friction in the BL regime decreases as the normal load (macroscopic mean contact pressure) increases. This effect is caused by the fact that the coefficient of friction of the boundary layer is not constant with the pressure (see Fig.4.13[b]).

As the macroscopic mean contact pressure increases for instance from 0.24 to 0.48 GPa, the amount of asperities which operate in the higher pressure region, 100 to 1000 MPa respectively, (low values for the coefficient of friction, see Fig.4.13) increases, and as a consequence the macroscopic coefficient of friction decreases.

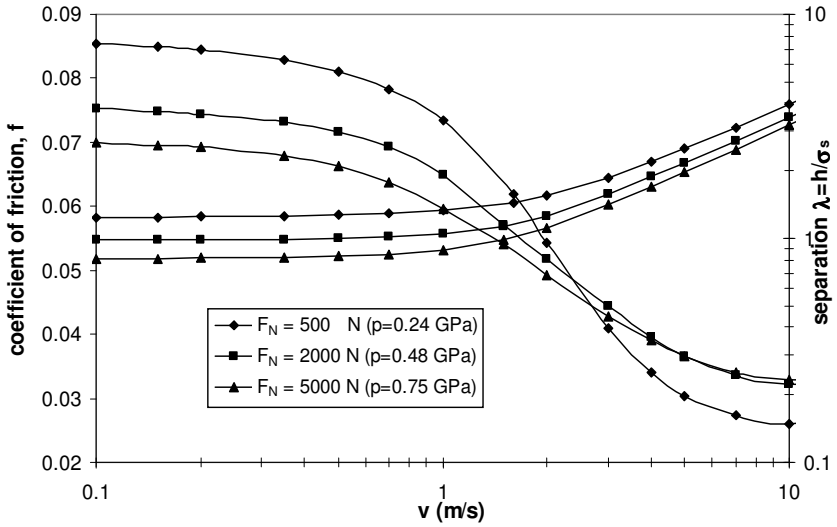

Fig.4.15: Stribeck curve and corresponding separation for a calcium carbonate lubricant. The normal load is varied from 500 N to 5000 N, see table 4.6.

It can be concluded from this section that when the coefficient of friction of the boundary layer is not constant with pressure, the macroscopic coefficient of friction in the BL regime varies with the load (macroscopic contact pressure). Therefore, when the shear stress - pressure dependency is not linear, it is very important to incorporate this effect in the mixed lubrication model. The disadvantage is that the shear stress-pressure behaviour for a certain boundary layer has to be determined experimentally. No model is available yet to predict the shear stress-pressure behaviour of the various boundary layers.
In the next section the conclusions concerning this chapter are drawn.

4.7 Conclusions

A deterministic contact model has been developed in order to calculate the Stribeck curve for a real distribution of the asperities. In section 4.3 a comparison between the deterministic and the statistic contact model on the Stribeck curve is made. It was shown that the Stribeck curve results obtained with the statistic and the deterministic contact models are significantly different when the distribution of the surface heights deviates from the Gaussian height distribution.
Next, the effect of the circular versus the elliptical asperity contact model on the Stribeck curve was investigated. It was found that the difference in Stribeck curve by using a sphere instead of ellipsoid for the asperity contact model, is negligible and therefore the circular contact is recommended due to its simplicity and applicability in deterministic contact modeling.
Further in section 4.5, the influence of the elastic versus elastic-plastic asperity contact model on the Stribeck curve was discussed. From the calculations it appears that the influence on the Stribeck curve of the elastic versus elasto-plastic contact is significant when the contacting surfaces are not run-in and is negligible when the contacting surfaces are run-in.
In section 4.6 the effect of the shear stress-pressure dependency of a boundary layer, in this case of a calcium carbonate lubricant, on the Stribeck curve, is presented. From the calculations it can be concluded that when the coefficient of friction of the boundary layer is not constant with the pressure, the macroscopic coefficient of friction in the BL regime varies with the normal load (macroscopic contact pressure) and therefore it is important to incorporate the shear stress-pressure behaviour in the mixed lubrication model.

References

Abbott, E.J. and Firestone, F.A. (1933), “Specific surface quality – a method based on accurate measurement and comparison“, Mech. Engr., Vol. 55, 569.

Chang, W.R. (1997), “An elastic-plastic contact model for a rough surface with an ion-plated soft metallic coating”, Wear, Vol. 212, 229-237.

Chang, W.R., Estion, I. and Bogy, D.B. (1987), “An elastic-plastic model for the contact of rough surfaces”, ASME Journal of Tribology, Vol. 101, 15-20.

Francis, H.A. (1976), “Phenomenological analysis of plastic spherical indentation”, ASME Journal of Engineering Materials and Technology, Vol. 76, 272-281.

Gelinck, E.R.M. (1999), “Mixed lubrication of line contacts”, PhD thesis, University of Twente, Enschede, The Netherlands.

Greenwood, J.A. and Williamson, J.B.P. (1966), “Contact of nominally flat surfaces”, Phil. Trans. R. Soc. London Series A, Vol. 295, 300-319.

Hertz, H. (1881), “Über die berührung fester elastischer körper”, Journal für die reine und angewandte Mathematik, Vol. 92, 156-171.

Johnson, K.L. (1985), “Contact mechanics”, Cambridge University Press, Cambridge, UK.

Tabor, D. (1951), “The hardness of metals”, Oxford University Press, UK.

Westeneng, A. (2002), “Modeling of contact and friction in deep drawing processes”, PhD thesis, University of Twente, Enschede, the Netherlands.

Zhao, Y., Maietta, D.M. and Chang, L. (2000), “An asperity microcontact model incorporating the transition from elastic deformation to fully plastic flow”, ASME Journal of Tribology, Vol. 122, 86-93.

Chapter 5

Experimental devices

5.1 Introduction

In chapter 3 and 4 the mixed lubrication model is presented for the statistical and as well as for the deterministic representation of rough surfaces. In this chapter the test rigs on which experiments were performed to validate the mixed lubrication model are described.
In the first section of this chapter a newly designed Surface Force Apparatus, on which the measured shear stress-pressure diagram for different lubricants was determined, is comprehensively described in section 2. The third section describes the pin-on-disc tribometer on which friction measurements were performed, for determining the Stribeck curves.

5.2 Surface Force Apparatus

5.2.1 Introduction

Many aspects of the micro-mechanisms involved in friction have been investigated extensively and reported in literature. Bowden and Tabor (1950) developed the theory of friction by considering the friction between surfaces as a collective behaviour of many sliding asperity contacts. Other authors like Briscoe et al. (1973) and Georges and Mazuyer (1991) showed that the asperity coefficient of friction in the BL regime is not constant with pressure when using different lubricants.
A series of apparatuses have been designed in order to measure the coefficient of friction of a single asperity contact. One of them, the Atomic Force Microscope (AFM), is the most known device which can measure friction of a microscopic

contact at atomic level. This technique deals with contact widths smaller than one micrometer, very low normal loads (< μN) and moving velocities in the order of micrometers per second. The aim of this technique is to examine the (micro) friction force at different deformation modes at atomic scale of surface layers.
The Surface Force Apparatus (SFA) is another well-known device which measures friction between two surfaces under rather low normal forces (μN-mN) and the contact area can be of the order of a few millimeters. Such an apparatus was developed by for instance Georges et al. (1991) for measuring friction forces between a sphere and a plane. In comparison with the AFM, this device can measure friction between surfaces with larger contact arear and normal loads.
In order to determine the shear stress as a function of pressure of a single asperity contact, a new Surface Force Apparatus was designed which operates with higher normal loads (mN-N) and larger velocity range (μm/s-mm/s). The new SFA (see Fig.5.1) is able to measure the friction force of a single asperity contact. In the following sections, the design of the SFA and its operating possibilities will be presented.

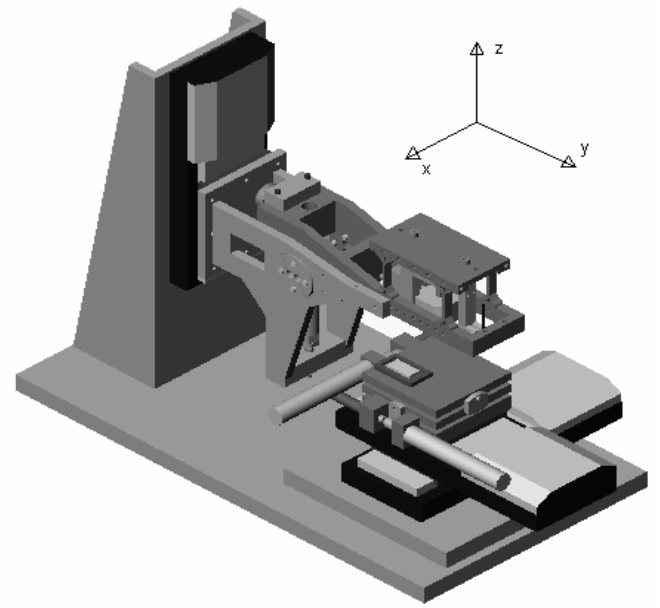

Fig.5.1: Setup of the Surface Force Apparatus.

5.2.2 Specifications of the SFA

Friction is stipulated by the material, the geometry of interface, the properties of the surfaces, the normal force, the relative velocity between the surfaces, and the environment (air humidity, temperature, vibrations). In order to measure the friction, the parameters mentioned above must be controllable. For this purpose the new SFA has to meet the following requirements:

- The material, surface properties, and geometry of the specimen and tip are precisely defined.
- The normal force is adjustable.
- The distance between probe and specimen in horizontal and vertical directions is controllable.
- The temperature is controllable.
- The sliding velocity over average rolling velocity, between probe and specimen is controllable.
- The influence of the environment should be limited.

The final requirements for the SFA are given in table 5.1. The range and precision of the requirements have been chosen on the basis of the tribological applications to be studied on the SFA and based on accumulated experience during designing other tribological measurement devices.

Table 5.1: Specifications for SFA.

property	range	precision
normal force	0.1 - 50 N	5 mN
friction force	0.1 - 50 N	5 mN
sliding velocity	0 - 50 mm/s	1 µm/s
sliding stroke	0 - 50 mm	1 µm
lateral stroke	0 - 50 mm	1 µm
vertical movement coarse (without contact) fine (contact)	 0 - 50 mm 0 - 200 µm	 5 µm 10 nm
contact temperature	0 - 250 °C	± 1 °C
slip	0 - 200 %	± 0.5 %

Based on these requirements, the SFA is built on four principal concepts. In the next sections these concepts will be presented.

5.2.3 Concept for the friction force measurement

An important question in designing the SFA is: How to measure and control the friction force and the normal force in combination with the displacements which appear in three directions (x, y and z). These forces and displacements should be independent. This means that by applying a force in one of the three directions, it does not result in displacements or forces in the other two directions. The most important principles which have been applied at this concept are:

- The stiffness of the device.
- The degrees of freedom.
- Symmetry.

For measuring the friction force, the design presented in Fig.5.2 is used. As it can be noticed, the elastic joints are placed symmetrically to the probe holder (see Fig.5.2 (b)) and are very thin in order to allow the frame to move in the sliding direction with as less elastic energy dissipation as possible. In the other two directions the friction measuring device is very stiff. A tip (probe) holder is mounted on the upper part of the frame and linked to one of the sides of the coupling element (see Fig.5.2).

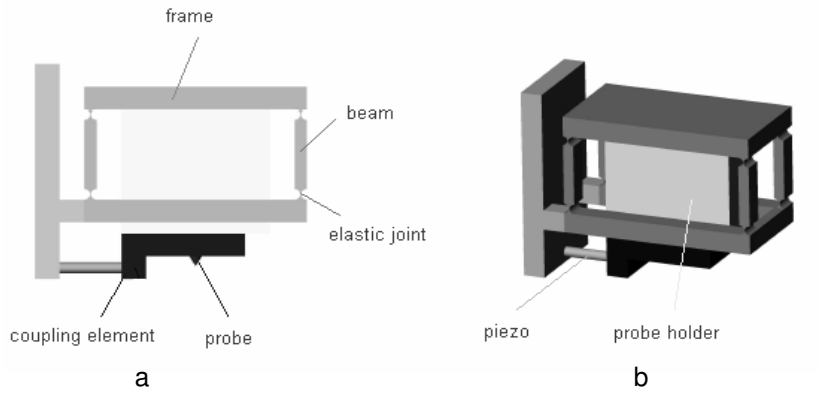

Fig.5.2: Concept of friction force measuring device.
a: front view. b: 3D view.

A piezo sensor is used to measure the friction force (see Fig.5.3[a]). Between the tip holder and sensor there is a coupling element (see Fig.5.3[b]) which bonds the holder and sensor and is flexible in the different directions except in the sliding direction (see Fig.5.3[c]). The coupling element plays a safety role in protecting the piezo sensor against the potential moments which could occur in sliding direction.

The piezo sensor generates a signal which is converted and recorded by the system (amplifier, digital converter and personal computer).

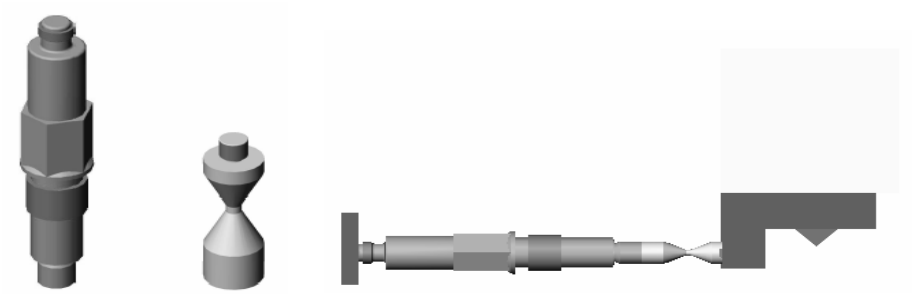

a b c

Fig.5.3: The two components for measuring friction force. a: piezo sensor. b: coupling element. c: connection between piezo sensor, coupling element and probe holder.

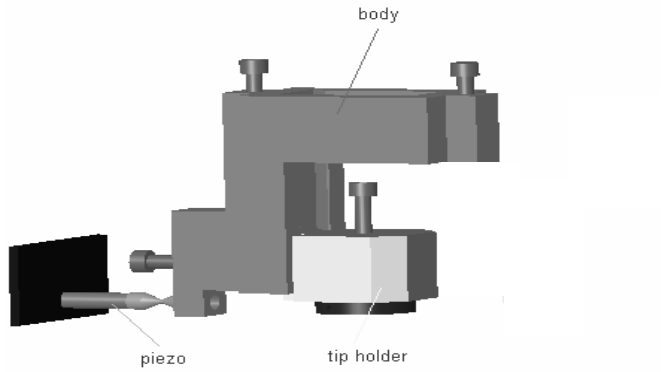

Fig.5.4: Concept of the friction force measuring device.

In Fig.5.4 the final design of the concept of the friction force measuring device is presented. This solution is simple and tips (balls) with different diameters and materials can be used.

5.2.4 Concept for measuring the normal force

In Fig.5.5 the design for applying and measuring the normal force is presented.

From symmetrical considerations (symmetrical dissipation of energy and symmetrical load distribution), two cross elastic joints were mounted symmetrically and connected together by a lever (see Fig.5.5[b]). In comparison with the elastic joints of the friction force concept, the cross elastic joints of the normal force concept only allows rotation around the pivoting point. A cross elastic joint consist of one horizontal beam (Fig.5.6[a]) mounted with one vertical beam (Fig.5.6[b]) by using four connection rolls (Fig.5.6[c]). Between these two elastic joints there is space in order to avoid contact between the beams and therefore energy dissipation.

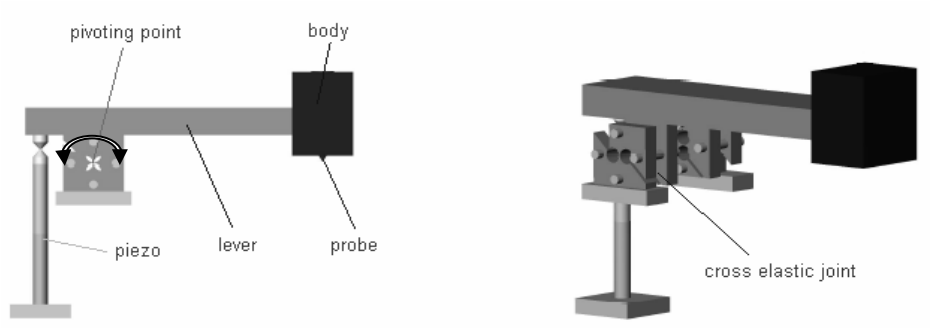

Fig.5.5: Concept of normal force measuring device. a: front view. b: 3D view.

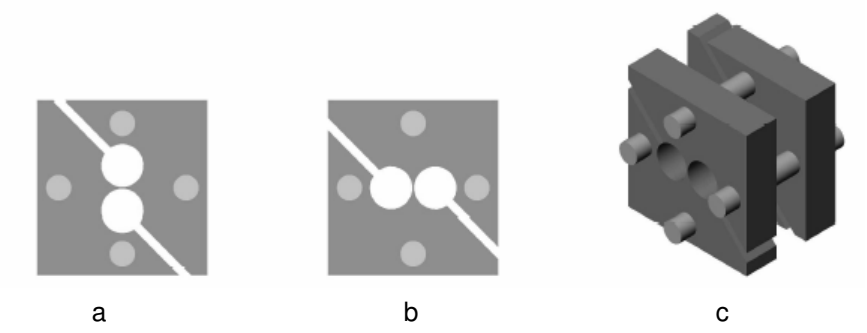

Fig.5.6: Design of cross elastic joint. a: horizontal beam. b: vertical beam. c: cross elastic joint.

This concept has a piezo sensor and a piezo actuator (see Fig.5.7[a] and Fig.5.7[b]) which are combined in one system which can measure and apply the normal force. The system is mounted at the lever at the opposite side of the friction force measuring device (see Fig.5.8) by using a coupling element (see Fig.5.7[c]). The coupling element plays the same protecting role like the one of the friction force

measuring device concept, i.e. stiff in normal direction, flexible in the other directions. The signals from the two piezos are recorded and controlled by the system (amplifier, digital converter and personal computer).

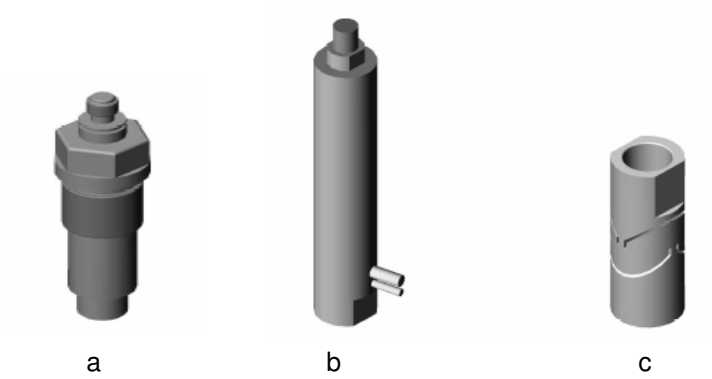

Fig.5.7: The three components for applying and measuring the normal force. a: piezo sensor. b: piezo actuator. c: coupling element.

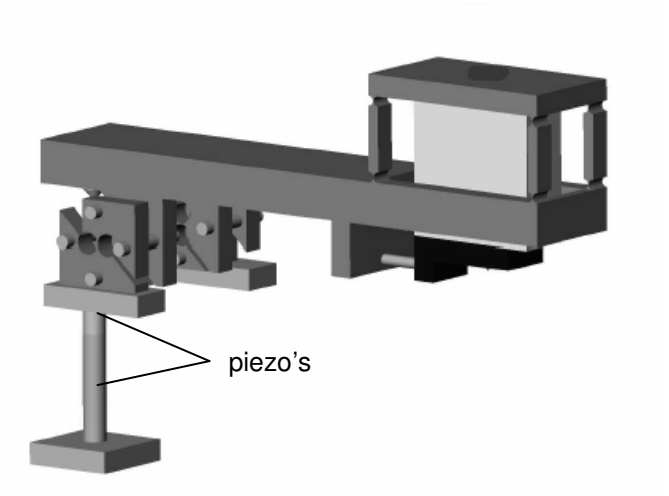

Fig.5.8: Concept of the normal force device together with the concept of the friction force device.

5.2.5 Concept of the specimen control

In designing the specimen control concept of the SFA, a few requirements must be achieved. The requirements are:

- Positioning the specimen in the horizontal plane.
- Moving the specimen in the sliding direction with the specified velocity in order to measure the friction force.
- Aligning the specimen in order to get a horizontal plan parallel movement.
- Controlling the temperature of the specimen.

The specimen control concept is shown in Fig.5.9. Two linear positioning stages were chosen for the positioning of the specimen in the horizontal plane (see Fig.5.11).

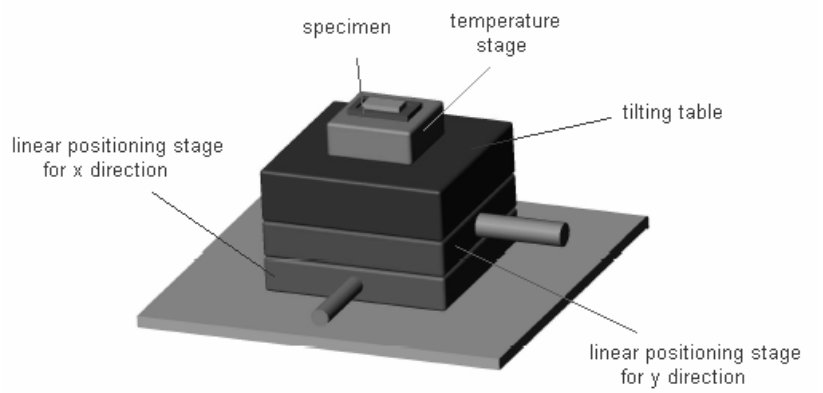

Fig.5.9: Concept of specimen control.

To get a horizontal plan parallel movement, the specimen is adjusted around the x and y axes with certain angles θ_x and θ_y. In Fig.5.10 the two angles which define the “alignments” of the specimen are indicated. To rotate the specimen, a tilting table (see Fig.5.12) is used and mounted on the linear positioning stage. The tilting table has two motors and two piezo sensors which control the tilt.

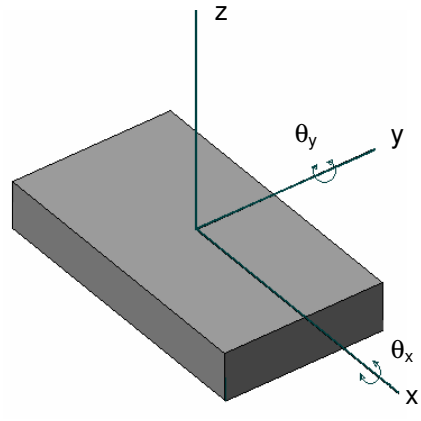

Fig.5.10: Tilting angles of the specimen.

The last requirement of this concept is to realize a certain temperature at the contact between the specimen and the tip. For this purpose a temperature stage is used. The temperature stage is mounted on top of the tilting table (see Fig.5.9) and is thermally isolated. The specimen is directly mounted onto the temperature stage so it is heated up to the desired temperature. During the measurement, when the tip is in contact with the specimen, the heat transfers to the tip and therefore the tip holder must also be thermally isolated from the lever frame.

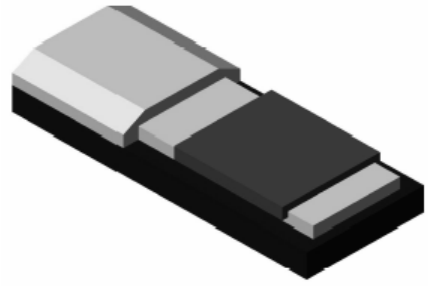

Fig.5.11: Linear positioning stage for x and y direction.

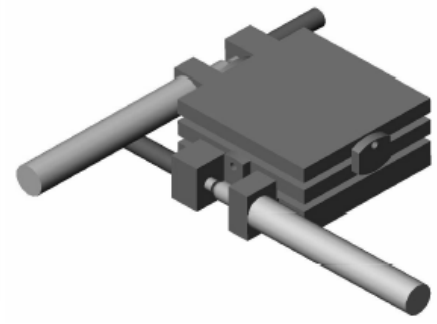

Fig.5.12: Tilting table.

5.2.6 The Surface Force Apparatus

In Fig.5.13 the final concept is schematically presented. An important point in performing good measurements is that the end of the tip is in the same plane as the piezo friction force sensor, pivoting point of the lever and the pivoting point of the coupling element of the piezo normal force sensor. These elements are aligned in order to avoid extra moments which could appear when the normal force and friction force are applied.

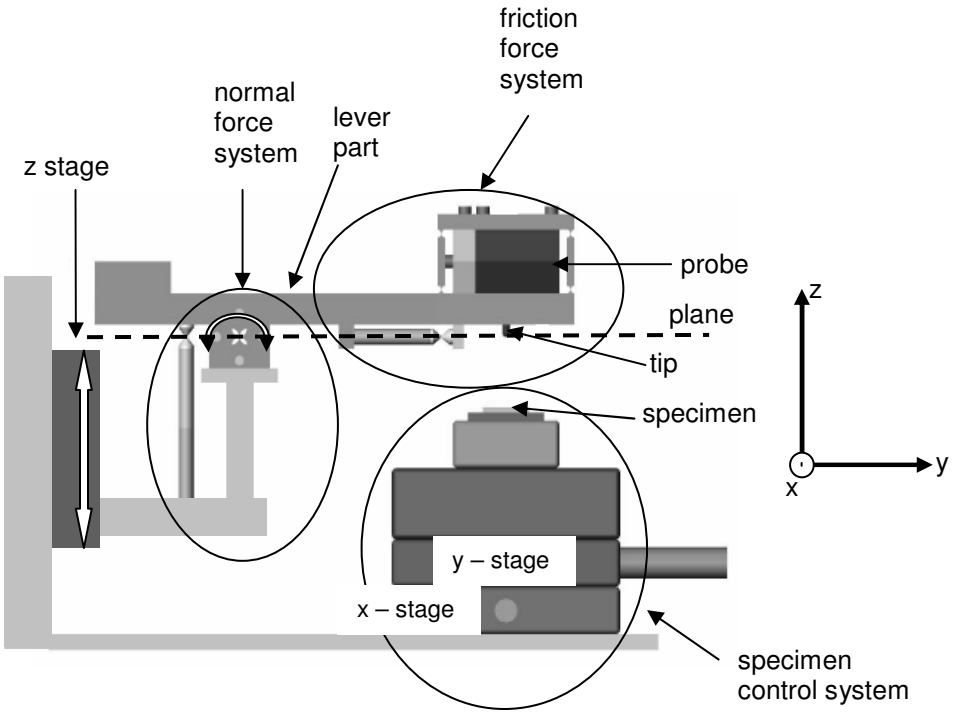

Fig.5.13: Front view of final concept.

The final design consists of two important parts: specimen part and lever part. The specimen part contains the components described in section 5.2.5. The linear stage for x direction, positions the specimen in x direction. The linear stage for y direction positions the specimen in y direction and respectively ensures the movement in the sliding direction. The specimen surface is made horizontally (plan parallel to the plane described before) by using a tilting table especially importat for the displacement controlled situation. The temperature stage ensures the desired

testing temperature of the specimen. The lever part consists of the components described in section 5.2.3 and 5.2.4. The linear stage for z direction, positions the lever part (course movement) in the vertical plane. By activation of the piezo actuator, a small rotation of the lever around the cross elastic joints takes place and the tip is moved vertically, coming into contact with the specimen.

Table 5.2: Spefications for adhesive and ploughing tests.

property	requested values		realized values	
	range	precision	range	precision
normal force	0.1 - 50 N	5 mN	0.1 - 45 N	2 mN
friction force	0.1 - 50 N	5 mN	0.1 - 50 N	0.5 mN
sliding velocity	0 - 20 mm/s	1 µm/s	0 - 50 mm/s	1 µm/s
sliding movement	0 - 20 mm	1 µm	0 - 50 mm	1 µm
lateral movement	0 - 20 mm	1 µm	0 - 50 mm	1 µm
vertical movement - coarse - fine	 0 - 50 mm 0 - 200 µm	 5 µm 10 nm	 0 - 50 mm 0 - 200 µm	 1 µm 9 nm
contact temperature	0 - 250 °C	± 1 °C	0 - 250 °C	± 1 °C
slip	0 - 200 %	± 0.5 %	0 - 200 %	± 0.5 %

During the concept phase, the choices concerning the design were based on the requirements from table 5.1. In this table the required values which the SFA should meet are indicated. In table 5.2 the specifications realized by designing the SFA are presented and a comparison with the required values is made. These values are stipulated by the properties of the piezo sensors, the linear positioning stages and the tilting table. The stiffness of the system is another factor which played an important role in designing the SFA. For more details regarding the stiffness, the reader is referred to Singerling (2002).
All the components of the SFA were machined and assembled together. In Fig.5.14 the new built Surface Force Apparatus is presented. Since the performances of the SFA have been established, the device is ready to perform measurements.
In order to perform measurements, the Surface Force Apparatus is made controllable by LabVIEW software.

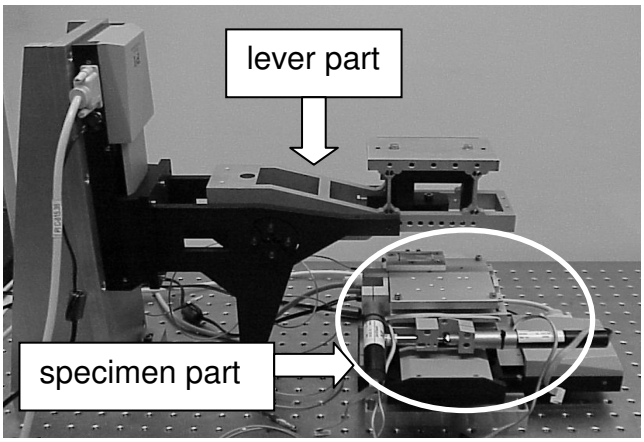

Fig.5.14: Surface Force Apparatus.

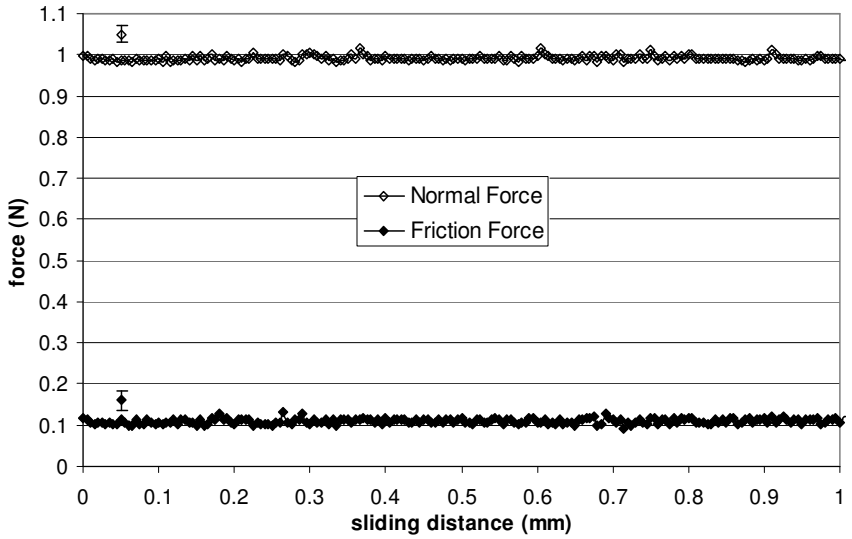

Fig.5.15: Initial measurements performed with the new SFA.
(↕ and ↕ are the measurement error bars).

In Fig.5.15 an initial experiment performed with newly designed SFA is presented. It should be mentioned that the results presented in Fig.5.15 are measured by the SFA in the displacement controlled mode (for instance for scratch tests) and therefore the normal force is influenced by the waviness of the surface of the specimen. In the case of the measurement presented in Fig.5.15, the specimen has a polished surface (Ra ≈ 4 nm) and the tip is a ball (Ra ≈ 8 nm). The sliding

distance is 1 mm and as it can be noticed the normal force is constant within the sliding distance and therefore in this case the waviness of the surface of the specimen within 1 mm is negligible. For a friction measurement, the normal force controlled mode is recommended for the SFA.

5.3 Pin-on-disc tribometer

The friction measurements conducted at multi asperity contacts, in order to obtain the generalized Stribeck curve, were performed on a pin-on-disc tribometer (see Fig.5.16).

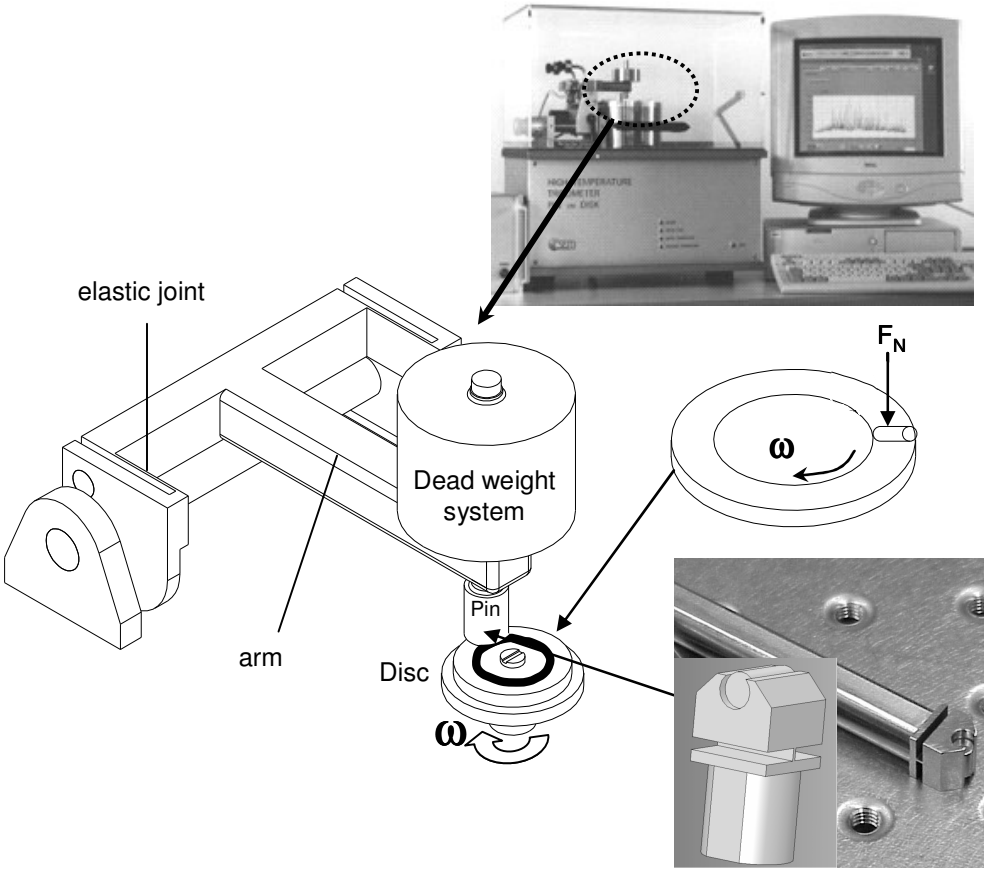

Fig.5.16: The pin-on-disc tribometer used for friction curve measurements.

The roller on disc geometry is used to obtain a line contact. In order to avoid misalignment problems, a specially designed roller holder is used which has an elastic joint (see insert of Fig.5.16).
The disc is mounted on a holder rotated by a motor. The motor is driven by a controller connected to a personal computer. A user can set the sliding velocity and the sliding distance required for a test. The roller is placed in a holder which is attached to an arm which is held by two elastic joints. The friction force is measured by a displacement transducer attached to the elastic joint. The normal force is applied by using a corresponding mass, placed on the top of the pin (see Fig.5.16).

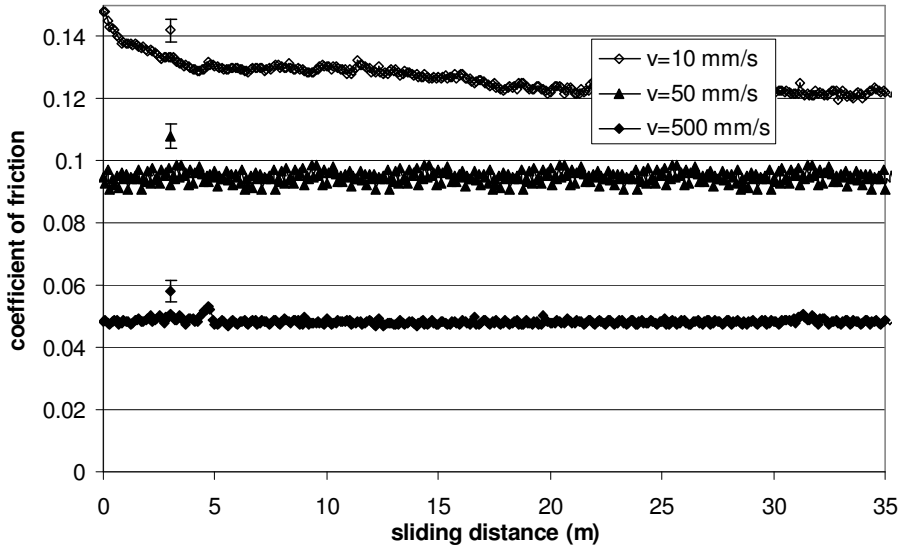

Fig.5.17: Measurements performed with the pin-on-disc tribometer at different sliding velocities. (Ŧ, Ŧ and Ŧ are the measurement error bars).

In Fig.5.17 an example of measurements performed with the pin-on-disc tribometer for a lubricated line contact at different sliding velocities is presented. For the first measurement, performed at 0.01 m/s, the friction decreases due to running-in, while for the other two measurements the friction stays constant with sliding distance (see Fig.5.17). As can be noticed the coefficient of friction decreases with increasing velocity due to the hydrodynamic effect.
In conclusion, accurate friction measurements can be performed on the well-known pin-on-disc tribometer by using a modified roller holder. For more detailed information concerning this tester the reader is referred to the website of CSEM.

5.4 Summary

In section 5.2 the newly designed Surface Force Apparatus is described and the final design is presented. The specimen is positioned by using two linear positioning stages. With the chosen tilting table, the surface of the specimen can be placed in the same plane formed by the elastic joint (pivoting point) and piezo friction forcer sensor. The temperature stage ensures that friction measurements can be performed at a certain temperature. The specimen and the tip are replaced fast and easily due to the detachable specimen holder and tip holder respectively. The stiffness and dimensions of the lever were chosen, based on the capabilities of the sensors introduced to the system. With these sensors the friction force and the normal force are measured. The modular construction and the simplicity of the design ensure a simple functionality of the SFA. The newly designed Surface Force Apparatus is available to measure friction of a single asperity contact accurately as shown with the initial experiment (see Fig.5.15) described in the second part of section 5.2.6. With the Surface Force Apparatus, one is able to measure the shear stress-pressure curve for different lubricants.
With the pin-on-disc tribometer (CSEM) friction experiments can be conducted to determine Stribeck curves.
In the next chapter the experimental results obtained with these two test rigs, i.e. the Stribeck curve and the shear stress-pressure curve, will be presented.

References

Bowden, F.P., Tabor, D. (1950), “The friction and lubrication of solids”, Part I, Clearendon Press, Oxford, UK.

Briscoe, B.A. and Tabor, D. (1973), “Rheology of thin organic films”, ASLE Transaction, Vol. 17(3), 158 - 165.

Eugen Butnariu (2003), “Surface force apparatus”, MSc thesis University of Twente, Enschede, The Netherlands.

George, J-M. and Mazurey, D.M. (1991), “Pressure effects on the shearing of a colloidal layer”, J. Phys. Condensed Matter, Vol.2, SA399 - SA403.

Singerling, B.F.S. (2002), “The plowing asperity test apparatus Twente”, MSc thesis University of Twente, Enschede, The Netherlands.

CSEM, http://www.csm-instruments.com.

Chapter 6

Experimental results

In the first part of this chapter the shear stress-pressure dependency measurements are presented. In order to determine the influence of the pressure on the microscopic coefficient of friction in the BL regime three different oils are used.
In section 6.2 comparisons between the deterministic and the statistical Stribeck curve model and measurements are made. In section 6.3 starved lubricated experiments are presented and discussed. Finally conclusions are drawn.

6.1 Shear stress-pressure dependency measurements

As it has been pointed out in section 2.2.3 there are boundary layers like calcium carbonate which are in a particular way sensitive to pressure instead of a simple linear dependency, see Fig.2.12 (curve 1 and 5). Calcium salts like calcium carbonate are widely used as an anti-wear agent in mineral diesel oils (Georges and Mazuyer 1990). In this section shear stress-pressure dependency measurements for three different oils will be presented. These experiments were carried out on the Surface Force Apparatus as described in section 5.2. The measurements were performed at room temperature (20°C) and the sliding velocity was 0.5 mm/s. As samples, hardened AISI 52100 steel plates of 40x15x8 mm with a CLA surface roughness of about 3 nm were used. As “tips”, whole or parts from hardened AISI 52100 steel balls with radii varying between 2 and 500 mm and a CLA surface roughness of about 5 nm were used. The tips and the samples were rinsed in an ultra sonic cleaner with ethanol and subsequently dried in hot air. Before measuring the friction the contact between the tip and the sample was run-in for about 1000 mm in order to obtain a stabilized coefficient of friction, see Fig.6.1. In Fig.6.2 the run-in surface of a ball of 6.35 mm radius is presented. The

radius of contact is about 62 μm which is in the range of the Hertzian contact width (55 μm).
In Fig.6.3[a] the shear strength and the microscopic coefficient of friction as a function of the mean contact pressure for the three different oils are presented. Oil 1 and oil 3 are typical traction drive oils and oil 2 is a diesel mineral oil which contains additives like calcium salts. In table 6.1 some properties of the lubricants used, are listed. As it can be observed from Fig.6.3[b] there is no significant variation of the microscopic coefficient of friction with the contact pressure for the two traction drive oils (oil 1 and oil 3).

Table 6.1: oil properties.

	Oil 1	Oil 2	Oil 3	unit	description
η_0 (20 °C)	0.0829	0.2	0.07	Pa·s	viscosity
η_0 (100 °C)	0.005	0.0078	0.007	Pa·s	viscosity
α	$2 \cdot 10^{-8}$	$2 \cdot 10^{-8}$	$2 \cdot 10^{-8}$	Pa^{-1}	viscosity pressure coefficient
τ_0	2.5	2.5	2.5	MPa	Eyring shear stress

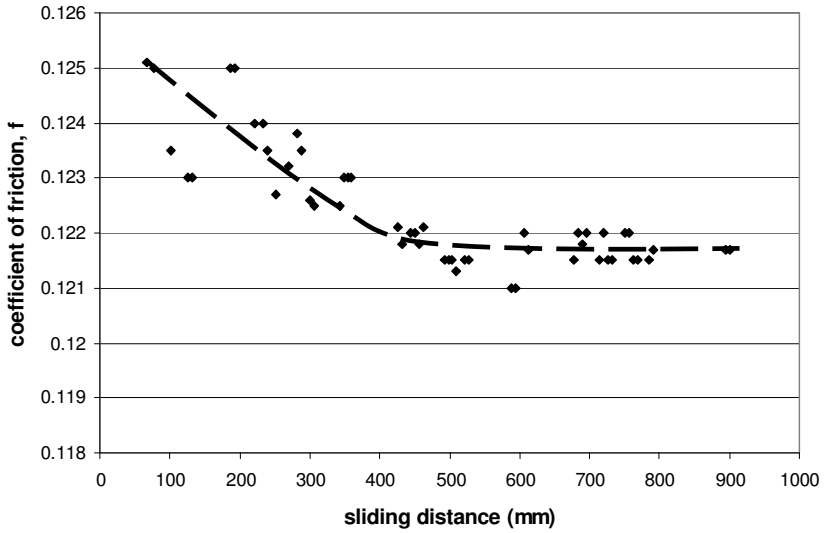

Fig.6.1: Coefficient of friction as a function of sliding distance during running-in for oil 1 (F = 4N, R = 6.35 mm).

For the diesel oil, when the mean contact pressure is higher than 600 MPa, the results shows a slight increase of the microscopic coefficient of friction of about 8 %. This variation of the microscopic coefficient of friction with the contact pressure is very small compared to the variation of the microscopic coefficient of friction of the specific fluids used by Georges and Mazuyer (1990) for a calcium carbonate

layer (see section 2.2.3, Fig.2.12 line 5) and therefore the variation of the macroscopic coefficient of friction in the BL regime with load is insignificant.

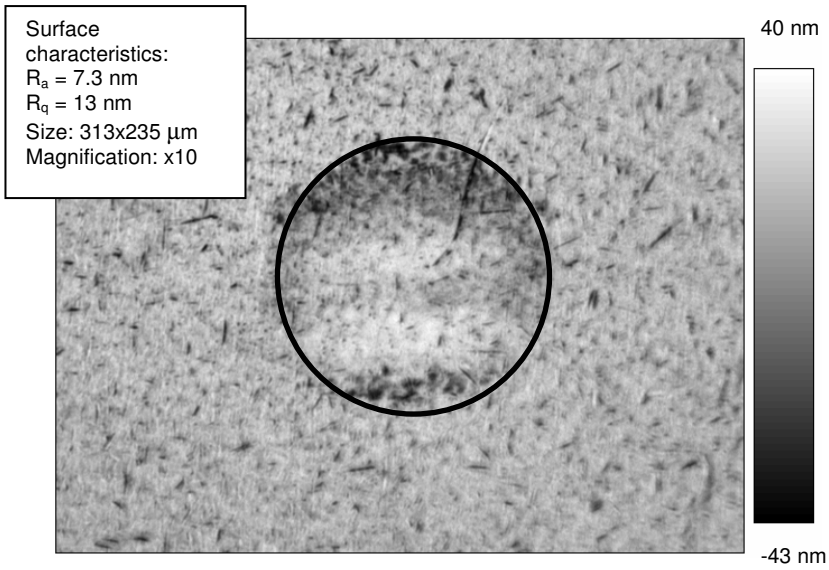

Fig. 6.2: The photograph of a surface of a ball of 6.35 mm radius after running-in at a load of 4 N.

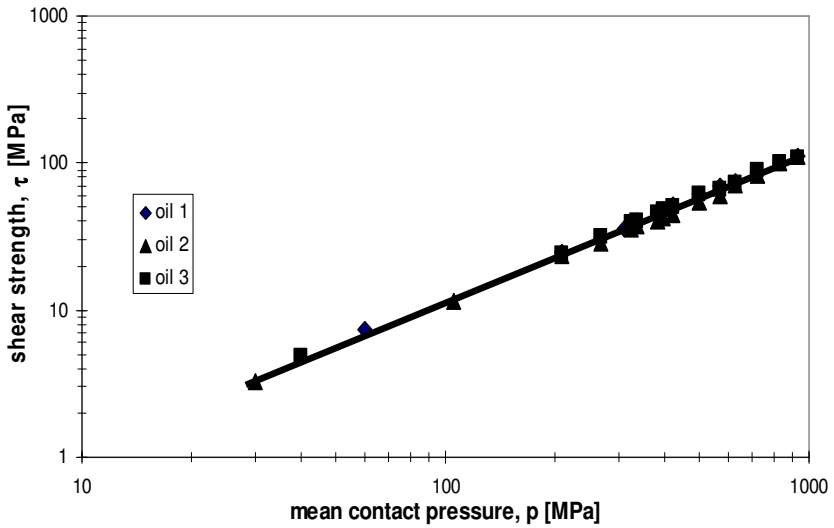

(a)

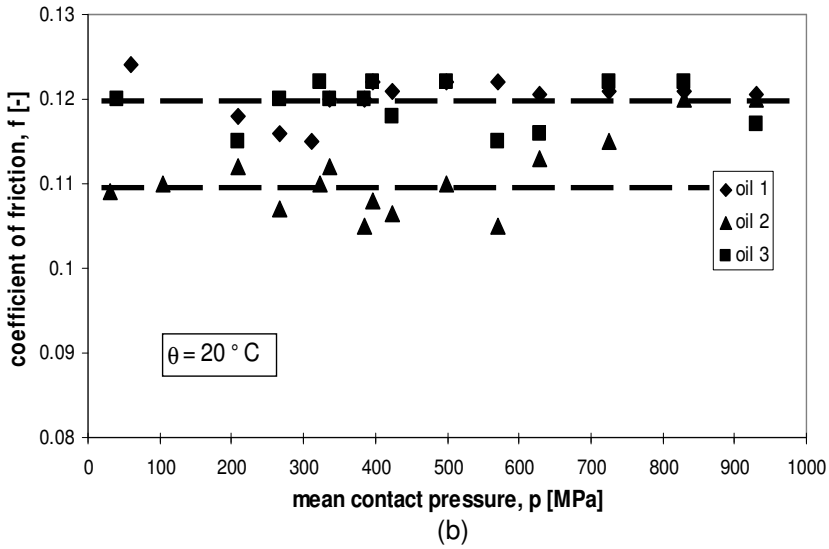

(b)

Fig. 6.3: The shear strength (a) and the coefficient of friction (b) as a function of the mean contact pressure. Oil 1 and oil 3 are traction drive oils and oil 2 is a mineral diesel oil.

In general it can be concluded that the variation of the microscopic coefficient of friction with contact pressure in the BL regime for most practical lubricants is almost constant. In fact the level of the coefficient of friction in the BL regime has a certain value for each type of lubricant.

6.2 Comparison between measured and calculated Stribeck curves

In order to validate the deterministic Stribeck curve model, experiments on the pin-disc machine have been performed by using three different lubricants (a traction oil, a mineral diesel oil and a base mineral oil). As samples, hardened AISI 52100 steel cylinders were used while the hardened AISI 52100 steel discs had polished surfaces. Prior to the friction experiments, a running-in procedure was performed near the transition from the BL to the ML regime for about 30 minutes for each new combination of sample and disc. After each measurement the surface topography of the cylinder and of the disc were measured by using an interference microscope. The digital data besides the operational conditions were used to calculate the statistical or deterministic Stribeck curve. In table 6.2 three cases are defined, together with the equivalent statistical roughness parameters. The real height

distribution versus equivalent Gaussian height distribution of the asperities of the cylinder surfaces for the three cases are depicted in Fig.6.4.

Table 6.2: Input parameters for the three cases.

property	value case1	value case2	value case3	unit	description
n_c	$3.5 \cdot 10^{11}$	$1.48 \cdot 10^{11}$	$2.9 \cdot 10^{10}$	m^{-2}	density of asperities of cylinder
β_c	$2.5 \cdot 10^{-7}$	$3.9 \cdot 10^{-7}$	$3.5 \cdot 10^{-6}$	m	radius of asperities of cylinder
σ_{sc}	0.26	0.23	0.092	µm	standard deviation of asperities of cylinder
n_d	$6.6 \cdot 10^{9}$	$2 \cdot 10^{10}$	$3.1 \cdot 10^{10}$	m^{-2}	density of asperities of disc
β_d	$3.8 \cdot 10^{-4}$	$7.28 \cdot 10^{-7}$	$5.5 \cdot 10^{-4}$	m	radius of asperities of disc
σ_{sd}	0.036	0.052	0.016	µm	standard deviation of asperities of disc
B	$5.5 \cdot 10^{-3}$	$5.5 \cdot 10^{-3}$	$5.8 \cdot 10^{-3}$	m	length of the contact
E'	231	231	231	GPa	combined elasticity modulus
R	$2.5 \cdot 10^{-3}$	$2.5 \cdot 10^{-3}$	$2 \cdot 10^{-3}$	m	reduced radius of cylinder
η_0	0.0829	0.232	0.9	Pa·s	viscosity
α	$2 \cdot 10^{-8}$	$2 \cdot 10^{-8}$	$2 \cdot 10^{-8}$	Pa^{-1}	viscosity pressure coefficient
τ_0	2.5	2.5	2.5	MPa	Eyring shear stress
f_c	0.125	0.12	0.12	-	coefficient of friction in BL
F_N	10	10	10	N	normal load
p	130	130	143	MPa	mean contact pressure

The statistic contact model takes into consideration the roughness of both surfaces, e.g. the surface of the cylinder and the surface of the disc. Because the roughness of the cylinder is higher than the roughness of the disc, the combined roughness of the contacting surfaces will not significantly change due to the roughness of the disc. For instance, for case 2 the standard deviation of the roughness of the cylinder is 0.23 µm and the standard deviation of the roughness of the disc is 0.052 µm resulting in a combined roughness of the two surfaces of 0.236 µm. Therefore, the comparison between the deterministic and statistic contact model is still realistic when using the combined roughness of the two contacting surfaces for the statistic model.

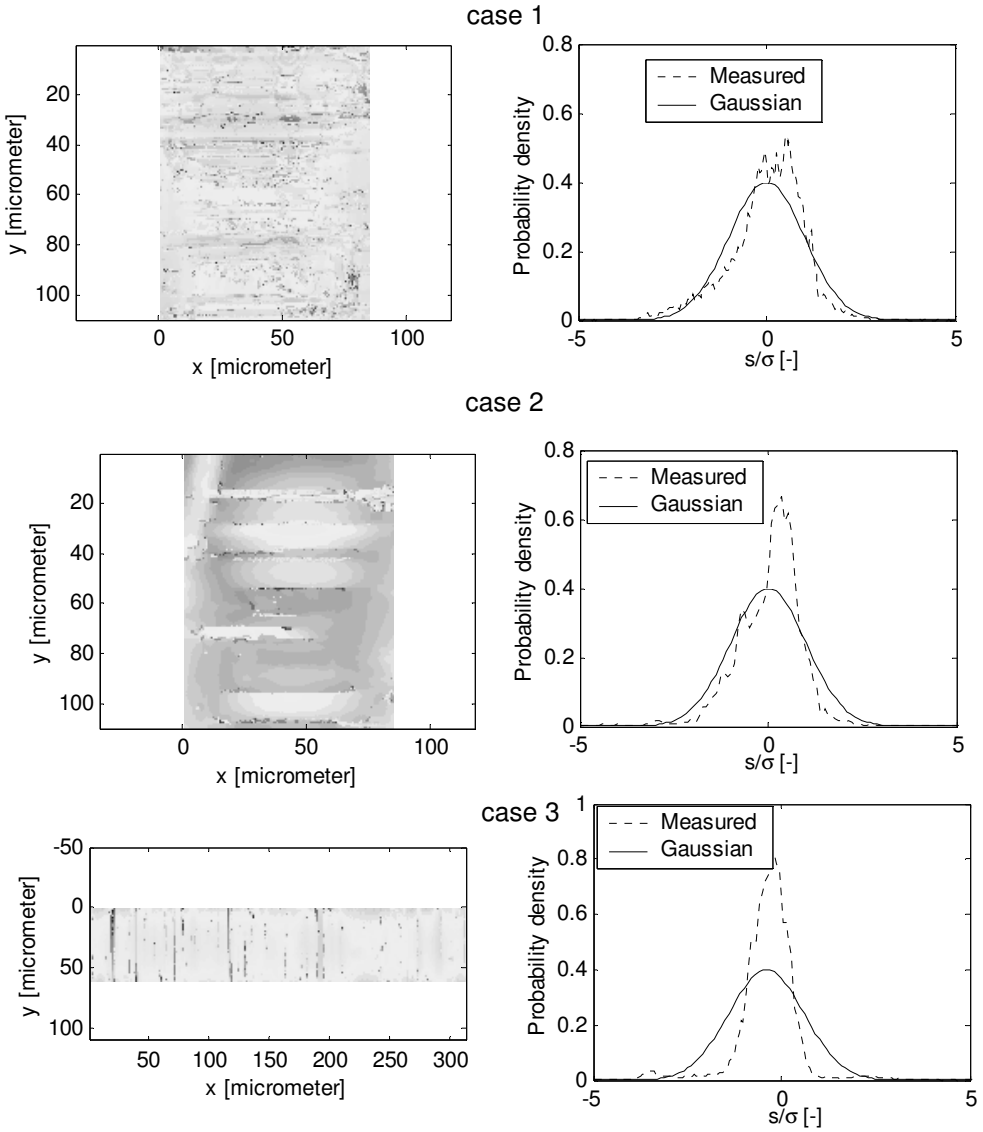

Fig.6.4: The surfaces of the cylinders together with their measured and equivalent Gaussian height distributions of the asperities for the three cases studied.

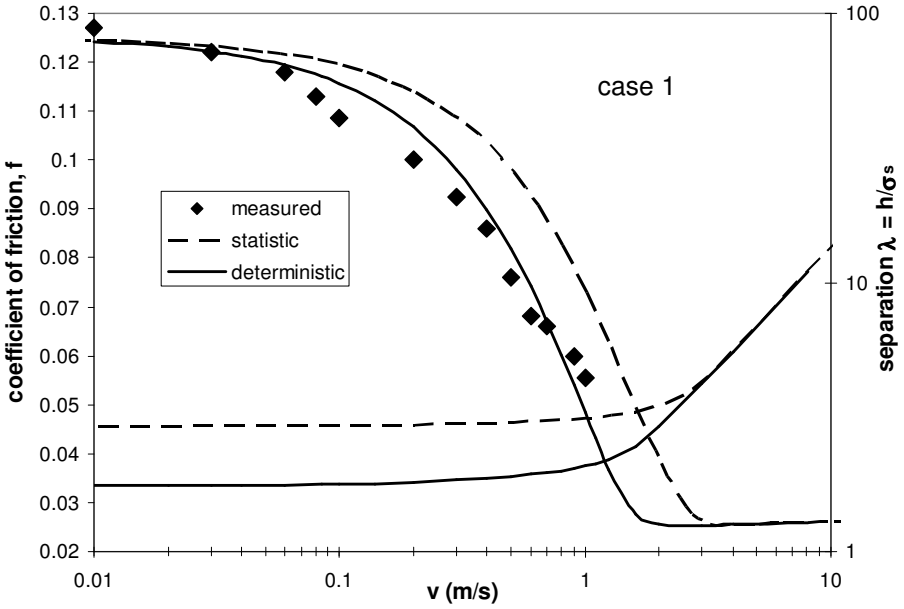
case 1
measured
statistic
deterministic
coefficient of friction, f
separation λ = h/σs
v (m/s)
0.13
0.12
0.11
0.1
0.09
0.08
0.07
0.06
0.05
0.04
0.03
0.02
100
10
1
0.01
0.1
1
10

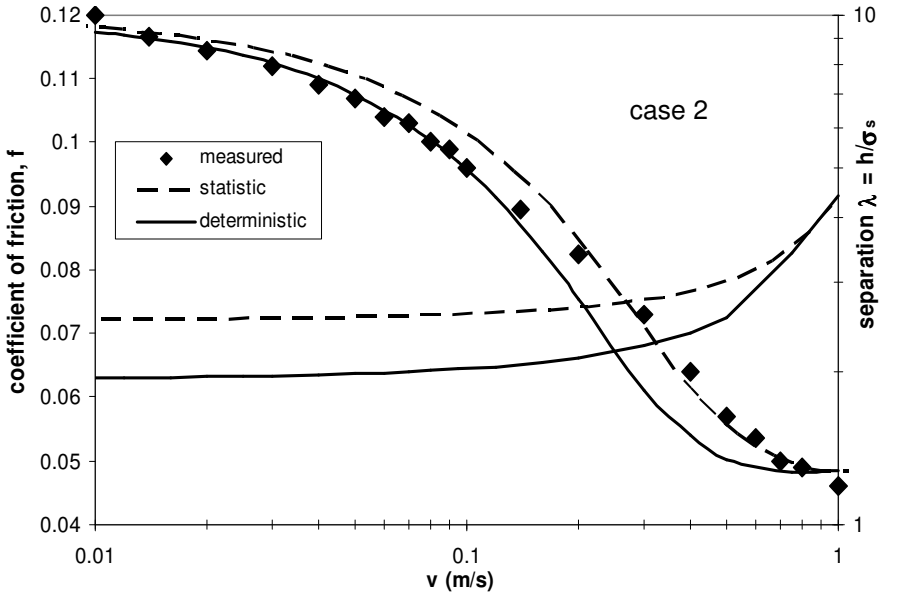
case 2
measured
statistic
deterministic
coefficient of friction, f
separation λ = h/σs
v (m/s)
0.12
0.11
0.1
0.09
0.08
0.07
0.06
0.05
0.04
10
1
0.01
0.1
1

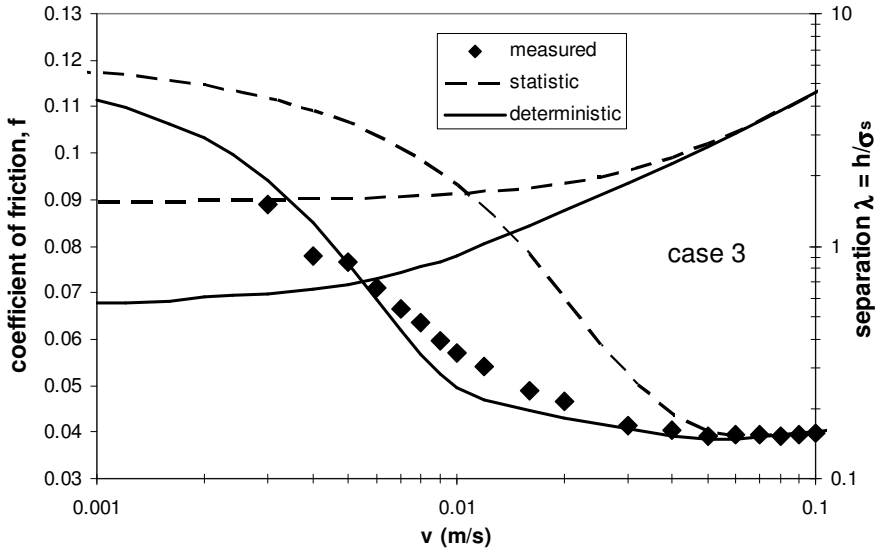

Fig.6.5: Comparison between measured and calculated Stribeck curves for the three cases, for the operational conditions see table 6.2.

In Fig.6.5 the comparison between the measured and the calculated Stribeck curve for the three cases is given. The Stribeck curve is calculated by using the statistic and the deterministic contact model respectively. As it can be seen in the three cases, the deterministic Stribeck curve model is in good agreement with the experiments (see Fig.6.5). The results given by the statistic contact model are close to the results given by the deterministic contact model (Fig.6.5, case 1 and 2) as long as the measured height distribution of the asperities is close to a Gaussian asperity height distribution (see Fig.6.4, case 1 and 2 when s/σ is between 1.5 and 3). As can be noticed the measured height distribution of the asperities in case 1 is a bit closer to the Gaussian distribution compared to case 2 in which s/σ is between 1.5 and 3 while in case 2 the statistical contact model is closer to the deterministic contact model compared to case 1. This unexpected difference may be explained by the stiffness of the surfaces which seems to be higher for case 2 due to a larger asperity radius i.e. the mean average asperity radius value is higher in case 2 than in case 1. Therefore, the separation in the BL regime for the deterministic contact model is closer to the statistic contact model for case 2 compared to case 1, and as a result in case 2 the statistical contact model is closer to the deterministic contact model compared to case 1.

For the deterministic and the statistical Stribeck curve model a shift in velocity of a factor of 5 is found in case 3 (see Fig.6.5, case 3) which is explained by the significant difference between the measured and the equivalent Gaussian height distribution of the asperities (see Fig.6.4, case 3). This difference between measured and equivalent Gaussian height distribution of the asperities gives a big difference in separation in the BL regime between the statistical and deterministic contact model and therefore a big difference between the statistical and the deterministic Stribeck curve.
Based on the results presented, it can be concluded that the calculations performed with the deterministic Stribeck curve model are in good agreement with the experiments, and the calculations given by the statistical Stribeck curve model are in agreement with the experiments when the height distribution of the asperities of a surface is close to the Gaussian distribution.

6.3 Starved lubrication

In section 3.5 a Stribeck curve model for starved lubricated line contacts was presented. In Fig.6.3 a comparison between measured and calculated Stribeck curve for respectively fully flooded and starved lubricated line contacts are made. The input parameters used, are presented in table 6.2, case 2. For the starved lubricated measurements the oil layer thickness ratio h_{oil}/σ_s which supplies the contact, was obtained by measuring the volume of the oil from the disc and the cylinder. After the measurement the disc and the cylinder were cleaned with ethanol which was collected in a glass recipient. The glass recipient was heated up at 60 °C so that the ethanol was evaporated. The weight of the oil which remained on the recipient was measured by using a balance with an accuracy of 0.01 mg. The mass of the oil was estimated by measuring the weight of the recipient with and without oil. The volume was calculated by knowing the density of the oil at 20°C. From the calculations the average value of the oil layer thickness ratio h_{oil}/σ_s which supplies the contact was 2.53. As it can be seen in Fig.6.6 there is good agreement between the calculated and the measured starved Stribeck curve.
Based on the results presented in this section, it can be concluded that the starved Stribeck curve model is in good agreement with the measurements.

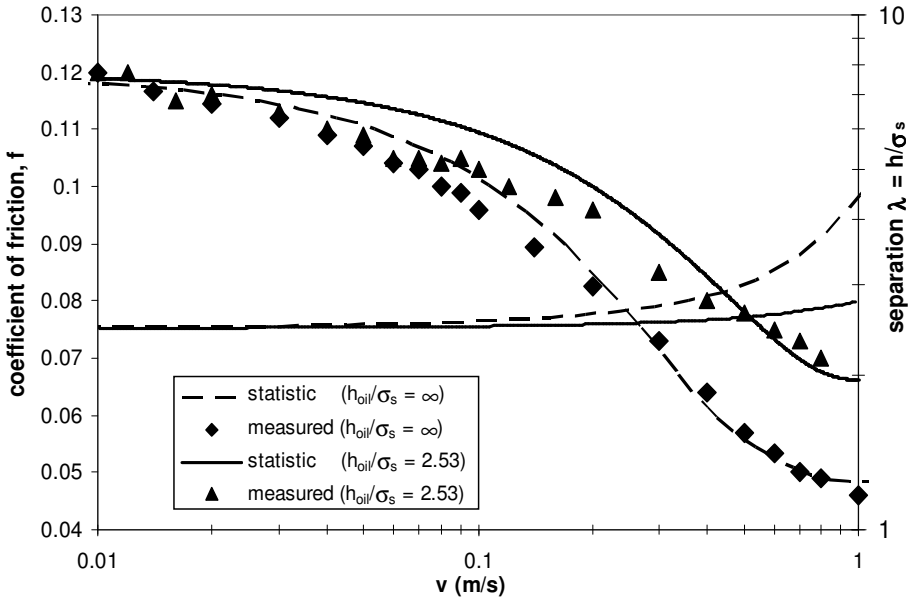

Fig.6.6: Influence of starvation on the Stribeck curve and the separation for case 2, see table 6.2

6.4 Conclusions

In the first part of this chapter, shear stress-pressure dependency measurements for three different oils were presented. It has been shown that in general the variation of the microscopic coefficient of friction with pressure in the BL regime is insignificant. The macroscopic coefficient of friction in the BL regime has a specific value for each type of lubricant and to obtain this value, it is sufficient to perform a single measurement at specific operational conditions in the BL regime, i.e. type of contact, macroscopic contact pressure and oil temperature.
In section 6.2 comparison between the deterministic and the statistic Stribeck curve model and measurements are made. Three cases are considered. Due to the fact that the deterministic contact model takes into account one rough surface, one of the contacting surfaces was chosen to be much rougher than the counter surface. The deterministic mixed lubrication model is in good agreement with the measurements conducted. From the calculations it appears that the statistic Stribeck curve model is in good agreement with the experiments when there is not much difference between the measured height distribution of the asperities and the

equivalent Gaussian height distribution of the asperities (see Fig.6.4 and 6.5). Therefore, the deterministic contact model is recommended due to its accuracy.
In section 6.3 a comparison is made between the measured and calculated Stribeck curve for the fully flooded and the starved lubricated line contacts respectively. In the case of starved lubricated measurements, the oil layer thickness ratio h_{oil}/σ_s which supplies the contact was measured and there is good agreement between the measured and the calculated starved Stribeck curve.

Reference

George, J-M. and Mazurey, D.M. (1990), “Pressure effects on the shearing of a colloidal layer”, J. Phys. Condensed Matter, Vol. 2, SA399 - SA403.

Chapter 7

Conclusions and recommendations

7.1 Conclusions

Chapter 3: Stribeck curve for statistical rough surfaces

A Mixed Lubrication model based on a statistic contact model for two rough surfaces including shear thinning lubricants and starved lubrication have been developed. In section 3.2 a statistical mixed lubrication model for highly loaded line contacts was presented. Next, the effect of two rough surfaces on the Stribeck curve was investigated by extending the statistical contact model of Greenwood and Tripp. The difference between the new contact model and the model of Greenwood and Williamson is that the new contact model takes into account the misalignment of the asperity couples resulting in a smaller separation under BL conditions, whereas the model of Greenwood and Williamson does not consider this effect and therefore the resulting separation in the BL regime is larger. It was shown that the difference in separation between the two models is significant when the two contacting surfaces have comparable roughness parameters. As a result, the Stribeck curve for equal rough surfaces will shift to the lower velocity region.
In section 3.4 the shear thinning effect was incorporated in the film thickness relation. The influence of the shear thinning effect on the Stribeck curve was investigated by varying two parameters, i.e. the low shear rate viscosity over high shear rate viscosity ratio η_0/η_∞ and the critical shear rate $\dot{\gamma}_c$. It was found that by increasing the viscosity ratio η_0/η_∞ the transition from the ML to EHL regime shifts to the higher velocity region while the friction in the EHL regime decreases. When the value of the critical shear rate $\dot{\gamma}_c$ decreases, the transition from the ML to EHL regime shifts to the high velocity region while the friction in the EHL regime is controlled by the viscosity-shear rate dependency.
In section 3.5 a model is presented which is able to predict the influence of starvation on the Stribeck curve. It was shown that for values of oil layer thickness

over roughness ratio (h_{oil}/σ_s) larger than approximately 6, the Stribeck curve and separation do not change. If oil layer thickness over roughness ratio is in the range of 6 to 0.7, the friction starts to increase and the film thickness decreases. When the oil layer thickness over roughness ratio is less than approximately 0.7, the Stribeck curve tends to transform into a straight line (constant friction level) and the separation stays on the same value as in the BL regime.

Chapter 4: Stribeck curve for deterministic rough surfaces

A deterministic contact model has been developed in order to calculate the Stribeck curve for a real distribution of the asperities. In section 4.3 a comparison between the deterministic and the statistic contact model on the Stribeck curve is made. It was shown that the Stribeck curve results, obtained with the statistic and the deterministic contact models, are significantly different when the distribution of the surface heights deviates from the Gaussian height distribution.
Next, the effect of the circular versus the elliptical asperity contact model on the Stribeck curve was investigated. It was found that the difference in Stribeck curve by using a sphere instead of ellipsoid for the asperity contact model, is negligible and therefore the circular contact is recommended due to its simplicity and applicability in deterministic contact modeling.
Further in section 4.5 the influence of the elastic versus elastic-plastic asperity contact model on the Stribeck curve was discussed. From the calculations it appears that the influence on the Stribeck curve of the elastic versus elasto-plastic contact is significant when the contacting surfaces are not run-in and is negligible when the contacting surfaces are run-in.
In section 4.6 the effect of the shear stress-pressure dependency of a boundary layer on the Stribeck curve, in this case of a calcium carbonate lubricant, is presented. From the calculations it appears that when the coefficient of friction of the boundary layer is not constant with the pressure, the macroscopic coefficient of friction in the BL regime varies with the normal load (macroscopic contact pressure).

Chapter 5: Experimental devices

In section 5.2 the newly designed Surface Force Apparatus is described and the final design is presented. The newly designed Surface Force Apparatus is available to measure friction of a single asperity contact accurately. With the Surface Force Apparatus, one is able to measure the shear stress-pressure curve for different lubricants.

Chapter 6: Experimental results

In the first part of this chapter, shear stress-pressure dependency measurements for three different oils were presented. It has been shown that in general the variation of the microscopic coefficient of friction with pressure in the BL regime is insignificant.
In section 6.2 a comparison between the deterministic and the statistic Stribeck curve model and measurements is made. Three cases are considered. Due to the fact that the deterministic contact model takes into account one rough surface, one of the contacting surfaces was chosen to be much rougher that the counter surface. The deterministic mixed lubrication model is in good agreement with the measurements conducted. From the calculations it is clear that the statistic Stribeck curve model is in good agreement with the experiments when there is a small difference between the measured height distribution of the asperities and the equivalent Gaussian height distribution of the asperities.

7.2 Discussion

In chapter 6 comparisons are made between the deterministic Stribeck curve model and the measurements performed. The velocity needed to operate in the EHL regime was low ($v < 1$ m/s) depending on the viscosity of the lubricant, roughness of the surfaces and the normal load. Thermal effects caused by frictional heating in these cases may be neglected. According to the thermal model of Bos (1995), for case 2 presented in section 6.2 for a velocity of 0.1 m/s and a coefficient of friction of 0.09 (see Fig.6.5), the increase in temperature over the bulk temperature would be about 0.3 °C which is negligible. In this section a discussion about the possible influence of temperature on the Stribeck curve is made.
In Fig.7.1 a comparison between the measured and the calculated deterministic Stribeck curve is made. The calculations are performed by using a thermal and an isothermal deterministic contact based friction model. For the deterministic thermal friction model, the model of Bos (1995) is used to calculate the contact temperature to determine the change in viscosity. The test conditions and the input parameters used for the calculations are presented in table 7.1. From Fig.7.1 it is clear that for high velocities the iso-thermal mixed lubrication model underestimates friction. The thermal mixed lubrication model predicts friction better.
The temperature effect on the Stribeck curve is investigated by simply calculating the increase of the temperature using the contact temperature model of Bos (1995) and subsequently calculating the decrease of the viscosity by using the viscosity-temperature dependency of the lubricant used. In Fig.7.2 the solution scheme used to calculate the deterministic Stribeck curve with temperature effect is presented.

Table 7.1: The input parameters

property	value	unit	description
n	$14.7\ 10^{9}$	m^{-2}	density of asperities
β	$1.5\ 10^{-5}$	m	radius of asperities
σ_s	0.23	µm	standard deviation of asperities
E'	$231\ 10^{9}$	Pa	combined elasticity modulus
p	134	MPa	mean contact pressure
η_0	$5\ 10^{-3}$	Pa s	viscosity (100°C)
α	$2\ 10^{-8}$	Pa^{-1}	viscosity-pressure coefficient
τ_0	2.5	MPa	Eyring shear stress
f	0.12	-	coefficient of friction in BL regime

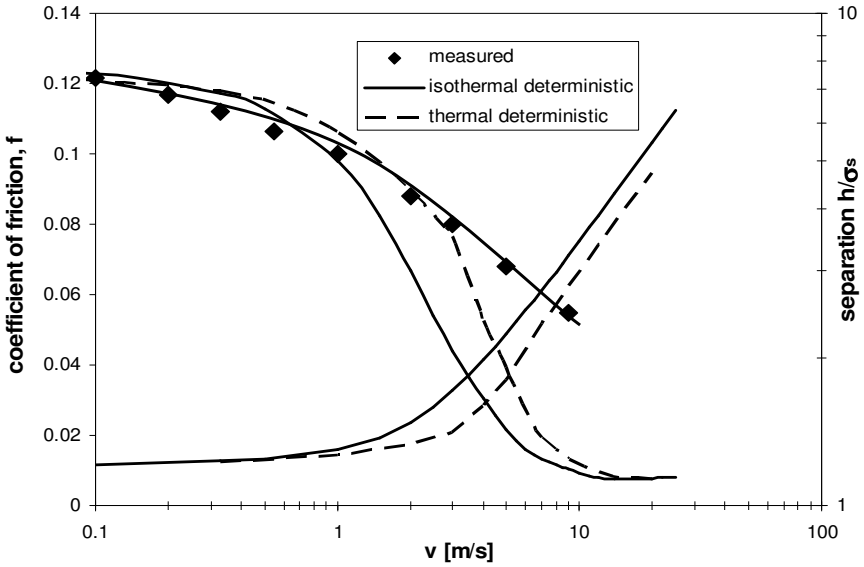

Fig.7.1: Comparison between the measured Stribeck curve and the calculated Stribeck curve with deterministic isothermal and deterministic thermal Stribeck curve model.

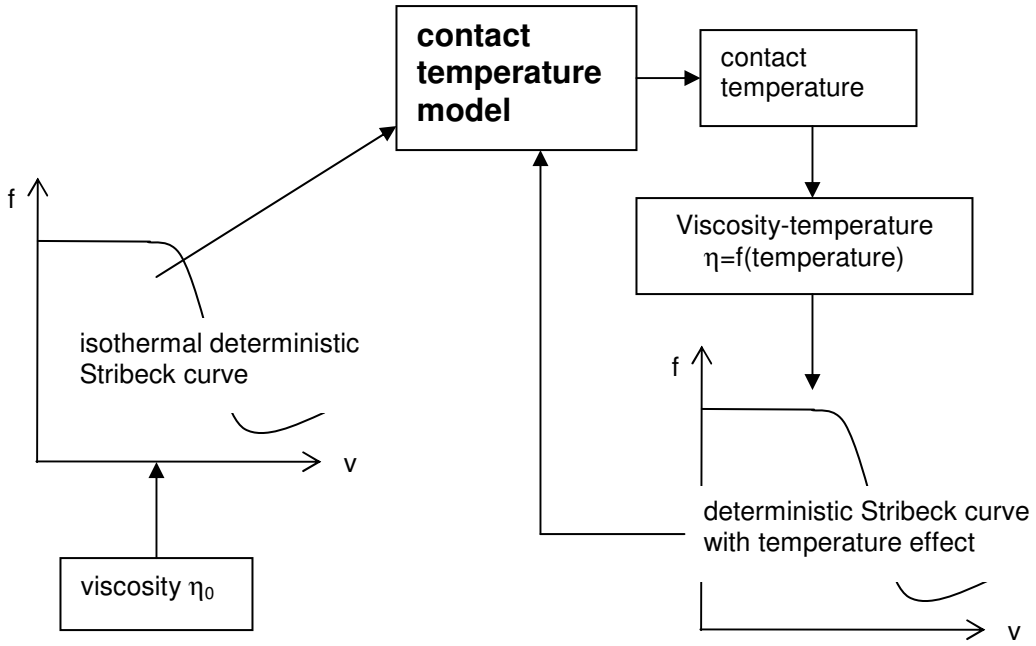

Fig.7.2: The solution scheme used to calculate the deterministic thermal Stribeck curve.

The discrepancy between the predicted and measured friction for high velocity region, say for this case > 3m/s is a consequence of the thermal model used. The thermal model of Bos is developed for elliptical contacts and the current thermal calculations were performed by using an equivalent elliptical contact instead of a line contact. The Péclet number used to calculate the contact temperature takes into account the geometry of the contact, therefore an improved thermal model for line contacts should be considered.

From above it can be concluded that there is thermal effect on the Stribeck curve when the contact operates at high velocity region (1 m/s to 10 m/s) and the existing contact thermal model of Bos (1995) gives good approximation of the contact temperature for velocities up to 3 m/s. For velocities higher than 3 m/s there is a discrepancy between measured and calculated temperature which gives difference between the measured and the calculated Stribeck curve. Therefore an improved temperature contact model which takes into account the line contact, should be developed.

7.3 Recommendations

In section 6.2 comparison between the deterministic and the statistic Stribeck curve model and measurements are made. It was shown that the deterministic mixed lubrication model is in good agreement with the measurements conducted. From the calculations it appears that the statistic Stribeck curve model is in good agreement with the experiments when there is a small difference between the measured height distribution of the asperities and the equivalent Gaussian height distribution of the asperities. The deterministic contact model takes into account one rough surface, one of the contacting surfaces was chosen to be much rougher that the counter surface. It is therefore desirable to develop a deterministic contact model which takes into account the roughness of both contacting surfaces.
In section 7.2 the influence of the temperature on the Stribeck curve has been discussed. It was shown that at high velocities the heat developed in the contact will give an increase of the contact temperature which will influence the Stribeck curve. Therefore it is desirable that a Stribeck curve model which takes into account the increase of the contact temperature due to frictional heating will be developed. In order to do this a contact temperature model for line contacts should be developed.

Reference

Bos J. (1995), “Frictional Heating of Tribological Contacts”, Ph.D thesis, University of Twente, The Netherlands.

Appendix A

Determination of roughness parameters

In chapter 3 calculations were performed using the roughness parameters n, β and σ_s. These parameters are obtained from roughness height measurements. In this appendix the calculation method of the roughness parameters n, β and σ_s is presented.

A.1 Density of asperities

First it must be established how a summit is defined. There are several definitions of a summit. When measuring a profile, a summit is generally defined as a point which is higher than its two neighbours. For a surface measurement there are basically two possibilities:

- A point is higher than its four direct neighbours. This is generally called a peak.
- A point is higher than its eight neighbours. This is generally called a summit (see Fig.A1).

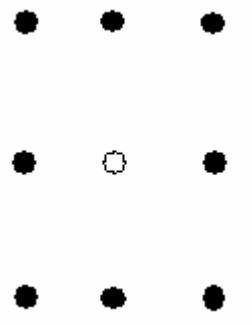

Fig.A.1: Definition of a summit.

Since the demand of a point to be a summit is stricter than the demand for a point to be a peak, there are always more peaks than summits on a surface.

The position of the summits being known, the number of asperities can be counted. By dividing this number through the surface area of the measured surface, the density of summits n per unit area is known.

A.2 The radius of asperities

The radius of an asperity β can be calculated in several ways. Greenwood (1984) introduced the 3 point definition:

$$\beta_x^{-1} = \frac{z_{x-\Delta x,y} - 2z_{x,y} + z_{x+\Delta x,y}}{\Delta x^2} \tag{A.1}$$

$$\beta_y^{-1} = \frac{z_{x,y-\Delta y} - 2z_{x,y} + z_{x,y+\Delta y}}{\Delta y^2} \tag{A.2}$$

with β_x and β_y the radii in, respectively, the x and the y direction, $z_{x,y}$ the local surface height at location (x, y) and Δx, Δy the step or pixel size.
The combined summit radius β_i of the radii in the two perpendicular directions β_x and β_y is obtained by:

$$\beta_i = \sqrt{\beta_{xi} \cdot \beta_{yi}} \tag{A.3}$$

The value of $\overline{\beta}$ used in the calculations is the average summit radius:

$$\overline{\beta} = \frac{1}{n}\sum_{i=1}^{n}\beta_i \tag{A.4}$$

The radii of the summits of the two contacting surfaces are calculated as:

$$\frac{1}{\overline{\beta}} = \frac{1}{\overline{\beta_1}} + \frac{1}{\overline{\beta_2}} \tag{A.5}$$

A.3 Standard deviation of the summits

The standard deviation of the summit heights σ_s can now be calculated from the measured summit distribution:

$$\sigma_s^2 = \frac{1}{n}\sum_{i}^{n}(s_i - d_d)^2 \qquad \text{(A.6)}$$

with s_i the height of summit i, n the number of asperities on the surface and d_d the distance between the mean line of the summits and the mean line through all points of the surface.
The standard deviation of the summits of two contacting surfaces are combined as follows:

$$\sigma_s = \sqrt{{\sigma_{s1}}^2 + {\sigma_{s2}}^2} \qquad \text{(A.7)}$$

with σ_{s1} and σ_{s2} the standard deviation of the summits of surface 1 and 2 respectively.

Appendix B

Summary of the Hertzian contact for the line, circular and elliptical contact

B.1 Line contact

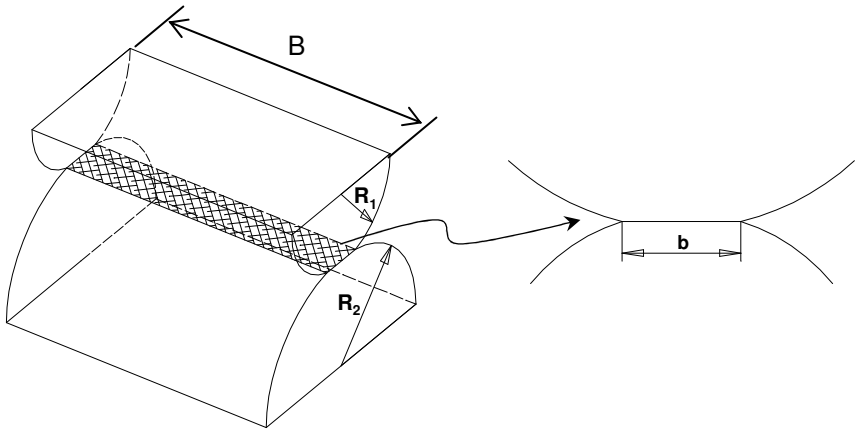

Fig.B1: Contact of two cylinders resulting in a line contact.

Suppose two cylinders (with radii of R_1 and R_2) are in contact under a normal load F_N, the contact width (b) can be calculated as:

$$b = 2\sqrt{\frac{2\frac{F_N}{B}R}{\pi E'}} \tag{B.1}$$

where B is the length of the cylinder, E' is the reduced elasticity modulus and R is the reduced radius respectively, defined as:

$$\frac{2}{E'} = \frac{1-\upsilon_1^2}{E_1} + \frac{1-\upsilon_2^2}{E_2} \tag{B.2}$$

and

$$\frac{1}{R} = \frac{1}{R_1} + \frac{1}{R_2} \tag{B.3}$$

The mean and maximum contact pressure can be calculated with:

$$p_m = \frac{F_N}{2Bb} \text{ and } p_0 = \frac{4}{\pi} p_m \tag{B.4}$$

B.2 Circular contact

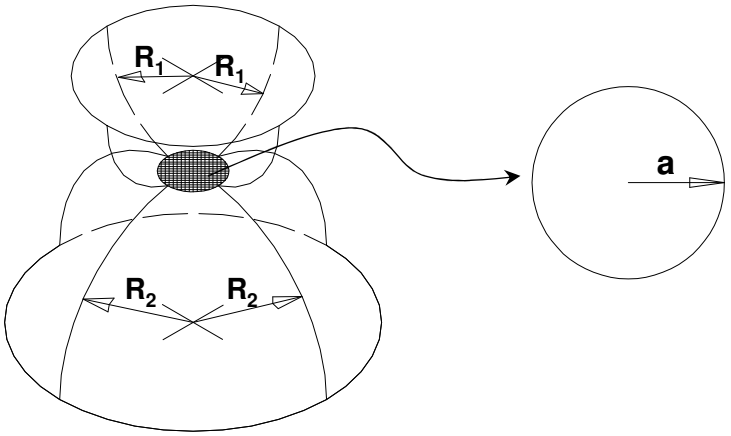

Fig.B2: Contact of two spheres resulting in a circular contact.

Consider two spheres (with radius of R_1 and R_2) are in contact under an applied load F_N. The contact area will be a circle. The radius of contact according to Hertz (1881) can be calculated as follows:

$$a = \left(\frac{3F_N R}{E'} \right)^{\frac{1}{3}} \tag{B.5}$$

with

$$\frac{1}{R} = \frac{1}{R_{1x}} + \frac{1}{R_{1y}} + \frac{1}{R_{2x}} + \frac{1}{R_{2y}} = \frac{2}{R_1} + \frac{2}{R_2} \tag{B.6}$$

in which E' is the reduced elastic modulus according to Eq. B2 and R is the reduced radius.
The elastic approach (δ) can be calculated as:

$$\delta = \left(\frac{9F_N{}^2}{8R(E')^2} \right)^{\frac{1}{3}} \tag{B.7}$$

The mean pressure (p_m) and the maximum pressure (p_0) can be calculated as:

$$p_m = \frac{F_N}{\pi a^2} \text{ and } p_0 = \frac{4}{\pi} p_m \tag{B.8}$$

B.3 Elliptical contact

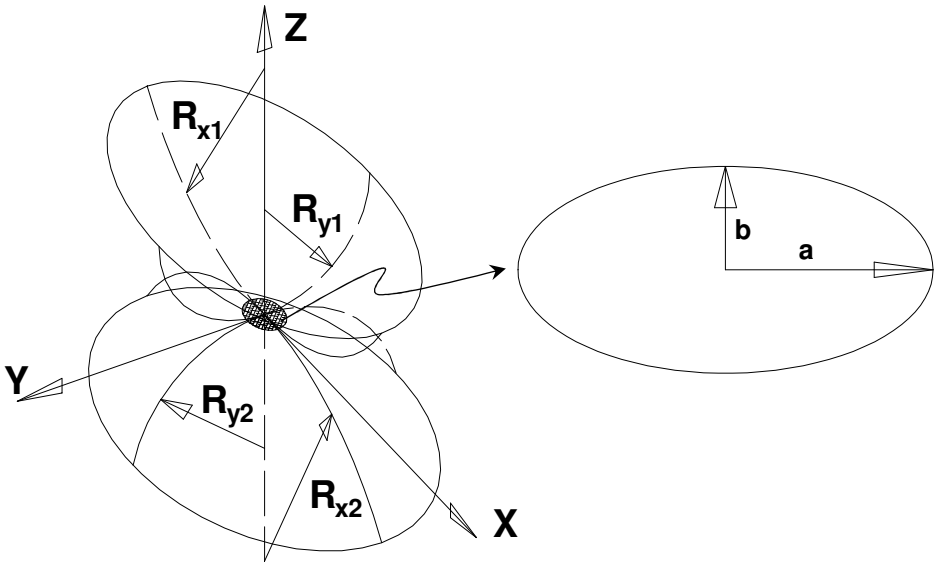

Fig.B3: Contact of two ellipsoids resulting in an elliptical contact.

Suppose two ellipsoids are in contact (see Fig.B3) under a normal load F_N, the contact area will be an ellipse. The major and minor axes of the contact area (a and b) and the normal approach (δ) can be calculated as follows:

$$a = \alpha\left(\frac{3F_N R}{E'}\right)^{\frac{1}{3}} \tag{B.9}$$

$$b = \beta\left(\frac{3F_N R}{E'}\right)^{\frac{1}{3}} \tag{B.10}$$

$$\delta = \gamma\left(\frac{9{F_N}^2}{8R(E')^2}\right)^{\frac{1}{3}} \tag{B.11}$$

where

$$\frac{1}{R} = \frac{1}{R_{1x}} + \frac{1}{R_{1y}} + \frac{1}{R_{2x}} + \frac{1}{R_{2y}} \tag{B.12}$$

and

$$\alpha \approx \kappa^{\frac{1}{3}}\left[\frac{2}{\pi}E(m)\right]^{\frac{1}{3}} \tag{B.13}$$

$$\beta \approx \kappa^{\frac{-2}{3}}\left[\frac{2}{\pi}E(m)\right]^{\frac{1}{3}} \tag{B.14}$$

$$\gamma \approx \kappa^{\frac{2}{3}}\left[\frac{2}{\pi}E(m)\right]^{\frac{-1}{3}}\left[\frac{2}{\pi}K(m)\right] \tag{B.15}$$

with

$$E(m) \approx \frac{\pi}{2}(1-m)\left\{1 + \frac{2m}{\pi(1-m)} - \frac{1}{8}\ln(1-m)\right\} \tag{B.16}$$

$$K(m) \approx \frac{\pi}{2}(1-m)\left\{1 + \frac{2m}{\pi(1-m)}\ln\left(\frac{4}{\sqrt{1-m}}\right) - \frac{3}{8}\ln(1-m)\right\} \tag{B.17}$$

$$\kappa \approx \left[1 + \sqrt{\frac{\ln(16/\lambda)}{2\lambda}} - \sqrt{\ln(4)} + 0.16\ \ln(\lambda)\right]^{-1} \tag{B.18}$$

$$m = 1 - \kappa^2 \tag{B.19}$$

$$\lambda = \frac{R_x}{R_y} \quad \text{for } 0 < \lambda \leq 1 \tag{B.20}$$

The mean pressure (p_m) and the maximum pressure (p_0) can be calculated as:

$$p_m = \frac{F_N}{\pi ab} \text{ and } p_0 = \frac{3}{2} p_m \tag{B.21}$$

Appendix C

Greenwood and Tripp's two rough surfaces contact model; equal radii of asperities

In 1970 Greenwood and Tripp published a paper in which they presented a contact model between two identical rough surfaces (n, β and σ_s of the two surfaces are the same). Let us consider the contact between two rough surfaces (Fig.C1) in which a contact between a particular asperity of one surface (z_1) and a particular asperity of the other surface (z_2) takes place. The shape of the asperity is assumed to be paraboloidal with:

$$y = f\{\rho\} = \frac{\rho^2}{2\beta} \tag{C.1}$$

where ρ, y are the horizontal and vertical distances from the summit and β is the radius of the summit.
The asperities are identical and therefore any contact will be symmetrically centered at a distance $\rho = r/2$ from each center, with r the misalignment distance between the opposing summits. The distances between the mean reference planes and the contact are:

$$z_1 - f\{r/2\}, \quad z_2 - f\{r/2\} \tag{C.2}$$

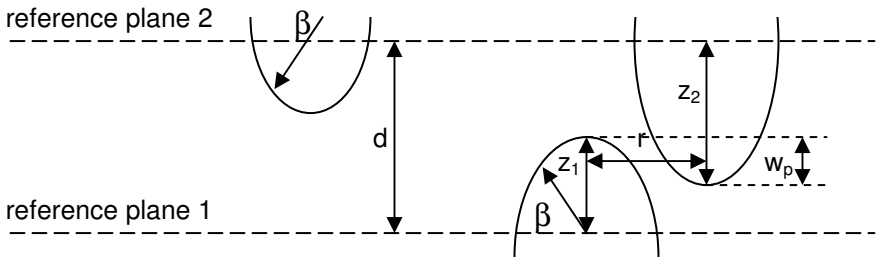

Fig.C1: The contact between two identical rough surfaces.

The overlap between the summits w_p is:

$$w_p = z_1 + z_2 - d \tag{C.3}$$

In order to have contact between the summits, the overlap should be at least equal or larger than 2·f{r/2} ($w_p \geq 2 \cdot f\{r/2\}$). Therefore, during loading the contact area A_r and normal load F_N depend on the interference w_p and the misalignment r:

$$A_r = A_r\{w_p, r\},\ F_N = F_N\{w_p, r\} \tag{C.4}$$

The number of asperities of the second surface with a height between z_2 and z_2+dz_2 situated between r and r+dr from asperity of surface 1 with a height z_1 and making contact with this asperity (z_1) is:

$$N = n \cdot 2 \cdot \pi \cdot r \cdot dr \cdot \phi\{z_2\} \cdot dz_2 \tag{C.5}$$

where n is the density of asperities of the second surface and $\phi\{z_2\}$ is the distribution of asperities of the second surface respectively.
The force on asperity z_1 due to asperity action of the second surface is:

$$F_N = \int_{z_2}^{\infty}\int 2\pi n F_N\{w_p - 2f\{r/2\}, r\}\phi\{z_2\} r dr dz_2 \tag{C.6}$$

In the same way considering the number of the asperities of the first surface with the range of heights between z_1 and z_1+dz_1 being $A_{nom}n\phi\{z_1\}dz_1$, the force acting on the contacting surfaces reads:

$$F_N\{d\} = 2\pi n^2 A_{nom} \int_{z_1}^{\infty}\int_{z_2}^{\infty}\int F_N\{w_p - 2f\{r/2\}, r\}\phi\{z_1\}\phi\{z_2\} r dr dz_1 dz_2 \tag{C.8}$$

The force does not depend on the individual height of an asperity but on their sum z_1+z_2 and therefore the distribution of asperities can be combined by setting z = z_1+z_2, as $\phi_0\{z\}$. The normal force becomes:

$$F_N\{d\} = nA_{nom} \int_{d}^{\infty} F_0\{w_p\}\phi_0\{z\} dz \tag{C.9}$$

where:

$$F_0\{w_p\} = 2\pi n \int_0^{\infty} F\{w_p - 2f\{r/2\}, r\} r dr \qquad (C.10)$$

is the force on one summit.
By following the same procedure, the total contact area reads:

$$A_r\{d\} = nA_{nom} \int_d^{\infty} A_0\{w_p\} \phi_0\{z\} dz \qquad (C.12)$$

where:

$$A_0\{w_p\} = 2\pi n \int_0^{\infty} A\{w_p - 2f\{r/2\}, r\} r dr \qquad (C.11)$$

is the contact area of one summit.
Greenwood and Tripp considered the case in which the asperities of the two surfaces have the same radius β and the asperity deform according to:

$$A = \pi\left(\frac{\beta}{2}\right) w, \quad F = \frac{2}{3} E'\left(\frac{\beta}{2}\right)^{1/2} w^{3/2} \qquad (C.13)$$

where $\beta/2$ is the combined asperity radius, $w=w_p-2f\{r/2\}$ is the "interference" and E' is combined elasticity modulus.
By considering the asperity deformation law, the Eq. C10 becomes:

$$F_0\{w_p\} = \frac{4}{3}\pi n E'\left(\frac{\beta}{2}\right)^{1/2} \int_0^{\infty} (w_p - \frac{r^2}{4\beta})^{3/2} r dr \qquad (C.14)$$

If the bracket $(w_p - r^2/4\beta)$ is negative the integral from Eq. C14 does not make sense therefore the integration limits are 0 to $(4\beta w_p)^{0.5}$. With this condition Eq. C14 reads:

$$F_0\{w_p\} = (8\sqrt{2}/15)\pi n E' \beta^{3/2} (w_p)^{5/2} \qquad (C.15)$$

The total normal force (Eq. C9) now becomes:

$$F\{d\} = (8\sqrt{2}/15)\pi n^2 E' \beta^{3/2} A_{nom} \int_d^\infty (z-d)^{5/2} \phi_0\{z\} dz \qquad (C.16)$$

By writing $z=s\cdot\sigma_s$, Eq. C16 reads:

$$F\{d\} = (8\sqrt{2}/15)\pi (n\beta\sigma_s)^2 E' \sqrt{\frac{\sigma_s}{\beta}} A_{nom} F_{5/2}\left\{\frac{d}{\sigma_s}\right\} \qquad (C.17)$$

Following the same procedure the contact area can be written as:

$$A_r\{d\} = \pi^2 (n\beta\sigma_s)^2 A_{nom} F_2\left\{\frac{d}{\sigma_s}\right\} \qquad (C.18)$$

and the number of asperities becomes:

$$N\{d\} = 4\pi (n\beta\sigma_s) n A_{nom} F_1\left\{\frac{d}{\sigma_s}\right\} \qquad (C.19)$$

In Eq. C.17, C.18 and C.19 the following integral identity is used:

$$F_j = \int_h^\infty (s-h)^j \phi(s) ds \qquad (C.20)$$

where j is a real number and $\phi(s)$ is the normalized Gaussian distribution function:

$$\phi(s) = \frac{1}{\sqrt{2\pi}} \exp\left(\frac{-s^2}{2}\right) \qquad (C.21)$$

with:

$$s = \frac{z}{\sigma_s} \qquad (C.22)$$